DEVELOPMENT OF HIGH STRENGTH MATERIAL FOR SMART AIRCRAFT BOLT

JEAN-MARIE VIANNEY VUGAMPORE

Thesis submitted in fulfillment of the requirements for a doctoral degree in the School of Mechanical Engineering at University of KwaZulu-Natal

Durban, South Africa

October 2005

Supervisor: Dr B. Verijenko

School of Mechanical Engineering

University of KwaZulu -Natal

ACKNOWLEDGEMENTS

I would like to express my deepest gratitude to Professor V. Verijenko, Dr B. Verijenko (my Supervisors) and Professor S. Adali for their financial support through the School of Mechanical Engineering and NRF bursary, their encouragement and guidance during my study.

I wish also to thank Mr. R. Bodger, Professor David Johnson and Dr Denys Slinchenko for their assistances in design and adaptation of testing equipment. Thank you to Bob Patent from Mintek, who manufactured most of the TRIP steels for this study. And finally thank you to my colleagues (PhD and Master Students) and Mechanical Engineering workshop staff for their assistance.

ABSTRACT

Scientists are constantly seeking new and convenient non-destructive damage assessment techniques. In fact, a global market has developed for structural health monitoring products. Many of the currently available techniques are expensive and difficult to implement. An inexpensive alternative is technology based on strain memory alloys. These materials encompass a vast array of alloys, from austenitic stainless steels through to the extremely high strength TRIP steels. All, however, have in common the transformation from paramagnetic austenite to ferromagnetic martensite upon application of strain. The degree of ferromagnetism can be directly correlated to the peak strain undergone by the material. Strain memory alloys are not as expensive to manufacture as some smart materials, and in addition are capable of bearing significant load, and it is therefore possible to manufacture entire components from these alloys, thereby producing what is known as a smart component, i.e. one that is capable of doing the job of an ordinary component while at the same time assessing its own peak damage levels. A possible application of this technology is that of wing bolts for the Hercules C130 aircraft. The material usually used to manufacture the aircraft wing bolts is HSLA steel (AISI 4340). A strain memory alloy was therefore developed to match the mechanical properties of 4340 steel, while also having the requisite properties to perform the self damage-assessment. Ultra high strength TRIP steels were identified as possible candidates, and four alloys selected for investigation. These alloys were melted and then thermo-mechanically processed using a rolling operation. All alloys were tensile tested and magnetic susceptibility monitored. The final material selected possesses an ultimate tensile strength (UTS) of between 1270 and 1500 MPa with 10 to 12% elongation. The stress / strain induced transformation begins to occur before the yield point, which is important because bolts must be replaced before they fail. Compression tests were also performed, and yielded similar results to those of the tensile tests, with martensitic transformation again beginning before plastic yield. The strain induced phase transformation was confirmed not only by magnetic susceptibility measurements, but also by metallographic inspection before and after testing. A subscale Smart bolt was designed, manufactured and tested for magnetic sensitivity using a smart washer.

DECLARATION

I declare that this dissertation is my own work except where due acknowledgement is made to others. This dissertation is being submitted for the degree of Doctor of Philosophy to the University of KwaZulu-Natal, and has not been submitted previously for any other degree or examination.

Jean-Marie Vugampore October 2005

Dedication

I would like to dedicate this work to my wife, Winifred Uwabakulikiza and my children, Ivan, David and Emmanuel.

Table of Contents

List of Figures:

Chapter 1

Chapter 2

List of Tables:

Chapter 1

Chapter 2

Chapter 3

INTRODUCTION

Aviation is generally considered to be an arena populated by safety critical structures. For this reason continuous research in important areas such as fatigue and corrosion of metallic aircraft structures has resulted in high levels of structural reliability. Materials science and engineering have developed theoretical understanding of metal mechanical behaviour, which equip the engineer to easily describe, quantify and predict loading conditions with high accuracy, allowing structures to be designed with reasonable damage tolerances. In this way the safety of the structure is increased, therefore minimizing the probability of mechanical failure, which may cause fatal accidents. These design practices are well supported by a routine inspection technology based on time services. During these periodic inspections the aircraft is out of service, and in the case of the C130 Hercules cargo plane, that amounts to approximately 200 man-hours per inspection. Down times double the cost to the company as flying personnel are paid on a periodic basis, and the company also loses revenue related to the down time or hiring of other aircraft. Smart damage monitoring has been shown not only to be an effective addition to conventional visual examination, providing reliable monitoring data useful in damage assessment and degradation evaluation, but can also significantly reduce down time if innovatively applied. A case in point revolves around the many bolted joints commonly found on aircraft.

Most aircraft have bolted joints somewhere on their structural assembly. In the case of the C130, the wings are bolted to the top of the fuselage, placing the bolts in a highly stressed area. Safety standards demand that these bolts all be removed for inspection at each 'major service'. Clearly a smart inspection technology that could significantly reduce inspection time and possibly eliminate the need to jack up and (in effect) remove the aircraft wing at each inspection would be highly beneficial. The possibility exists that bolts could be manufactured from TRIP steel that would allow them to act simultaneously in the capacity of damage indicator and structural load bearing element (double application). TRIP steels (or Transformation Induced Plasticity steels) have a paramagnetic austenitic crystal structure at room temperature, but upon application of

strain, this transforms to ferromagnetic martensite [7-8]. This transformation is irreversible, and there is therefore a direct correlation between the peak strain (a measure of the accumulated damage) and the percentage martensite present in the microstructure, expressed as:

$$V_{fm} = f(\varepsilon) \quad (1)$$

Where V_{fm} is the volume of transformed fraction of martensite

A measurement of the magnetic susceptibility can thus be correlated with the peak strain or damage levels within the material [4]. A hand-held monitoring device that measures magnetic susceptibility could then be used to monitor bolt health in situ (without removal) thereby providing information regarding bolt health without bolt removal. The disassembly and re-assembly that can result in damage to the bolts (helping to propagate or speed up failure) would be avoided. And, the inspection time would be reduced from the 200 man-hours usually required (due to access difficulties) to a few minutes [2].

The aim of this work is partly to investigate the possibility of using smart aircraft wing bolts, but primarily to develop a high strength strain memory alloy capable of bearing the required load (in terms of the military specification for C130 wing bolts) as well as producing the correct transformation characteristics to allow early detection of damage. In order to accomplish this task several sub-tasks must be performed, among them an extensive literature survey, formulation of candidate alloys, rigorous testing of candidate materials including tensile, compressive, and impact testing, all in conjunction with magnetic susceptibility monitoring to determine transformation characteristics. The effects of temperature [2], strain rate [2], material processing [5, 9, 10] and compositional effects [2] will all be important variables.

TRIP steels were originally discovered when researchers were searching for an alternative to high strength low alloy steels. The extraordinary combination of strength and ductility as well as excellent fatigue performance (due to the phase transformation) was what attracted all the attention approximately 40 years ago [3-5]. No one at that time thought of using the change in magnetic susceptibility (accompanying the phase

transformation) as a damage monitoring mechanism. In order to do just that, however, alloying chemistry must be correctly tailored to achieve just enough austenitic stability to produce the paramagnetic austenite at room temperature, but also just enough instability to allow the phase transformation under the action of strain. The formulation of appropriate candidate alloys will therefore require an in depth understanding of the effects of individual alloying elements on both mechanical properties as well as transformation characteristics.

Closely associated with the alloying chemistry (and having a direct bearing on the transformation characteristics) is the material processing commonly known as Prior Deformation of Austenite (PDA) that is used to raise the strength of TRIP steels. The nature, temperature and degree of this warm work have all been shown to have an effect on the strength of the material produced.

The testing of candidate alloys will begin with tensile testing (including magnetic susceptibility monitoring), primarily because the first criterion that any material to be used in military aircraft bolts must meet, is that of tensile yield strength. Thereafter, if the candidate material makes the grade, it will be further tested to assess compressive transformation characteristics, impact properties and importantly, the effects of temperature on the transformation characteristics of the alloy. Once complete this battery of tests will produce an alloy or set of alloys that meet the strength criterion of the military specification. The work cannot hope to produce a complete working smart aircraft bolt because the scope of work (which includes the fatigue testing of prototypes) required for this, is just too large. The concept of the smart bolt can however be furthered by considering how the bolt design can be modified to incorporate a damage measuring device within the design. For this purpose a scaled down prototype machined from strain memory alloy material can be tested.

CHAPTER 1

STRAIN MEMORY ALLOYS

The development of a smart aircraft bolt capable of bearing the normal load, while at the same time providing an indication of its own damage level, requires the use of a smart material. The only class of smart material capable (at reasonable cost) of fulfilling this dual role is that of strain memory alloys. Strain memory alloys effectively memorize the peak strain experienced by the material, and can be considered to be at their most useful when used as passive peak monitoring devices. Strain memory alloys encompass a broad range of austenitic ferrous alloys, but TRIP steels can be considered to be a special class of these alloys, with ultra high strength possible.

The TRIP (transformed induced plasticity) phenomenon was observed in austenitic steels in the 1970 s. It has since become a topic of immense interest for scientists due to the extraordinary combination of strength and ductility that can be produced using this effect. Research proves that the strain induced phase transformation is responsible for the large values of ductility and strain hardening that is observed in these steels [2, 4, 5, 11-17]. Early work in this area was centred on understanding the nature of the phase transition [18-20]. Recent developments in the steel industry use the TRIP phenomenon as part of dual phase steels (which contain retained austenite) that transform when pressed using sheet metal forming operations. Besides the obvious advantages offered by the above mentioned structural properties, the strain induced phase transformation from an austenitic face centred cubic (FCC) parent phase to a martensitic body-centred cubic (BCC) product phase results in a change in the magnetic properties of the steel.

The magnetic signature of TRIP steel depends on the fraction of martensite present and this increases as the transformation progresses with increasing strain [8], as shown in Figure 1.1 which follows.

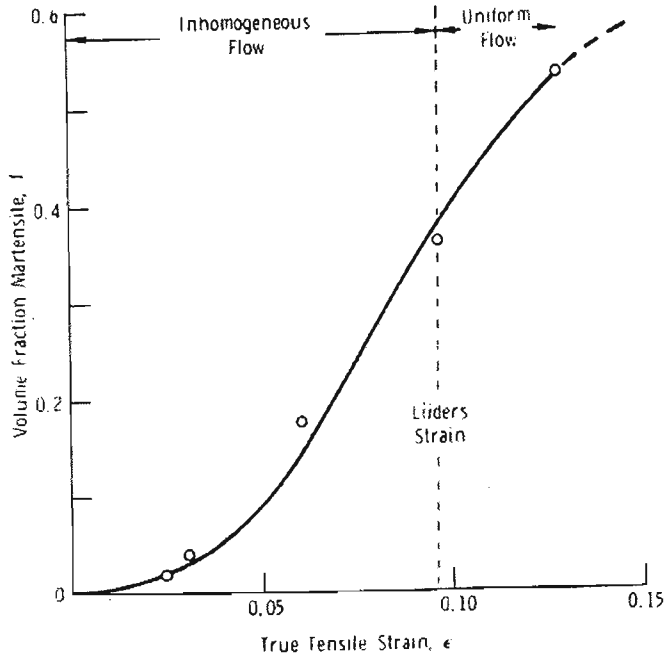

Figure 1.1 Volume transformed stress-strain induced martensite versus strain [21]

This aspect of the TRIP Steels makes them an inherently SMART material. The strain induced martensite transformation may be controlled by alloy chemistry and thermo-mechanical processing of the material (warm rolling [22] and pre-straining). To obtain the highest yield strengths it is necessary to thermo-mechanically process the material [5-6, 9, 12, 13, 23, and 24]. The ultra-high strength developed in TRIP steels can actually surpass traditional high strength structural steel such as 4340 (AISI), which is currently used in aircraft landing gear and similar applications.

1.1 Alloying Chemistry

An austenitic steel alloy composition that exhibits TRIP behaviour within the operating temperature range of –50°C to +50°C, is required. In order to obtain the desired level of austenite stability, austenitic stabilising elements are added in appropriate amounts. The Schaeffer-de Long Diagram [40] gives a visual representation of the effects of various alloying elements on the phases that will be present (see Figs 1.2-1.8). Figure 1.9 shows an approximate region identified to contain smart alloys. Individual alloying effects, however, deserve closer scrutiny. The most commonly used elements are Fe, C, Cr, Ni,

Mn, Si, N, Mo and P. Strain memory alloys are based on iron for the important allotropic change accompanied by a change in magnetic permeability that makes the material smart. All other elements may have one of two basic effects, according to the Wever classification [25]:

- Austenitic stabilisers are those that expand and open the γ field.
- Ferrite stabilisers are those that contract and close the γ field.

1.1.1 Elements that create an open γ field

These elements include nickel, manganese, cobalt, and the inert metals ruthenium, rhodium, palladium, osmium, iridium, and platinum.

Nickel and manganese stabilise the γ phase at room temperature if they are added in sufficient quantity. They also depress A_{e1} and A_{e3} temperatures on the iron-carbon phase diagram.

Nickel: Figure 1.2 shows the effect nickel has in stabilising and enlarging the austenite or gamma loop. Nickel is the most used austenitic stabiliser in austenitic stainless steels, and also improves corrosion resistance in neutral and weak oxidising media [26]. Improvement of ductility and formability (FCC structure at room temperature), as well as depression of the M_s temperature (see Fig 1.3) all result from nickel additions.[11, 27 - 29].

A study investigating the base alloy of Fe-0.3C-2Mn-9Cr-X Ni (X varying from 8 to 16%) directly shows the stabilising action of nickel [30].The 8% Ni alloy was unstable, while the 12% Ni alloy was metastable, showing transformation. The 16 % Ni alloy was however a totally stable alloy [27, 31].

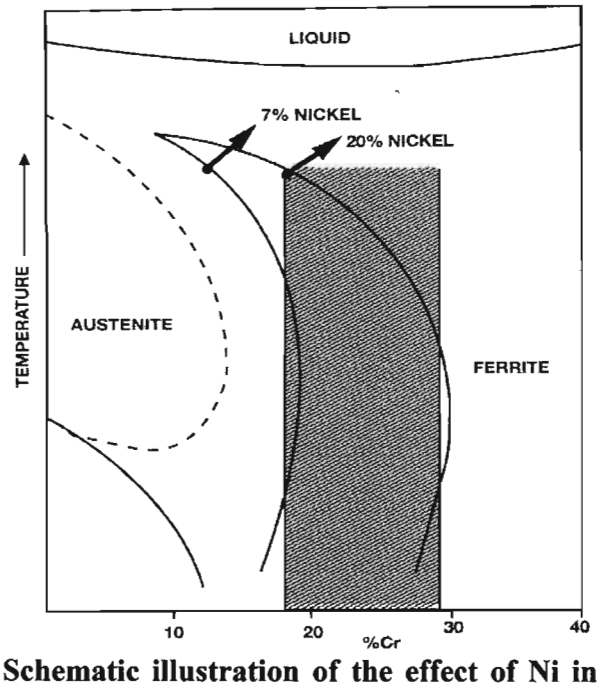

Figure 1.2 Schematic illustration of the effect of Ni in shifting Gamma Loop and stabilizing austenite down to low temperatures [97]

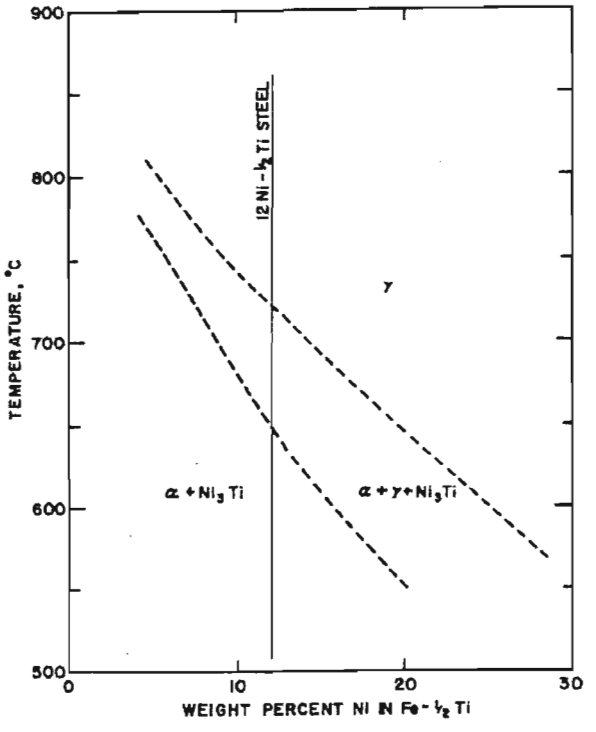

Figure 1.3 Phase diagram of the Fe-Ni-Ti system showing the transformation temperatures for the steel 12Ni-0.5Ti [28]

Manganese: is only half as effective as an austenitic stabiliser when compared with nickel, but has the added effect of lowering the stacking fault energy. When the stacking fault energy is lowered sufficiently, enough stacking faults form which promote the formation of an intermediate (HCP) ε martensite [4, 32-36] between the austenite and stable α' martensite phases [6].

To produce a Fe-Mn-Cr austenitic steel in which ε martensite is formed, manganese content of 10% or greater is required, while 13-18% Cr stabilizes the α phase field sufficiently to cause the transformation from ε to α martensite [63, 64]. This important group of alloys is cheaper than the well-known Fe-Cr-Ni stainless steels; and can also be manipulated to improve the transformation temperature and strain rate insensitivity of the strain induced martensitic transformation [6]. Temperature and strain rate sensitivity are not advantageous for practical use of the strain memory technique and must be eliminated if possible. However promising and attractive this alloy group may be though, it will not be considered for the aircraft bolt application, as it does not achieve the required high strength.

1.1.2 Elements that expand the γ field

These elements are carbon (C), nitrogen (N), copper (Cu), zinc (Zn), and gold (Au) but this field is cut short by the formation of compounds [31].

Nitrogen: many researches have concentrated on the replacement of Ni by N [7, 31, 37-38]. One such study replaced approximately 2.5%Ni with 0.2 % N [7]. The stability of austenite was not quite the same as in the original alloy, but comparable properties were attained in terms of work hardening rate. It has been found that too high a nitrogen level might delay cracking after deep drawing operations [39], and cracking may get worse with time, because of the embrittling effect of nitrogen on martensite.

Carbon: is an austenite stabilizer, but care must be taken to avoid the formation of free chromium carbides, which arise as the solubility of carbon decreases with decreasing temperature (in sensitizing range 400-950^{o}C). Elements such as Ti, and niobium are often

added to inhibit this effect [26]. Carbon also depresses the M_S temperature [18] by around 10°C for every 0.01% C. The austenite-martensite transformation starts at a temperature referred to as M_s and continues with respect to decreasing temperature down to a temperature referred to as M_f, at which the reaction ceases even though retained austenite may still exist [31,40]. Martensite forms in the range $M_s - M_f$ only with decreasing temperature [41]. These temperatures are influenced by the composition of the steel and particularly the carbon (see Fig 1.4), nickel and manganese contents.

If complete dissolution of carbides in austenite prior to quenching is assured, the M_S temperature may be calculated by the following expression for any alloy containing around C= 0.2 to 0.85 % and Cr less or equal to 1.5%.

M_S (°C) = 523 - (361 x %C) - (39 x %Mn) – (19 x %Ni) – (39 x % Cr) – (28 x % Mo) (2)

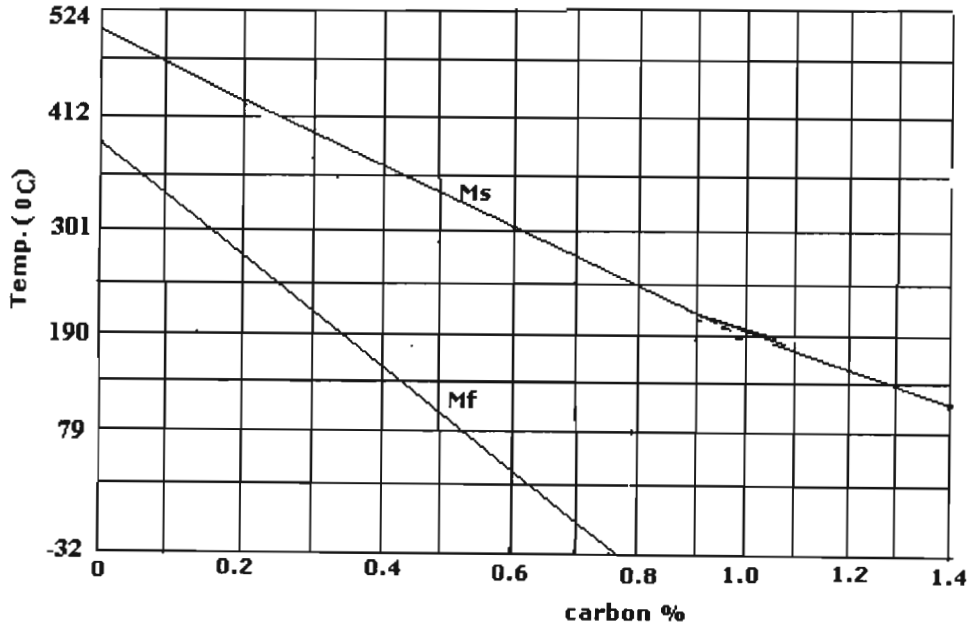

Figure 1.4 Influence of carbon on M_S and M_f temperature [31]

Copper: Besides the austenitic stabilising effect of copper, it has good corrosion characteristics [39], but with a small negative effect on ductility [37]

1.1.3 Elements that promote the formation of BCC iron

By creating a γ loop on the phase diagram, the α and δ phases became continuous [26]. These alloys cannot be heat-treated by using the γ/α-phase transformation. The group of elements which promote this behaviour include: silicon (Si), aluminium (Al), beryllium (Be), and phosphorus (P). Carbide formers (like Cr, Mo Ti, and vanadium (Fig 1.5) are also part of the same group (see Fig 1.5-1.6)).

Chromium: is commonly added for corrosion resistance; and forms a passive protective oxide film on the outside air-exposed surface. A minimum of 12-13 % Cr is required to assure this stainless effect. There is an austenite to ferrite transformation on cooling from the γ loop. For chromium content greater than 13%, a transformation does not occur, and a solid solution of Cr in α ferrite is formed (see Fig 1.5). The formation of carbides in strain memory alloys is a positive phenomenon [6], as they enhance dislocation multiplication and pinning at elevated temperatures. Thermo-mechanical processing and the presence of carbides substantially increase the yield strength at room temperature [42].

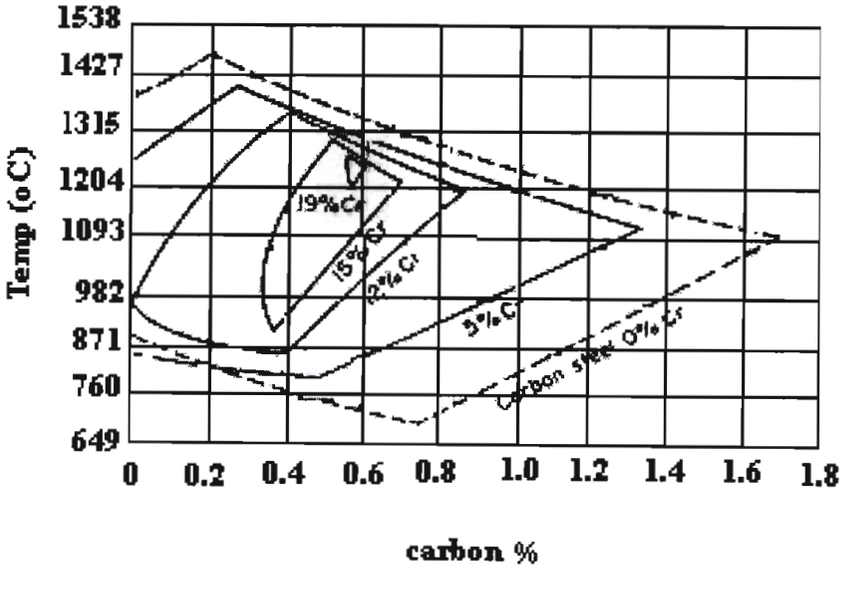

Figure 1.5 Effect of chromium on the austenite phase region [41]

Molybdenum: is the most effective of the above mentioned three carbide formers in enhancing strain-hardening properties, and Cr the least effective. Mo and V produce strain hardening that is independent of temperature and strain rate [43, 44]. Molybdenum is a ferrite stabiliser, the effect of which can be seen in Fig 1.6. Molybdenum carbides are effective barriers to plastic deformation [42], and account for secondary hardening after tempering in the range 500-600°C.

Mo and Si both improve corrosion resistance [45, 46], Mo specifically the pitting and crevice corrosion resistance in chloride atmospheres [26].

Al is added to improve high temperature scaling, and is commonly added, like Ti and Nb, to combine with interstitial elements and thus prevent sensitisation.

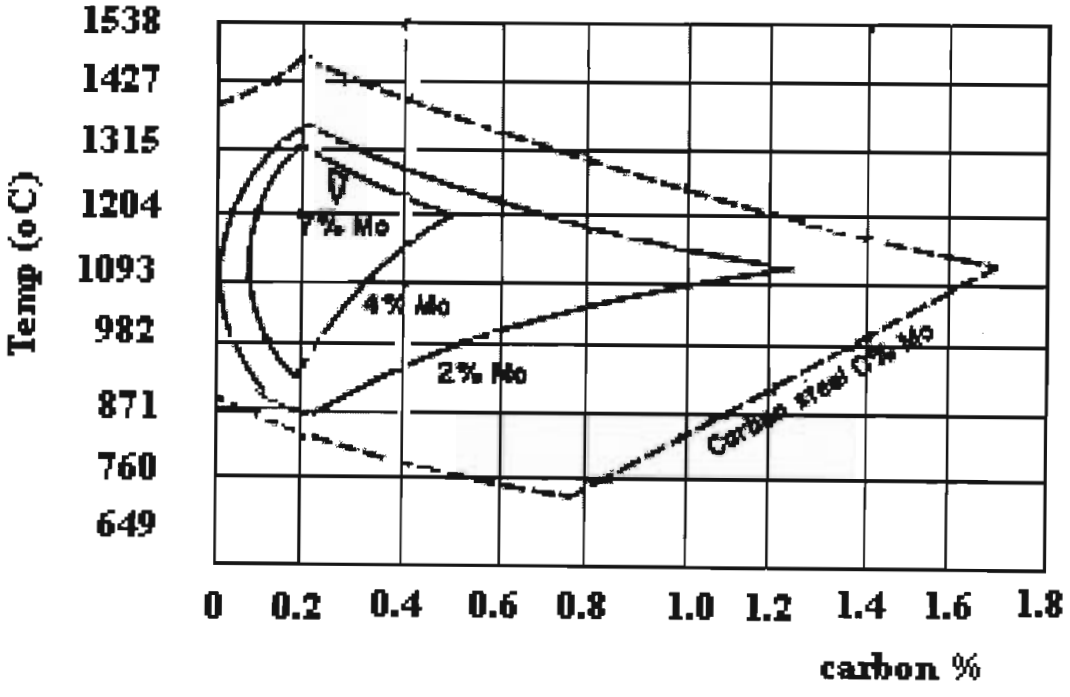

Figure 1.6 Effect of molybdenum on the austenite phase region [41]

1.1.4 Elements that contract the γ field

These are boron (B), and the carbide formers tantalum, niobium, and zirconium. Niobium (0.13-0.22 %) is commonly added as a grain refiner [11], which may improve strength. The effects of all the elements discussed above can be summarised in Table1.1 below [6]. The general effect of alloying element on hardness (strength) of α -iron is shown in Fig 1.7.

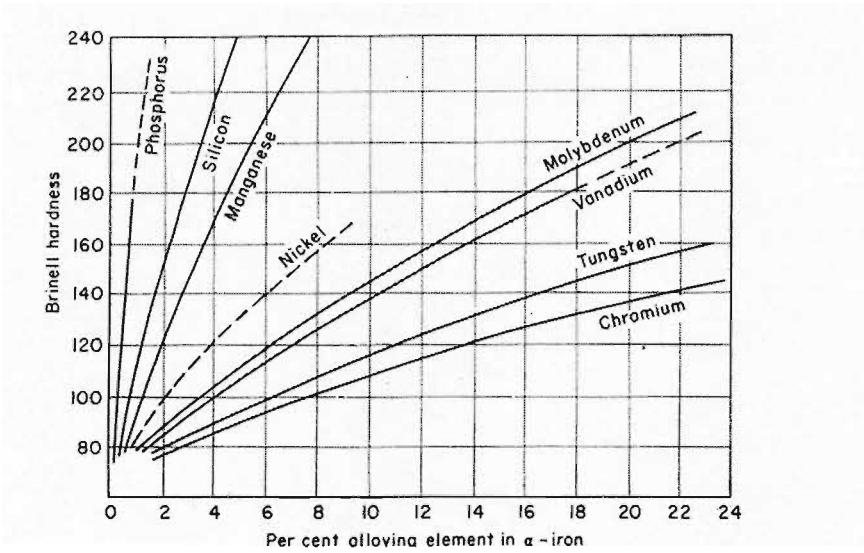

Figure 1.7 Hardening effect of various elements as dissolved in pure iron

Table 1.1 General effect of alloying elements on the stability of austenite and the properties of stainless steel

	Promotes	Effect on properties
Cr	Ferrite	Improves general corrosion resistance and resistance to oxidizing environments and lowers the SFE
Ni	Austenite	Improves general corrosion resistance and resistance to reducing environments, **austenitising index 1**
C	Austenite	Increases strength, decreases corrosion resistance, **austenitising index 30**
N	Austenite	Increases strength, improves pitting resistance, raises SFE, **austenitising index 25**
Mn	Austenite	Improves hot cracking resistance, increases solubility of nitrogen, austenite stabilizer, lowers SFE, **austenitising index 1/2**
Mo	Ferrite	Improves pitting and crevice corrosion resistance, increases work hardening, lowers SFE
Nb	Ferrite	Forms stable carbonitrides to resist sensitization, grain refinement
Si	Ferrite or neutral	Improves wetting and flow, improves high temperature oxidation and carburization resistance
Ti	Ferrite	Forms stable carbonitrides to resist sensitization
Al	Ferrite	Improves high temperature oxidation and decarburization resistance
Cu	Austenite (weak)	Improves resistance to reducing environments. Can be used for precipitation hardening
S	Neutral	Improves machinability, promotes hot cracking
P	Ferrite	Increases strength, promotes hot cracking

The effects of the various alloying elements have been discussed in terms of the stability of the γ phase at room temperature in relation to iron, but the interaction of alloying elements is complex. Damage detection based on strain memory alloys requires the production of an austenitic alloy at service temperature (range -50^0C to $+50^0$C) which transforms to martensite when undergoing deformation. In formulating candidate chemistries, the Schaeffer-De Long diagram in Figure 1.8 (which predicts the phases present in stainless alloys), is useful. The chromium and the nickel equivalents are calculated as follows:

$$C.E=\%Cr+\%Mo+\%1.5Si \quad (3)$$

$$N.E=\%Ni+30\%C+0.5\%Mn+\%Co+25\%N \quad (4)$$

A region where smart steel or strain memory alloys are likely to be produced has been identified by Paton [30] in Fig 1.9.

A balanced quantity of austenitic former or stabilizers and ferrite stabilizers must be met, in order that the austenite is stable at the service temperature but at the same time be destabilized by lattice perturbation to transform to martensite. For strength, processing and manufacturing reasons, chemistries were formulated to avoid the production of ε martensite. [47, 48].

1.2 Material Processing

After casting, metals usually undergo further processing in order to optimize the properties, homogenise the microstructure, and possibly shape the material. This processing is usually divided into hot working which is deformation of metal at high temperatures and does not produce any strengthening in the metal and cold working which is a simultaneous deformation of metal by which the metal is strengthened. After mechanical processing heat treatment may be carried out in order to modify or eliminate the residual stress and the strengthening obtained during cold work. By controlling

deformation and heat treatment, metal parts are transformed into useful shapes whilst improving their mechanical properties.

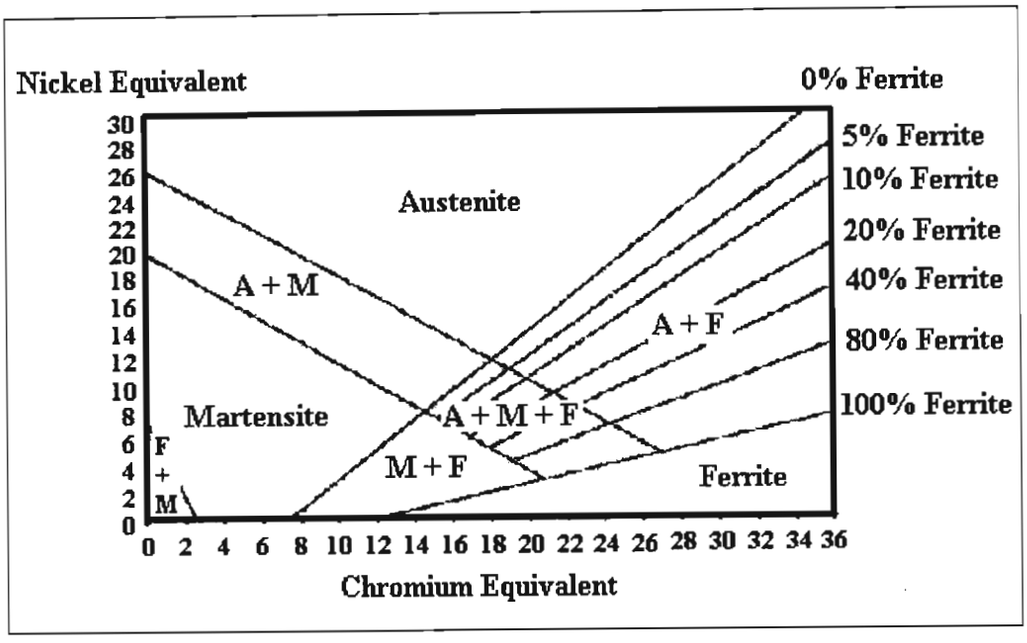

Figure 1.8 De Long Diagram

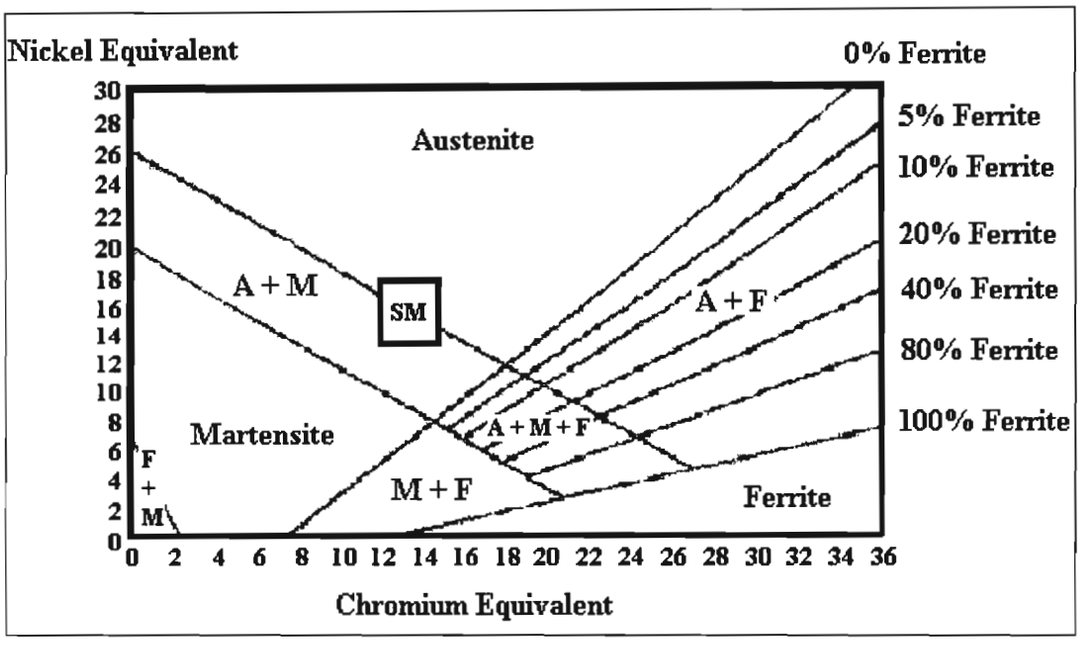

Figure 1.9 De Long diagram showing the area for TRIP steel or Smart steel

1.2.1 Strain hardening mechanisms

The strengthening obtained by cold working, which is brought about by slip or twinning, becomes progressively more difficult. This is called strain hardening or work hardening. When a stress greater than the yield strength is applied to a metal, a permanent deformation (plastic) is caused. Each time we apply a higher stress than the yield strength, and then unload the material, the yield strength and tensile strength increase but the ductility decreases. The metal is strengthened until the yield strength, the tensile strength and the breaking strength are equal and there is no more ductility. At this point metal can be plastically deformed no further. The response of metal to cold working is given by a strain-hardening coefficient n, which is the slope of the plastic portion of the true stress-strain curve on a logarithmic scale, described by the equations (5-7) below. Metals with low strain-hardening coefficients respond poorly to cold working

$$\sigma_t = k\,\varepsilon_t^{n} \text{ or} \qquad (5)$$

$$\ln \sigma_t = \ln k + n \ln \varepsilon_t \qquad (6)$$

$$k_t = \sigma_t; \text{ when } \varepsilon_t = 1 \qquad (7)$$

Where σ_t = true stress,

ε_t = true strain,

k= modulus of elasticity

This hardening which is obtained by the movement, restriction and multiplication of dislocations requires that materials have ductility. When a stress greater than the yield strength is applied to a metal, dislocations begin to slip. Dislocations moving on a slip plane encounter obstacles that pin the ends of the dislocation line. As we continue to apply the stress, the dislocation attempts to move by bowing in the centre, a dislocation loop is produced and when the dislocation loop finally touches itself, a new dislocation is created. The original dislocation is still pinned and can create additional dislocation loops. This mechanism for generating dislocations is called a "Frank-Read" source.

The number of dislocations may increase to about 10^6 of dislocation lines per cubic millimetre of metal. The more dislocations we have, the more likely they are to interfere with one another and the stronger the metal becomes.

1.2.2 Melting and Processing of TRIP Steel (thermo-mechanical processing)

The processing of TRIP steel or any strain memory alloy follows the elements of normal processing but with some modification. The process begins in a vacuum induction furnace. Molten metal is cast into ingots and is then hot rolled to produce wrought material from which all casting imperfections are eliminated. In order to increase the yield strength to a value acceptable for the aircraft wing bolt, the material would usually be cold worked or heat-treated. In this case, both methods are unacceptable, because the γ/α transformation would not produce martensite, as strain memory alloys are designed so that austenite is stable at working environmental temperatures (which must be above M_S temperature), and because normal cold work (usually at room temperature, which is below the M_D temperature) will induce the martensite transformation reaction.

Two new methods for increasing the yield strength, without creating martensite, have been investigated. The first method makes use of the unusual TTT diagram created by strain memory chemistry, a process commonly known as ausforming [49-50]. The benefit of ausforming is two fold: it increases the diffusivity of alloy carbide formers as well as providing structural contributions to strengthening (dislocations and precipitates) [50]; and the second method is a cyclic heat treatment method (reverted austenite [51]).

1.2.3 Time Temperature Transformation curves

The common method used to study phase transformation (a phase diagram) is quite simple when dealing with a two or three element alloy composition. In reality alloys are engineered with more than three main elements in order to meet the high environmental and mechanical performance required by modern industry, apart from additional unintentional impurities. In complex alloys phase diagrams become complex and difficult to represent graphically, let alone interpret. Establishing a TTT diagram for the identified alloy chemistry is one method used to solve this dilemma. On the TTT diagram, isothermal transformations are represented as functions of time and temperature. Figure 1.10 shows the simplest type of TTT curve, that of a plain carbon eutectoid steel.

From martenite start (M_S) to martensite finish (M_f) temperatures, there is spontaneous thermal formation of martensite (with decreasing temperature) which is used for the classic γ/α heat treatment. Although strain-induced martensite forms above the temperature range of the spontaneous martensitic transformation, the proximity of the M_s – M_f temperature range to the operating temperatures of the strain memory sensor have an effect on the strain-induced formation of martensite. The temperature above which strain induced martensite ceases to form is called M_d [30] temperature, which is experimentally determined for a given alloy composition and may change for different loading conditions [8, 10, 17, 33, 44, 52, 54-55, 61].

Alloying elements, such as nickel and manganese, which expand the γ field, depress the position of the TTT curve with respect to temperature. Those alloying elements that favour the ferrite phase raise the curve higher with respect to the temperature.

While Figure 1.10 shows the TTT curve for plain carbon eutectoid steel, the diagram is radically altered with the addition of sufficient alloying elements, to produce the curve shown in Figure 1.11, which presents a metastable bay, allowing for useful thermo-mechanical processing, without transformation.

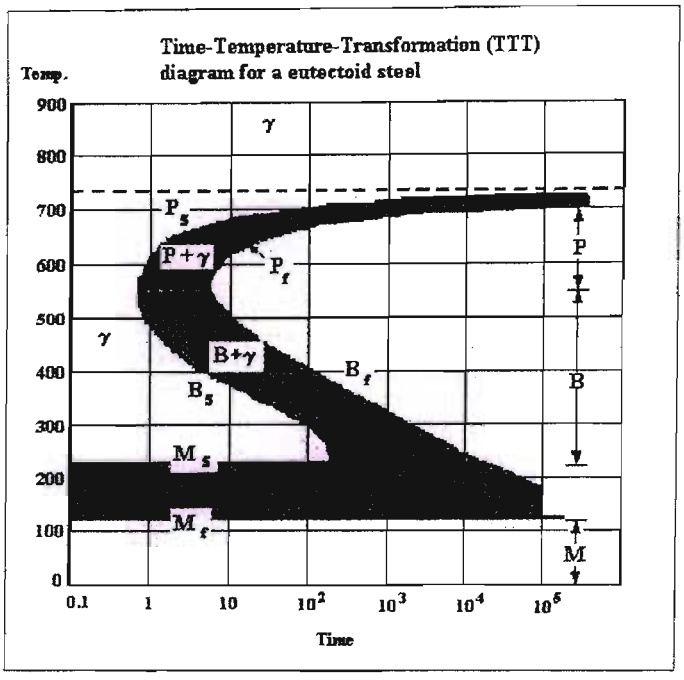

Figure 1.10 An example of the TTT curve for a plain carbon eutectoid steel

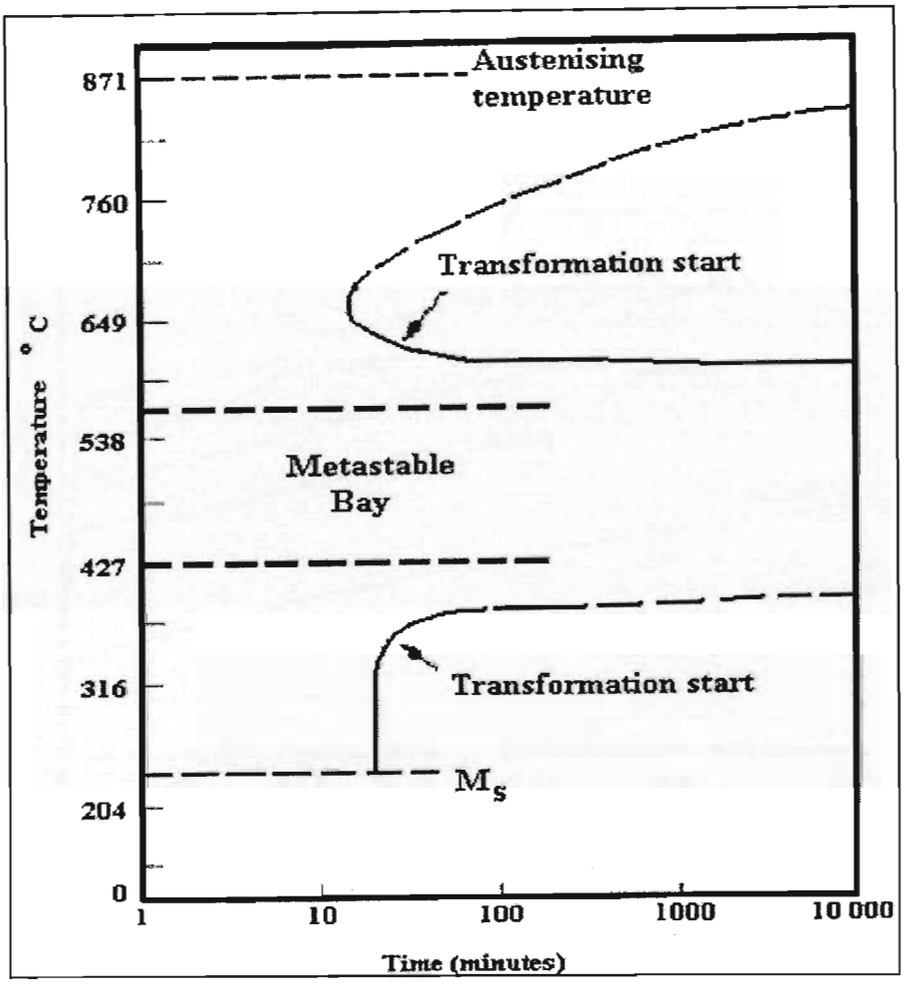

Figure 1.11 An example of a metastable austenitic bay engineered into the TTT curve by alloying chemistry [49]

1.2.4 Warm work

The metastable bay makes possible the processing of strain memory alloys, in this temperature range [49]. The warm work imparts strength to the material, as the bay is below the recrystallisation temperature. This thermo-mechanical process is preferably accomplished by rolling rather than by extrusion [49], but hot hammer forging may also be employed. The high loads and therefore large rollers required for this rolling are expensive, especially when the temperatures under consideration are high enough to degrade the roller surfaces. This means that most commercial cold working mills are unwilling to perform this type of operation on their equipment. A combination of processes is therefore used to adjust rod size to fit into smaller rolling mills. For ultra-

high strength material a high reduction (80+%) is necessary, and the size of the structural element to be produced must be borne in mind since there is not much scope for machining without producing undesirable transformation.

This most common method of increasing the strength in metastable alloys, is termed Prior Deformation of Austenite (PDA) and is a modified form of the technique of thermal-mechanical processing commonly known as Ausforming (when mechanical work is applied to steel in metastable austenitic condition, a substantial increase in tensile strength and yield strength takes place). The effect of the PDA on strength is illustrated in Figure 1.12, where the suffixes /1, /2, /3 and /4 imply, 20%, 40%, 60% and 80% work respectively.

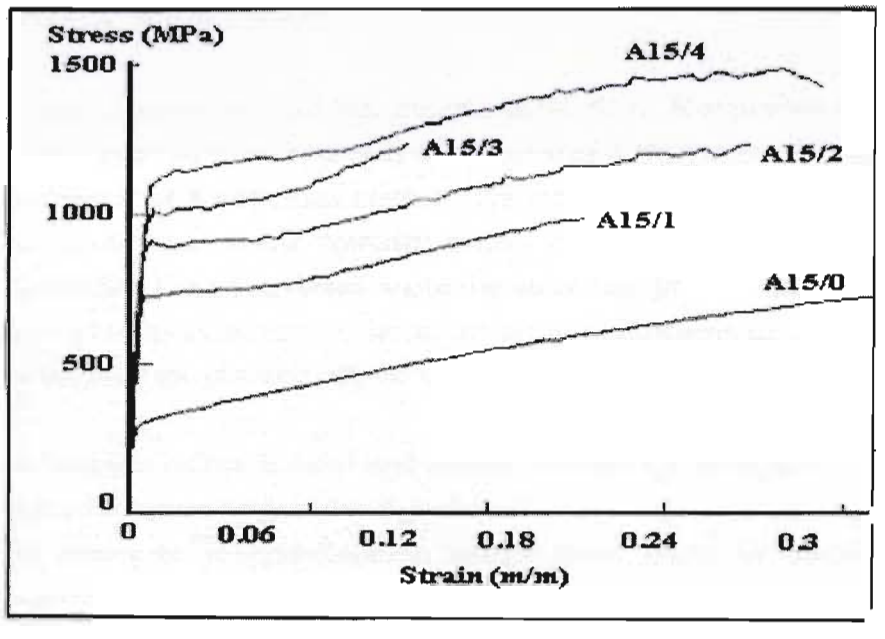

Figure 1.12 Effect of the amount of PDA on the strength of TRIP steel

The range of temperatures through which the PDA is performed, falls within the sensitizing temperature range of 450-950^{o}C. In this temperature interval carbides are precipitated if carbide-forming elements are present in the alloy chemistry. Carbides are known to raise the M_d temperature [12, 13]. During PDA the density of dislocations also increases and the dislocation substructure imparted by PDA strongly influences the

martensitic nucleation dynamics [6]. The strengthening effect of the PDA may be optimized by choosing a warm working temperature just above the M_d temperature for a given chemistry [30, 32].

1.2.5 Thermal processing only

Koppenaal proposed another method for increasing strength [51, 56-59], by cyclic quenching to liquid nitrogen temperatures (–175°C) and then reheating to room temperature. In these experiments, using the 2nd alloy in Table 1.2 below, the hardness of his samples ranged from 31.5 to 33 HRC (martensite + austenite). The samples were then immersed in salt baths (500-940°C) and air-cooled to room temperature, and produced a hardness of 27.5 HRC (which is greater than for as-quenched austenite) The microstructure produced was termed reverted austenite. Kopenaal's experiment increased the hardness of austenite from 80 HRB to 27.5 HRC. After several cycles were performed on the alloy (Fe-24.5Ni-4.1Mo-0.29C), the final hardness (after 5 cycles) was 44HRC (see Fig 1.13 and Table 1.3) and the yield and UTS were comparable to values produced in thermo-mechanically processed TRIP steel.

Table1.2 Comparison of thermal cycling and thermo-mechanical processing

Alloy	Treatment	σ_y(MPa)	UTS (MPa)
Fe - 24Ni - 4Mo - 0.3C	Thermo-mechanical reduction of 80% at 517°C	1131	1214
Fe - 24.2 Ni - 4.1Mo -.029 C	5 thermal cycles between–175°C and 722°C	1117	1331

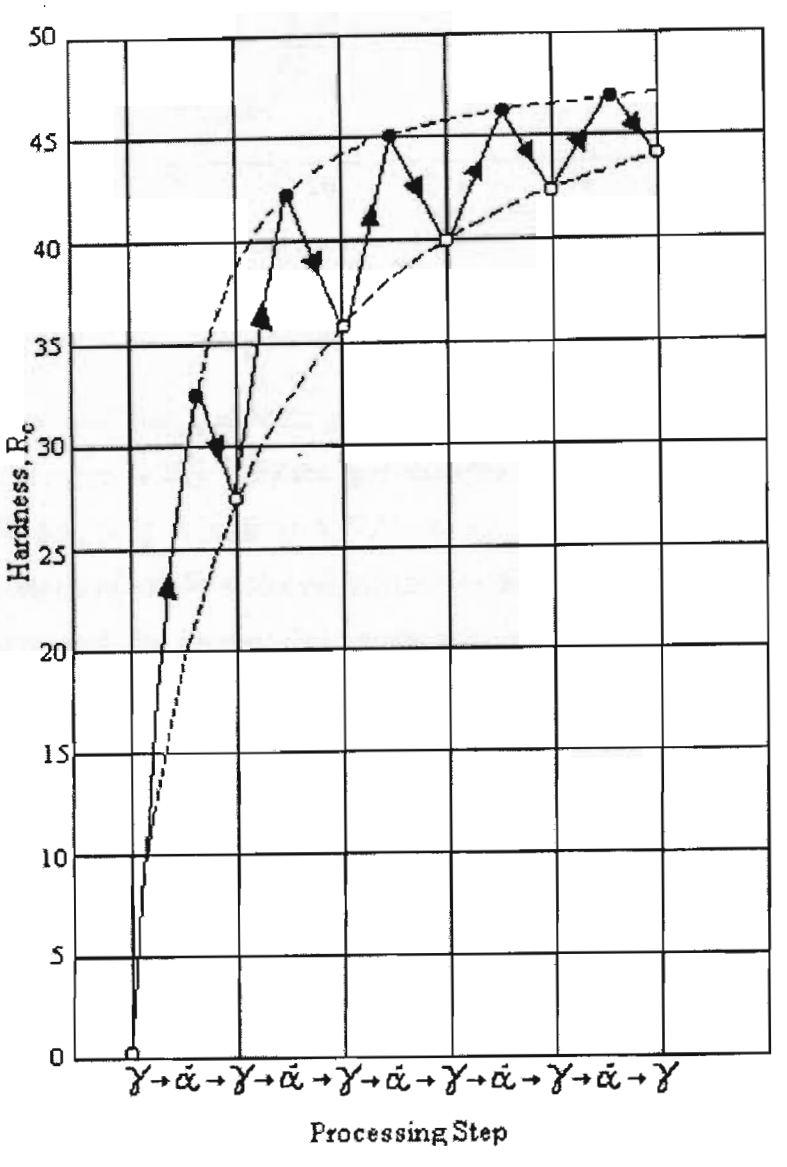

Figure 1.13 Illustration of increasing strength by cyclic quenching to liquid nitrogen temperatures and reheating back to austenite

1.3 Transformation characteristics and factors affecting them

Transformation characteristics are affected by a number of factors including individual alloying elements, dislocation substructure and stacking faults. The substitutional elements responsible for austenitic stabilization prevent a change of a crystal structure on cooling to room temperature [60], but the crystal structure is in a metastable state. Changes occur during cold working when movement of atoms occurs along the crystal planes, (slip planes), within the grains. Constraints are thereby eased and there are enough nucleation sites for a crystal structure change to take place at extremely small localized areas along the slip planes [8, 61, 62]. Tiny patches of martensite are then formed.

Martensite formed in this way is lower in carbon, tough and of varying crystal structure (BCC or hexagonal close packed HCP). It is different from the martensite formed in martensitic stainless steel. The normal austenite to martensite volume expansion takes place and these small martensite islands act as keys along the slip planes. Further movement is thus inhibited making the steel harder, stronger and resistant to further distortion by cold work. Austenitic stainless steel can be work hardened, and extremely high strength levels can be developed by this mechanism (over 2200 MPa in cold drawn wire).

When manganese (Mn) replaces nickel, this work hardening phenomenon occurs more rapidly. Austenitic stainless steel exhibits a slight degree of ferro-magnetism, which depends on the amount of cold work and chemical composition of the steel. Solution annealing can remove the work hardening condition: the steel is heated to approximately 1050 $^{\circ}$ C, and the martensitic precipitates then dissolve and are taken back into the equilibrium solution of a fully recrystallized austenitic structure.

In the past, studies evaluating the behaviour of Fe-Mn and Fe-Mn-Cr alloys were conducted in parallel with those involving the conventional austenitic stainless steels (AISI300 series materials) [63, 64]. Technically the Fe-Mn-Cr austenitic steels are not TRIP steels, but they do transform sequentially from face centered cubic to hexagonally

close-packed to body-centered cubic [65] (or B.C.Tetragonal depending on the carbon concentration of the strain-induced martensite) The transitional H.C.P. ε phase observed in Fe-Mn alloys is also observed in ternary alloys based on Fe-Mn containing either Ni, Cr, Co or C.

On a weight percentage basis, C has the greatest effect on the transformation characteristics of alloys, its effect being to lower both the M_d and M_s points of the TRIP steel [8].

In the ternary alloys studied, ε was never formed unless the percentage Mn present was such as to have allowed ε to form in a simple Fe-Mn binary alloy of the same Mn content. This suggested that Mn was the primary cause of ε formation in the ternary alloys. The effect of Cr and Co in Fe-Mn ternary alloys was to favour the formation of α_2 at the expense of ε, this despite Co itself undergoing a martensitic transformation from F.C.C. (β) to H.C.P. (α). The effect of nickel was to stabilize γ at the expense of ε. Thomson [65] used a high temperature X-ray diffraction technique; and determined that no ε phase could be detected prior to or during the course of the γ to α_2 transformation in plain Fe-8% Ni or Fe-19% Ni alloys. Using a similar technique to that cited above, no ε phase was detected in Fe-10% Cr-8 % Ni alloys or in an Fe-18 % Cr-4 % Ni alloy. This confirms Otte's conclusion [95] that there is a minimum total Ni+Cr content above which ε will form in an Fe-Ni-Cr alloy. This total is probably about 24%. It was also found that ε and α_2 appeared simultaneously at sub-zero cold working in a commercial 18% Cr-8% Ni alloy. The conclusion of this work was therefore that α_1 probably nucleated from ε and also directly form γ.

A similarity in microstructure was noted between the γ + ε (F.C.C. and H.C.P) phases observed in binary and ternary Fe-Mn alloys and Fe-Cr-Ni alloys, such as Co, Co-Ni, Cu -Si, Cu-Zn-Ge and Au-Cd, in all of which F.C.C. and H.C.P. phases were present together. The martensitic mode of formation for the H.C.P. phase is well-documented for

binary [12] as well as ternary Fe-Mn alloys, Fe-Ni-Cr alloys [64, 66] Co [67] and Co-Ni alloys [68].

It is also suggested in literature that the transitional H.C.P. ε phase observed in Fe-Mn base and Fe-Ni-Cr alloys should be considered as a phenomenon distinct from the possible occurrence of stacking faults in these alloy systems [4, 32-34, 36, 69].

1.3.1 Inhomogeneous transformation

The deformation associated with phase transformation has been reported to be inhomogeneous along the gauge length of the tensile specimens during the initial stages of plastic deformation [2, 4-5, 21, 52, 70-71]. When interrogating the ferromagnetic response of the material therefore, provision must be made to accommodate this inhomogenity. A ferromagnetic sensor, such as a Hall sensor, which measures the localized ferromagnetic response of the sensor element in the location where the *Hall sensor* is positioned, will produce a localized rather than overall measurement. Measurement of the ferromagnetic response using an induction coil arrangement will produce a reading that reflects the overall behaviour of the deforming gauge length. The reading is then an average response, which takes into account the deformation occurring within the entire gauge length of the sensor element. Another solution to this inhomogeneous nucleation is for the specimen to be designed to include a stress concentration in the area where the sensing coil is located (reduction of the section by a groove).

Strain-induced phase transformations are responsible for delaying mechanical instability and necking in unaxial tensile testing [71]; the increased uniform plastic deformation observed in these alloys corresponds to increased levels of energy absorption capacity, as seen in equation (8) below.

$$E_v = \sigma(\varepsilon)d\varepsilon \qquad (8)$$

Where $\sigma(\varepsilon)$ represents the true stress as a function of true strain

The unstable region in the TRIP steel component transforms from the weaker austenitic phase to the stronger martensitic phase resulting in the region becoming locally stronger

than the surrounding material so that deformation continues without the formation of a true neck. This process is repeated throughout the deforming gauge section.

1.3.2 Temperature Influence on Strain-Induced Martensite Transformation

Experiments have shown that more martensite forms as the deformation temperature decreases [8, 13, 23, 31, 33-35, 47, 53, 72, 73]. The temperature sensitivity of the transformation kinetics with respect to plastic strain is greatest at temperatures just above the M_S temperature. In Figs 1.14 - 1.15, one can see that the quantity of strain-induced martensite formed decreases when the temperature is increased and the error introduced by this temperature dependence increases as the amount of martensite formed increases, as seen in Fig 1.16. The optimum solution to the temperature dependence issue is to identify alloy compositions with little or no temperature dependence. After thermo-mechanical processing, Fe-Mn-Cr alloys are good in this case.

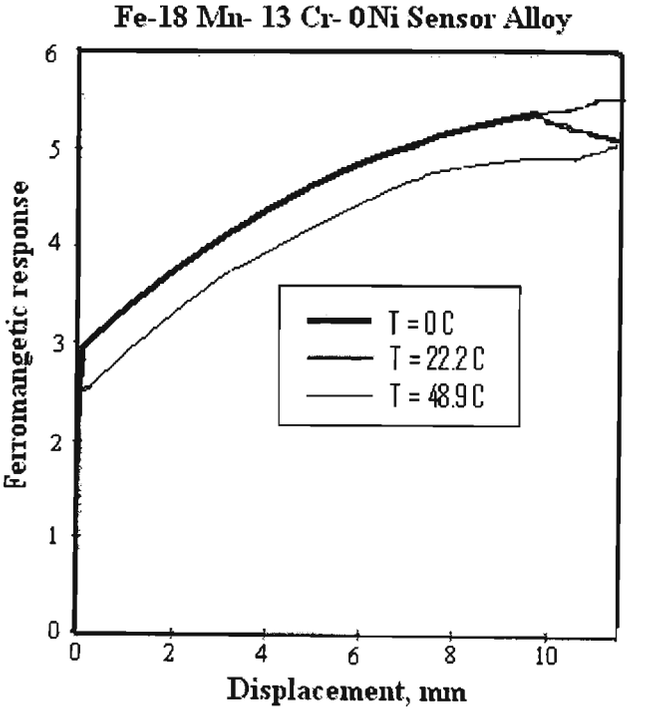

Figure 1.14 Ferromagnetic response curves of Fe- 18Mn-13Cr-0Ni sensor alloy at three temperatures

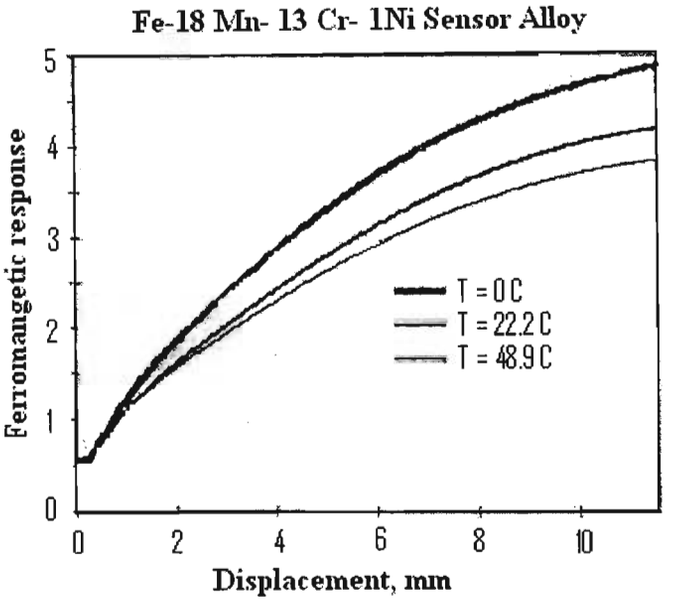

Figure 1.15 Ferromagnetic response curves of Fe-18Mn -13Cr-1Ni sensor alloy at three temperatures

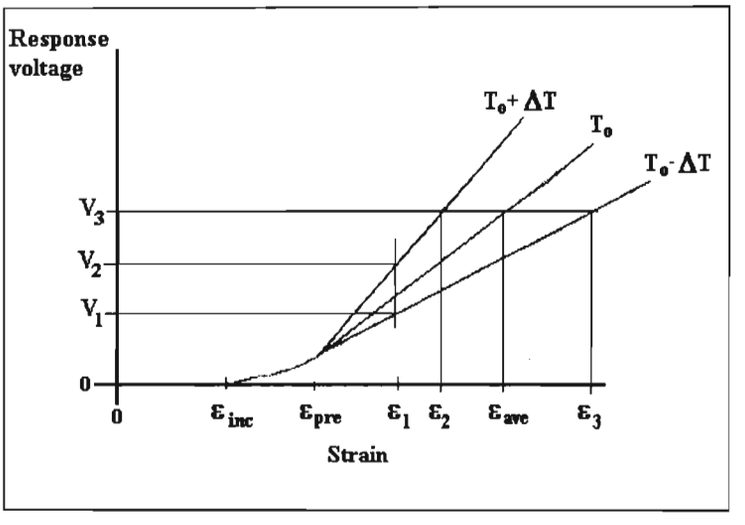

Figure 1.16 Illustration of possible error in reading on strain memory sensor due to the temperature dependence of martensite formed in normal strain memory alloy

1.3.3 Effect of tensile speed

The effect of test conditions on the mechanical properties of austenitic stainless steels has been discussed by Lincoln and Mather [74], Krivobok and Talbot in [75], Waston and Christian [76], Carlsen and Thomas [77], Form and Baldwin [73], Powell, Marshal and Backolen [78], and Breedis and Roberton [79]. But the work of Bressanelli and Moskowitz is especially relevant to this subject [80].

An increase in tensile speed results in an increase in specimen temperature (see Fig 1.17), and an increase of the temperature causes a decrease in the amount of transformed martensite (see Fig 1.18). Optimum martensite formation for the highest elongation can be obtained in slow-speed testing by optimization of composition and/or the deformation temperature. It can be obtained in high-speed tests, but only if specimen heating is prevented (see Fig 1.19). Various investigations have indicated that both the tensile strength and tensile elongation decrease rapidly with increasing test-speed [2, 14, 33, 34, 53, 71, and 73]. However, there are some differences of opinion concerning the reason for this behaviour. The decrease in strength is readily explained but not the decrease in elongation. It is implied that martensite formation during straining has a beneficial effect on elongation. This is contrary to the opinions of Cohen [18].

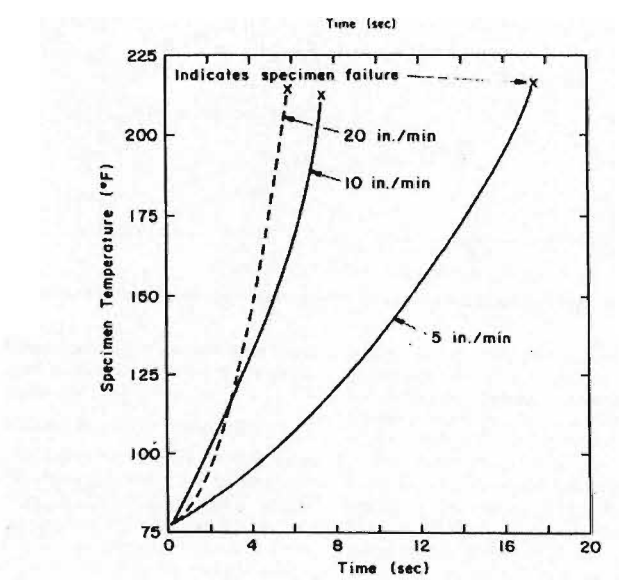

Figure 1.17 Time-Temperature profiles for specimen heating at various tensile speeds [80].

Form and Baldwin [73] concluded that the effect of test speed on specimen temperature, and hence the effect on the austenite to martensite reaction, could not account for all the observed effect. Bressanelli and Moskowitz in 1966 attempted to determine and explain the effect of the test speed on the tensile properties of metastable austenitic stainless steels, and undertook a study. In order to gain a complete understanding of the effect of tensile speed on tensile properties, particularly on tensile elongation, the effects of composition and temperature on tensile properties were studied. All steels in that study were completely austenitic prior to tensile testing and all had a fine grain size (smaller than ASTM 7). Furthermore, none of the steels formed any martensite when cooled to –100°F (-73°C), the lowest test temperature used [80].

The slower speed resulted in a greater amount of martensite formation for a given strain (elongation) than the higher speed (see Fig 1.18). With the faster speed, transformation occurred at a relatively low rate. The work-hardening coefficient w decreases with increasing test speed. The specimens tested at faster speed in water showed much higher martensite contents than specimens tested at fast speed in air (see Fig 1.19). The specimen tested above the M_D temperature (260°C) revealed that no detectable transformation to martensite occurred during tension. Tests on 310 steel at 0.5 and 20 in/min showed an absence of any martensite transformation, with no change in strengths 89 - 91.5 ksi (613-631MPa) and elongation 42 to 44%, and no magnetic response (martensite formation).

Bressanelli and Moskowitz concluded that the decrease in tensile strength and work hardening rate of metastable austenitic stainless steels with increasing test speed is primarily due to a decrease in the amount of martensite formed during testing. The decrease in martensite with the increasing speed in turn, is related to the increased temperature of the specimens during testing at high speed (see Fig 1.17). The test in a water bath shows that speed does not directly affect tensile elongation (see Fig 1.19). The effect on elongation must be related to increased temperature [80].

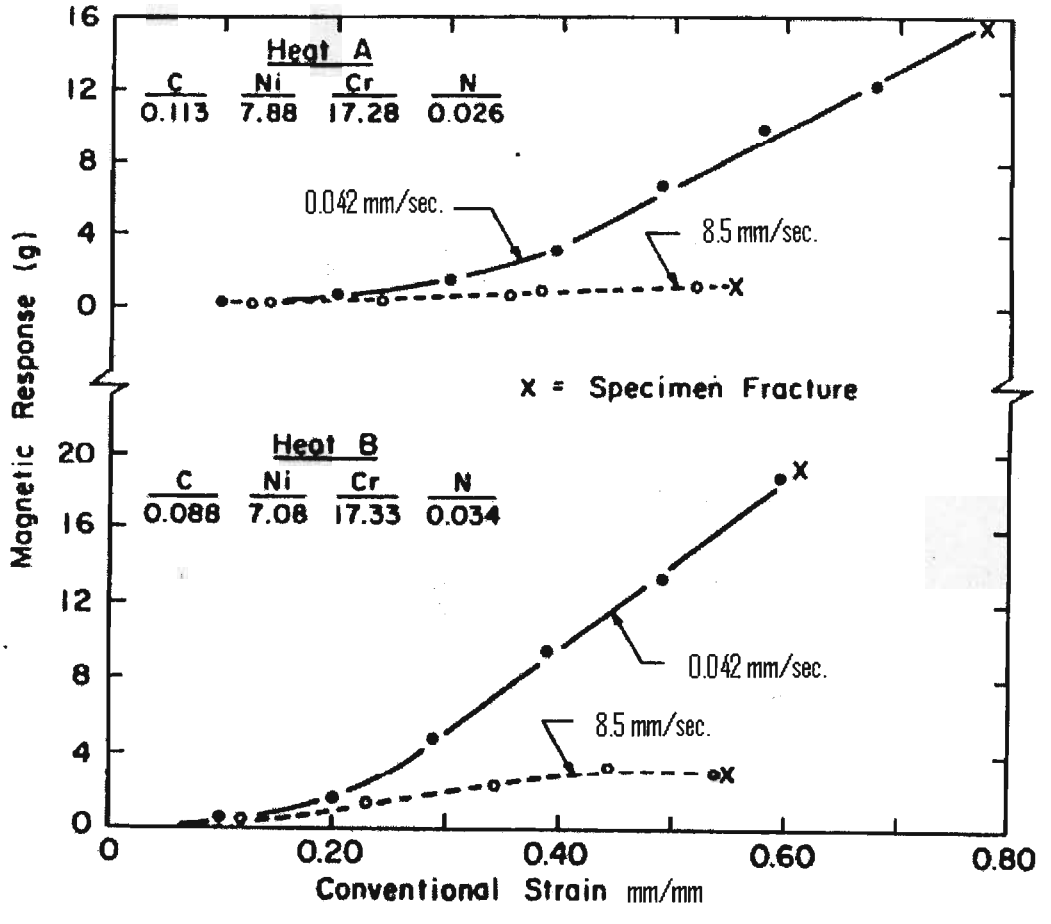

Figure 1.18 Effect of testing speed on martensite formation (magnetic response) during testing [80]

It has been determined empirically that sensor alloys which are based on carbon-free chemical formulations do not display strain rate effects that are considered to be large enough to present a problem (see Fig 1.20).

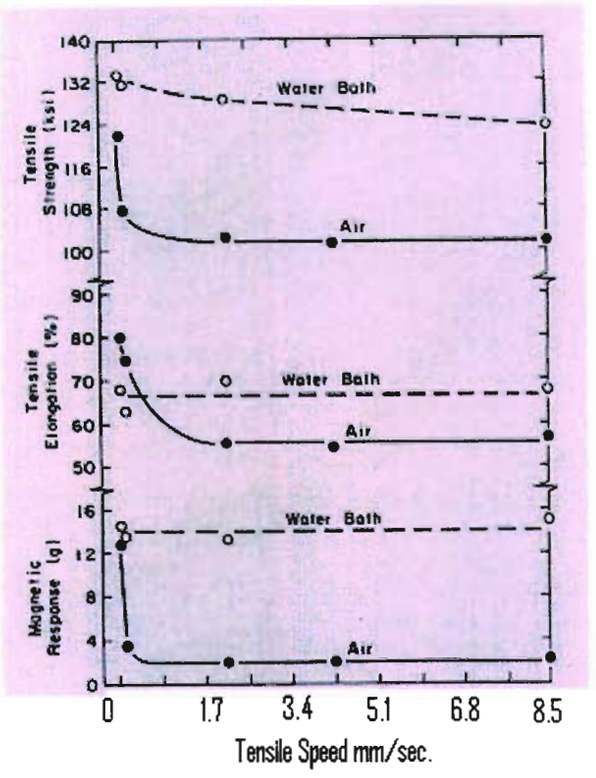

Figure 1.19. Comparison of tensile properties at varying speeds for specimens tested in air and in a water bath [80].

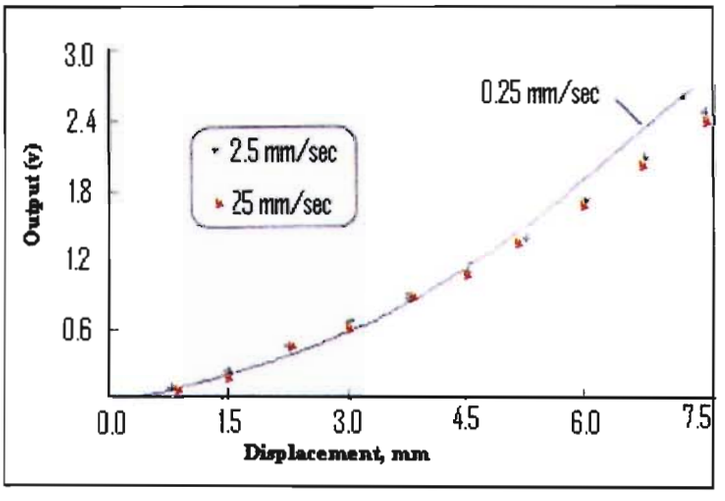

Figure 1.20 Hall unit output as a function of displacement for three different strain rates for carbon-free alloy [93, 96].

1.3.4 Effect of PDA on martensite transformation

The PDA above the M_d temperature creates a high dislocation density in the metastable alloy and thereby increases the number of nucleation sites for martensite. Carbide formation occurring during this process alters the chemical composition of alloy and some austenitic stabilizers are leached out of the austenitic matrix, thereby destabilizing it chemically [9], as can be seen in Figure 1.21.

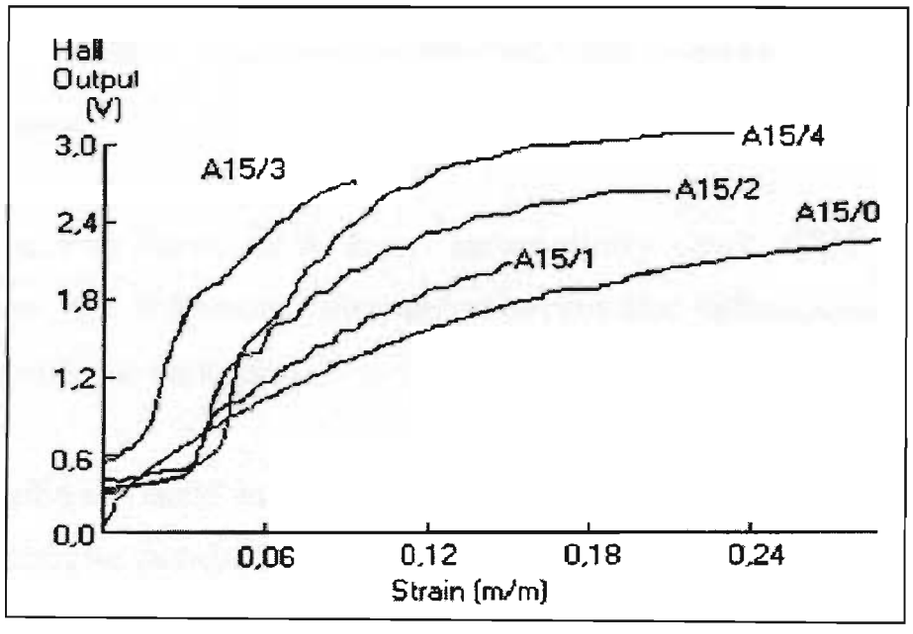

Figure 1.21 Influence of % PDA on austenitic strain induced transformation [6, 93]

The maximum strengthening and strain-induced transformation effect are obtained at temperatures close to the M_d temperature [30, 32]. The volume of martensite at a given strain varies with the temperature of the PDA as well as with the amount of PDA. Higher temperature PDA also produces a lower M_d [6].

The strain induced martensite reaction depends on five parameters [30]:

- The chemistry
- The processing history
- The environmental temperature
- Strain rate, and
- Loading condition

The martensitic product phase is also influenced by PDA. It has been found [49] that the martensite produced from worked austenite is finer than that produced in non-worked austenite. The reasons for this include:

- More nucleation sites for the martensite, which is due to the increased grain boundary area.
- Bending the austenite lattice may restrict the martensitic shear to shorter plate lengths.
- Heavily worked slip bands block the process of advancing martensitic plates [52].
- Distorted austenite grain boundaries may be more effective in limiting the size of martensite plates.

1.4 Mechanical properties of strain memory alloy

The strain induced martensite transformation affects mechanical properties of these alloys differently compared to ordinary material [30]

1.4.1 Stress strain curves

The stress-strain curve for an ordinary alloy is expressed mathematically in equation (9) as follows,

$$\sigma = K\,[\ln(1+\varepsilon)]^{n} \qquad (9)$$

Where σ is the true stress

ε is the true strain

K is austenite strength factor (constant)

n is strain hardening index (constant)

This expression does not hold true for TRIP steel. Various investigations [14, 43, 81], have found that the strain-induced decomposition of austenite to martensite is responsible for this irregularity.

Ludwigson and Berger [81] proposed an amended flow curve equation to incorporate the true stress contribution of both austenite and martensite at any level of strain in equation (10).

$$VFM = \{1+\varepsilon^{-B}/A\}^{-1} \quad (10)$$

Where VFM is the volume fraction of martensite,

ε is strain,

A is a measure of potential to transform, and

B is a measure of the autocatalytic nature of martensitic transformation

The true stress σ may then be expressed as follows in equation (11):

$$\sigma = K[\ln(1+\varepsilon)]^{N}(1-VFM)+C(VFM)^{q} \quad (11)$$

Where K is the austenite strength factor,

N is the austenite strain-hardening index,

C is the martensite strength factor, and

q is the martensitic strengthening index.

Indices n and B are constant [6], but K, C, q and A are influenced by alloy chemistry [81]. Interstitial elements such as carbon and nitrogen increase K and C, and the yield strength. Substitutional elements (Ni, Mn, Cr) seem to have no effect on K, and slightly increase C; Ni has no effect on C. A is decreased by Mn, Ni, and Cr, but decreases more substantially with carbon and nitrogen. q is reduced by carbon and nitrogen, and extended by Ni. Martensite and austenite are strengthened by both carbon and nitrogen. Strain hardening is also enhanced by carbide forming elements such as Mo, V and Cr. [81].

1.4.2 Ductility

The high ductility of strain memory alloys is attributed to the transformation induced by deformation [65, 82] (see Figure 1.22) which shows a comparison of strength and ductility for ordinary steel, hot rolled metastable alloys, and TRIP steel after PDA. Best elongations have been recorded at an optimum rate, between the M_S and M_D temperatures [30, 83- 85]

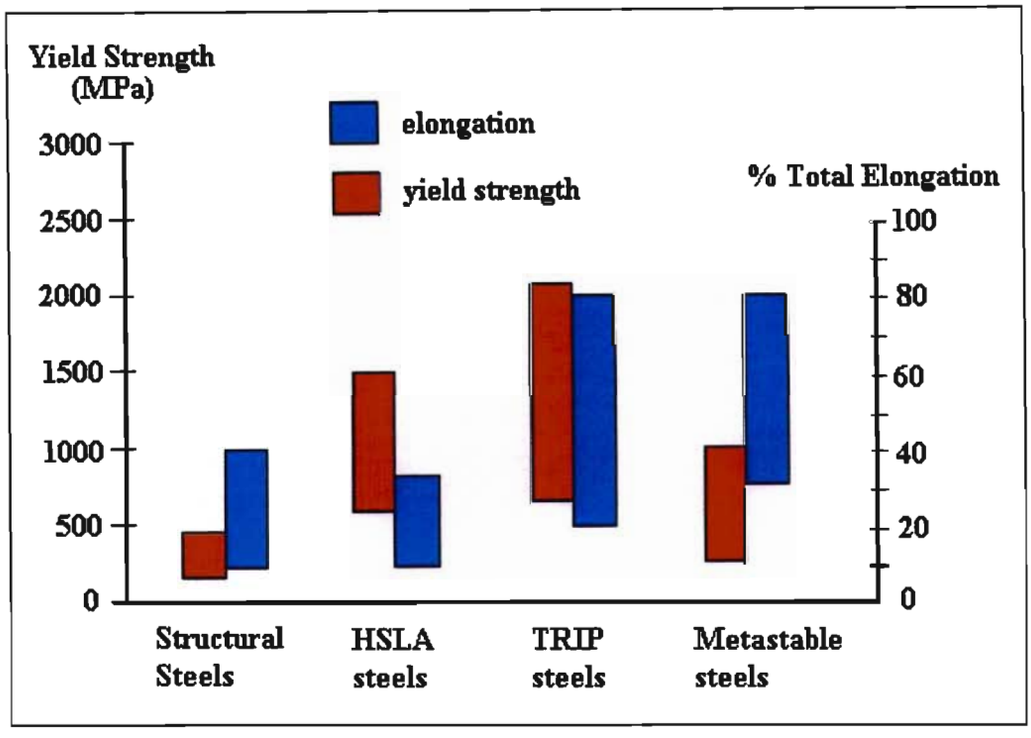

Figure 1.22 Comparison of strength and ductility for various grades of steel

1.4.3 Fatigue properties

G.R. Chanani [9] found the beneficial effect of strain induced martensite transformation with regard to fatigue crack propagation. Fig 1.23 shows a comparison between the fatigue properties of TRIP steel and those of conventionally melted 4340 steel, electro-slag remelted (ESR) 4340, high-strength alloy 300M (currently used in landing gear application) and high performance alloy HP9-4. The ultimate tensile strengths and fatigue endurance limits for 10^7 cycles are plotted for fatigue tests with a minimum to maximum load ratio, R, of 0.1. It can be seen in Fig 1.23 that TRIP steels displayed good fatigue properties, particularly the higher strength materials, where the combination of tensile

strength and fatigue endurance limits are superior to those of the other materials shown in Figure 1.23 [3, 9, 15, 65, 86, 87].

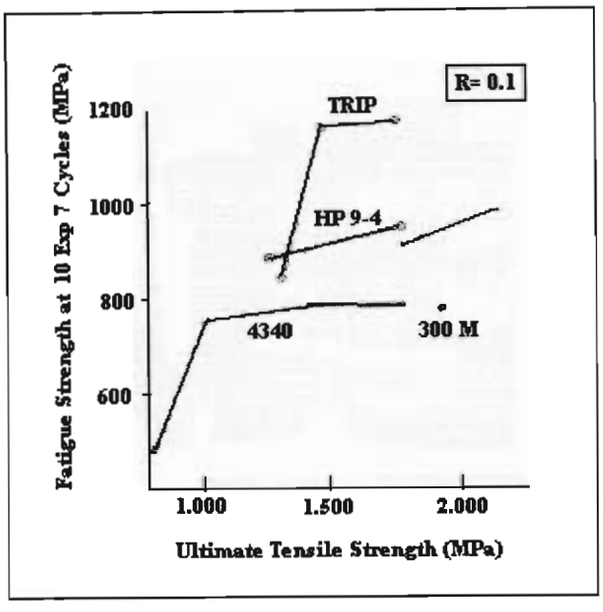

Figure 1.23 High-Cycle Fatigue Properties of TRIP Steel and High Performance Structural Steels [93]

1.5 Specific requirements and proposed alloys for investigation

In order to meet the strict requirements for the aircraft bolt application, high strength TRIP steel is required. The Fe-C-Cr-Ni family gives promising results after 80%PDA at 450°C, with a carbon concentration of 0.35% to increase the strength. At this carbon concentration, the strain induced martensite reaction may be inhibited at room temperature. The ductility will also be reduced by the PDA and the high carbon content (brittle material). The PDA is, however, favourable to increase the strain induced martensite transformation.

A TRIP steel with strengths, both yield and fatigue endurance, which surpass those of conventional high strength structural material for an aircraft bolt application needs to be used. No current commercially available material meets the requirements. As a result, the

focus of this work revolves around developing the alloy chemistry and thermo-mechanical processing for TRIP steel for the smart aircraft bolt application.

The following requirements (see Fig 1.24) for the material for the smart aircraft wing bolt must be achieved:

1. Yield strength similar to or higher than AISI 4340 (HSLA steel) currently used for the aircraft wing bolt;
2. Resistance to corrosion in a high altitude environment (moisture);
3. Low incubation strain or stress for strain induced transformation in the temperature range of $-50^{\circ}C$ to $50^{\circ}C$;
4. Costs involved in material melting and processing should be as low as possible;
5. Simple monitoring using conventional techniques should be found.

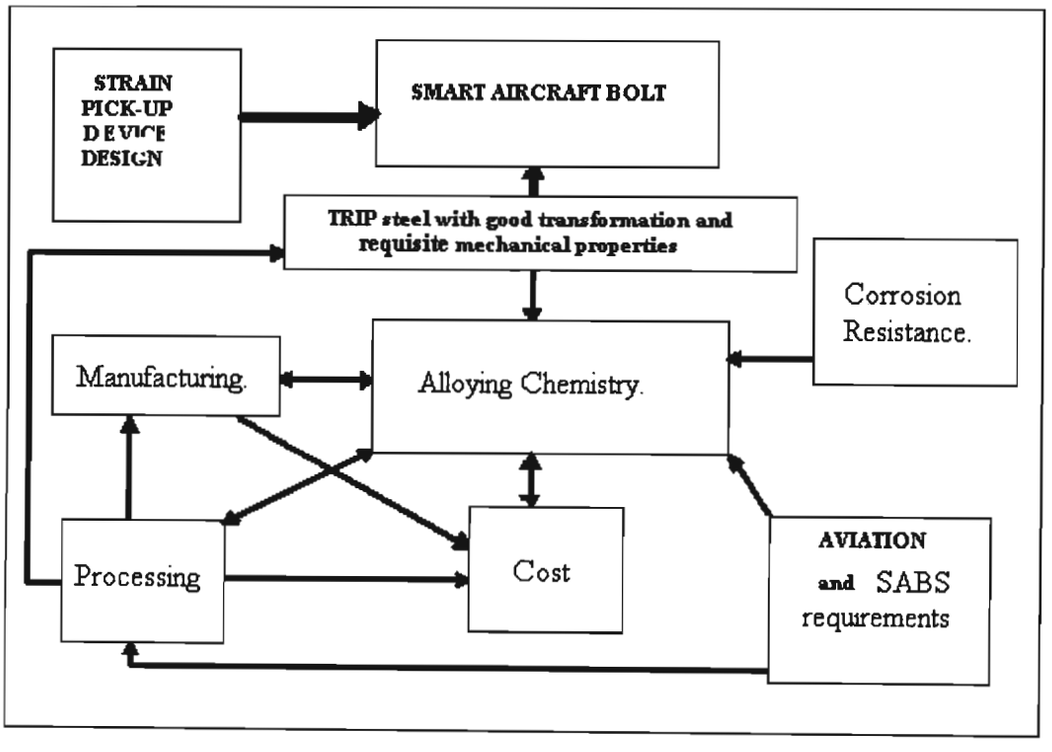

Figure 1.24 Aircraft smart bolt manufacturing is influenced by different factors

1.6 Experimental alloys selection

By using information gathered from previous research four alloy compositions (listed below) are proposed.

Alloy 1: **Fe-9.00Cr-8.00Ni-3.50Mn-0.50Si-0.35C** has a calculated chromium equivalent C.E = 10 and a nickel equivalent N.E = 20. This alloy is located in the austenitic area in the Schaeffer-De Long diagram, and from that standpoint it is expected to be austenitic after warm processing. On the strain-induced transformation side, Alloy 1 will have good strain-induced phase transformation, (see Figs 1.9 and 1.25), and the 0.35% C and 0.5% Si will assure the high strength required for aircraft bolt.

Alloy 2: **Fe-8.5Cr-8.4Ni-2.10Mn-2.0Mo-0.5Si-0.3C** is designed with a small modification from Alloy 1 with an addition of 2% Mo. Molybdenum is a good strengthener and ferrite stabilizer element. It is for this reason that the carbon content (Alloy 1) is reduced from 0.35 to 0.30% C and chromium from 9 to 8.5% Cr. Nickel content is slightly increased from 8 to 8.4% Ni as manganese is reduced from 3.5 to 2.1% Mn (both being austenite stabilizers). The calculated C.E = 11.3 and N.E = 18.4 fall in the austenite area in the De Long diagram near the border of the smart region (see Figs 1.9 and 1.25) and should therefore have acceptable strain-induced phase transformation. The element content of 0.30% C, 2% Mo and 0.5% Si should raise the strength of this alloy to the required strength for aircraft bolt manufacturing.

Alloy 3: **Fe-12.00Cr-1.50Ni-10.00Mn-0.25C** is manganese based TRIP steel. In general this class is cheaper than the nickel based class of strain memory alloys and is usually considered for low strength applications. Manganese based alloys are hard and difficult to machine, and they are not cold worked or warm rolled as Mn tends to cause cracking during the cold work operation. Alloy 3 with its manganese base is included in this study in order to verify how it will respond to the PDA and how much strength may be induced within this alloy by the warm processing. The 12% chromium content is chosen for full

corrosion resistance in normal atmosphere and 1.5% Ni is added in order to avoid the stress assisted phenomenon. The carbon content is reduced to 0.20% as Mn will also contribute to increasing the strength of the alloy. Alloy 3 has a chromium equivalent estimated to be C.E = 12, and N.E = 14. It falls in the austenite-Martensite field on the De Long diagram (see Figs 1.9 and 1.25) and it will be a metastable alloy that undergoes phase transformation when deformed.

Alloy 4: **Fe-12.00Cr-9.00Ni-1.00Mn-0.50Si-0.35C** has 12% Cr which assures the corrosion resistance in normal atmospheres. It has a calculated chromium equivalent (C.E) equal to 13 and a nickel equivalent (N.E) equal to 20. It is in the austenite field in the De Long diagram and will therefore transform well. The content of 0.35% C and 0.5% Si contribute to increasing the strength of the alloy to the aircraft bolt strength level.

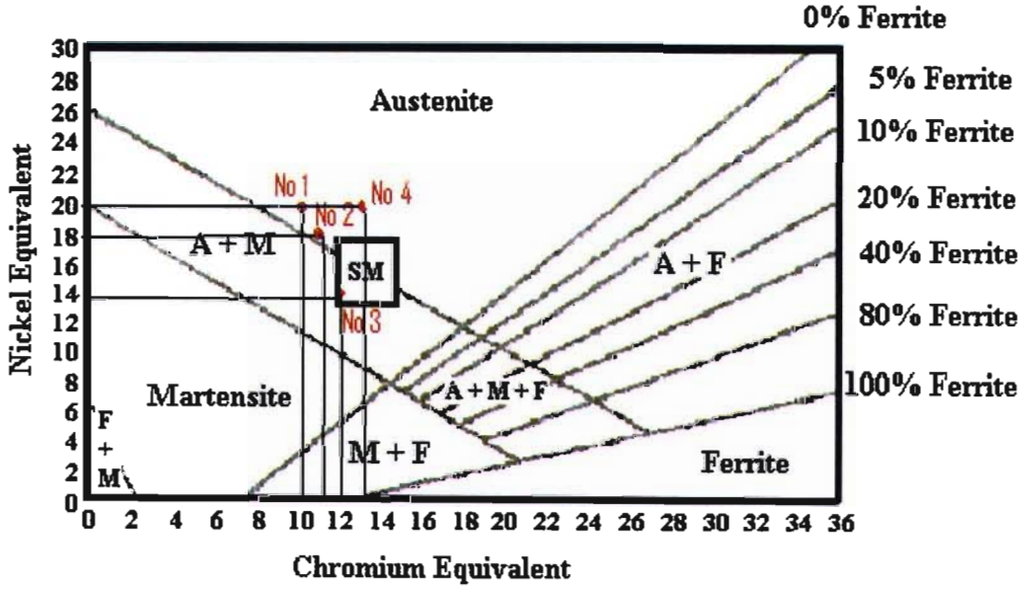

Figure 1.25 De Long diagram showing location of selected strain memory alloys

Alloy five (304 stainless steel) is added to the batch as a reference alloy (with data base in [88]) for calibration and correlation of the magnetic response to the volume of martensite fraction [88, 31]. It will be hot rolled only. The chemistry is **Fe-18.12Cr-8.60 Ni-0.055 C-0.20 Co-0.14Cu-0.14 Mo-0.14 W [29].**

As a high quality material is desired, oxygen, nitrogen, sulphur and phosphorus must be kept as low as possible. A primary hot rolling (aproximatly 50% reduction) or forging to break down casting anomalies is followed by a warm work at 450°C taking the form of rolling or forging. In order to achieve the high strength requirement, an amount of warm work equal to 80% reduction or more, is necessary. Due to the high forces required to roll the cross section for a full bolt prototype, a scaled down version will be produced to prove concept, and avoid the expense incurred by a full-size cross-section.

CHAPTER 2

EXPERIMENTAL PROCEDURES

Strain memory alloys (as a group) do encompass some commercially available stainless steels; however, the compositions that will produce the ultra high strength (i.e.: those with substantial carbon and nickel required for the smart aircraft bolt) are not commercially available. Small batches of experimental compositions had, therefore to be melted and processed in research laboratories. Because the facilities available for performing the PDA or warm rolling were limited in size in the research laboratories in South Africa, the size of the bolts that could be manufactured was also limited. This chapter deals with the specifics of the methodology used to produce the experimental materials and the means by which they were tested. The results of rigorous testing are shown in Chapter 3.

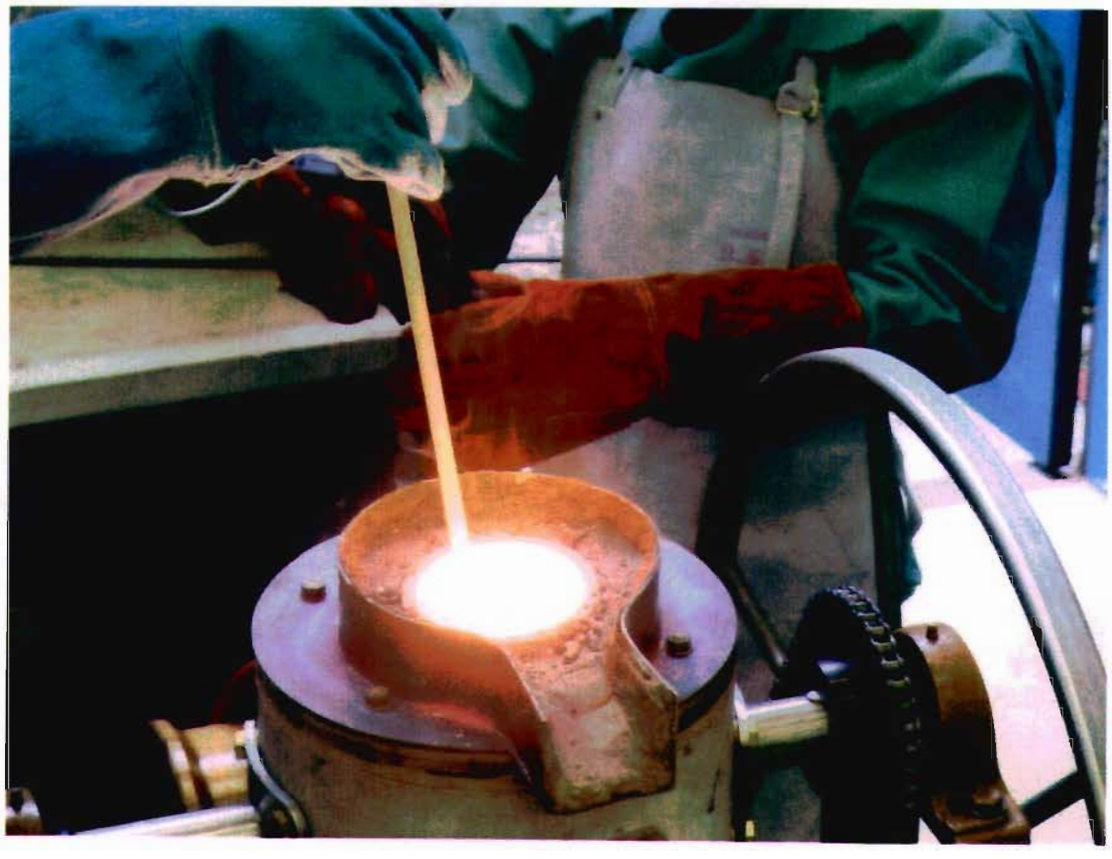

Figure 2.1 A 5 kg induction furnace

Three melting of the target chemistries were done altogether; the first melting was done merely to assess the amount of PDA that could successfully be put into the material, and the consequent strength achieved; and for this only Alloy 1 was melted. Tensile test results for the first melting are presented later in this chapter. The second melting was used to perform not only strength tests, but also to test the transformation characteristics of the alloys. This melting also showed up a slight processing problem in that some decarburization had occurred on the material surface during heat treatment. A third melting was therefore commissioned with closer control on material processing. The following notation will be adopted to identify alloys. The first number is the alloy number and the melt (whether 1st, 2nd, 3rd) will be denoted /1, /2, /3. ie melt 3 of alloy 1 is denoted alloy 1/3

2.1 Melting

Some of the alloys within this study were melted at University of KwaZulu-Natal (UKZN) using a 5kg open induction furnace Fig 2.1, but at the time these alloys could not be processed at the University. These samples were used as microstructure testers, while determining the correct etching procedure for TRIP steel. Almost all the materials for this study were melted and processed at Mintek[1]. All alloys were melted using the same procedure for melting and processing. They were melted in a vacuum induction furnace using a pure source of raw materials, as the refinement of liquid metal under laboratory conditions is not easy. The target chemistries for this study (which were formulated after extensive literature survey) are tabulated in table 2.1 below, for easy reference.

Table 2.1 Targeted chemistries for study

Element	C	Si	Mn	P	S	Mo	Cr	Ni	O	N	Fe
Alloy 1	0.35	0.50	3.5	-	-	-	9.00	8.00	-	-	Balance
Alloy 2	0.30	0.50	2.10	-	-	2.0	8.50	8.40	-	-	Balance
Alloy 3	0.25	-	10.0	-	-	-	12.0	1.50	-	-	Balance
Alloy4	0.35	0.50	1.00	-	-	-	12.0	9.00	-	-	Balance

[1] Mintek is a parastatal research organization with both extractive and physical metallurgy research programs.

2.2 Alloys processing

For all the chemistries, a 5 kg, 68 mm thick ingot was cast. After solidification, each ingot was soaked at 1200°C for 1 hour. They were then hot flat forged to a 37mm thick slab. After hot forging, the 37 mm thick ingot was soaked at 550°C for 1 hour. A series of rolling passes inducing approximately 4% reduction, and reheating for 5 min in between passes, were then performed. A plate of average thickness 10 mm was produced. The level of reduction achieved varied from one chemistry to the next, between 75% and 80%. The limit on the reduction was considered to be the onset of cracking in the plate. Plates of 600 mm x 65 mm size, with 13 mm thickness, were manufactured after 75% warm rolling reduction at 550^0C. After processing, the plates were wavy and some plates presented small cracks (see Figure 2.2 and Table 2.2 below).

Table 2.2 Physical characteristics of as-received plates, 75% warm rolled (second experimental melting).

ID	% warm reduction	Magnetic susceptibility (H/m)	Cracks	Deformation (Waves)
Alloy 1/1	80		Start cracking	-
Alloy 1/2	75	0.54	Negligible	Non straight
Alloy 2/2	75	0.24	Negligible	Non straight
Alloy 3/2	75	0.018-0.045	Present	Non straight
Alloy 4/2	75	0	Negligible	Non straight
304	-	0	None	Straight
Mild steel	-	0.34, 0.51, 1.6	For comparison	

Figure 2.2 Warm rolled plates to 80% reductions showing cracks Alloy 1/1

Alloys 1/3, 2/3, 3/3 and 4/3 were melted, cast in ingot, and heat-treated under a more controlled protective atmosphere in order to avoid decarburization during warm processing.

2.3 Flattening Press and Laser Cutting

As mentioned above in Table 2.2, and confirmed below in Figures 2.3-2.4, warm rolled plates were received in a wavy state (not straight).

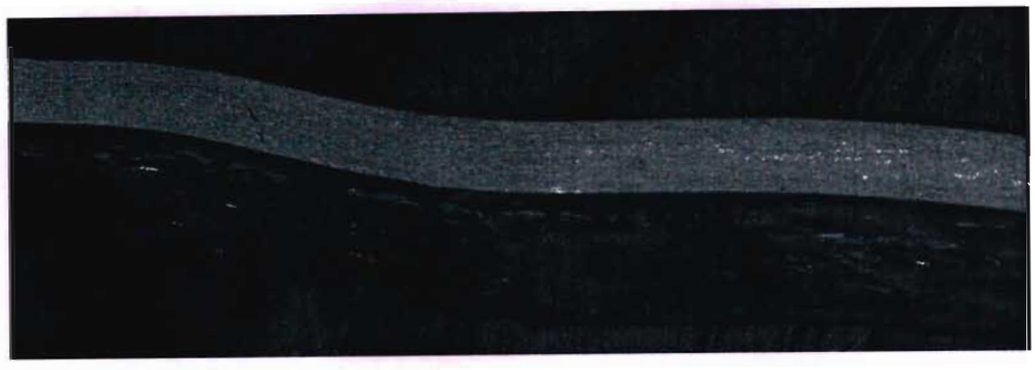

Figure 2.3 Wavy plates by rolling milling operation (2nd melting)

Figure 2.4 Top views (above) and side views (below) of wavy plates (3rd melting), which need to be straightened

As straight strips (see Fig 2.5) for tensile sample fabrication are needed, a flattening process had to be performed on these plates. They were then cut into strips for sample machining.

A cold pressing (deformation) would induce martensitic phase transformation, which cannot be allowed as this reaction must take place when the sensor is strained **during service**. Hot pressing also cannot be used, as the work hardening from warm work induced in that material would be lost if heated above the recrystallisation temperature. The plates were therefore warm pressed at 550°C (same as warm rolling temperature), using a press with a force of 1.7 MN in the UKZN workshop. The plates were then laser cut into strips for tensile sample machining, as mechanical cutting is difficult because this material is hard. During both operations, measurement of the magnetic permeability of the plate material was done at every step, to be sure that the material did not transform to martensite. Confirmation of non-transformation is given in table 2.3, which shows an essentially unchanged magnetic susceptibility, for each batch as it passed through the various operations.

It is however interesting to note that the third melting of each alloy, as well as 4/2, showed much lower magnetic susceptibility than most of the second melts. This implies that the closer control on the carbon content produced better levels of austenitic stability with no martensite originally present at room temperature

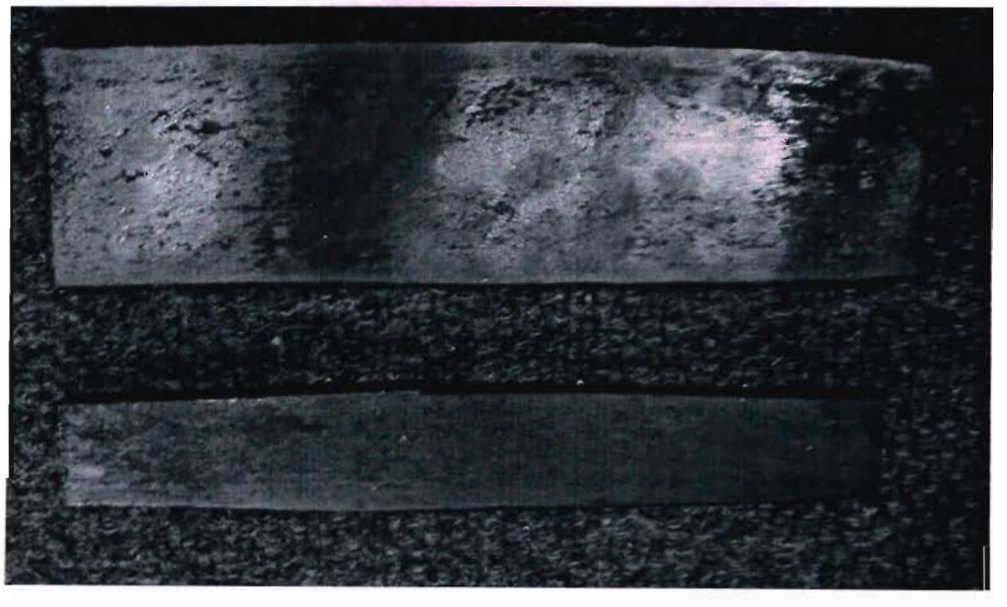

Figure 2.5 Plates flattened by pressing at 550°C (warm) Alloy 4 /2

Table 2.3 Verification of possible strain-induced transformation during flattening pressing proccess

ID	Before pressing μ (H/m)	After pressing at 550°C μ (H/m)	After laser cut μ (H/m)
1/2	0.56 – 0.65	0.50 – 0.64	0.27
1/3	0.04 – 0.07	0.065 – 0.075	-
2/2	0.33 – 0.35	0.24 – 0.47	0.15
2/3	0.077 – 0.085	0.095 – 0.099	-
3/2	0.09 – 0.14	0.08 – 0.09	0.09
3/3	0.030 – 0.039	0.031 – 0.034	-
4/2	0.00– 0.052	0.00- 0.052	0.053
4/3	0.036 – 0.046	0.039 – 0.041	-

2.4 Chemical analysis

It is very important to know the correct chemistries for all processed materials, as the kinetics of the strain induced martensite transformation reaction is dependent on the alloy chemistry, thermo-mechanical history (processing), environment and deformation parameters (test condition).

A chemical analysis was done by Spectro-chemical method of analysis after processing and test results are tabulated below in table 2.4. Oxygen and Nitrogen analysis were done by wet chemical analysis. the first melting of alloy 1 reveals that 0.28% C content is achieved, while the expected carbon content is 0.35%.

For the second and third melting Spectro-chemical analyses were simultaneously done at Mintek and at Umgeni Iron Work Foundry Ltd. Divergences in chemical test results done at Mintek on cast ingot and at Umgeni Iron Foundry on warm processed plates at the outside plate surface were significant. Even the results for chemical analysis tested inside the plate were different from expected values of carbon concentration. It was therefore decided to send the material to an independent laboratory, with equipment that is regularly calibrated. The chemical analyses shown in Table 2.4 were

all done by the independent laboratory, and the difference between melts (especially with regard to the carbon content) is clearly visible. The carbon contents of all the chemistries were less than the target, for the second melting.

The carbon content of Alloy 3/2 is particularly bad; a difference is also noted between the plate surface and the plate core. This means that decarburization occurred during heat treatment of the cast ingot and during thermo-mechanical processing (warm rolling at 550°C). This may result from a chemical reaction occurring during heat treatment. When steel is heated in an open furnace, in the presence of air and products of combustion, two surface phenomena may be involved: oxidation, and decarburization [31]. For the 3rd melting, heat-treatment was done in a more controlled protective environment. From Table 2.4 it can be seen that there are still differences in chemical composition between as-received and expected material, especially with carbon content, but the chemistries are much closer when the protective atmosphere is used during heat treatment. However there is obviously still a loss or burn-off of certain elements during the original melting which is difficult to predict with any consistency.

Table 2.4 Discrepancies in chemical composition between as-received and expected materials, the % Fe is the balance

ID	%C	%Ni	%Mn	%Cr	%Si	%S	%P	%Mo	C E	N E
Expected 1	0.35	8.0	3.5	9.0	0.5	-	-	-	**10**	**20**
1/1	0.28	9.21	3.69	10.11	0.71	.004	0.01	-	11.7	19.5
1/2	0.16	8.31	4.00	8.14	0.53	.007	.005	0.03	9.00	17.8
1/3	0.30	6.30	3.86	9.09	0.61	.015	.011	-	10.0	17.2
Expected 2	0.30	8.40	2.10	8.50	0.50	-	-	2.00	**11.3**	**18.4**
2/2	0.21	8.91	2.57	8.00	0.60	.006	.005	1.91	10.8	17.8
2/3	0.33	8.49	2.63	8.75	0.44	.016	.013	1.70	11.1	20.4
Expected 3	0.25	1.50	10.0	12.0	-	-	-	-	**12**	**14**
3/2	0.19	1.33	10.5	11.6	0.08	.010	.005	0.03	11.7	12.3
3/3	0.20	1.86	10.14	9.66	.068	.014	.011	0.13	9.8	12.9
Expected 4	0.35	9.00	1.00	12.00	0.50	-	-	-	**13**	**20**
4/2	0.29	9.48	1.13	11.6	0.56	.007	.005	0.01	11.9	18.8
4/3	0.35	8.89	1.64	11.95	0.58	.012	.011	.002	12.8	20.2

2.4.1 Conclusion

Carbon is an important element of this study, as it is both an austenitic stabiliser and a strengthening element for steel (interstitial and carbide forming). And this may negatively affect the transformation and mechanical properties of these alloys. The nickel and manganese contents are however similar to those expected.

2.5 Hardness Tests

After chemical testing, it was necessary to verify if melted alloys were qualified for high strength strain memory application by using simple tests that did not require expensive sample preparation and testing operations. Hardness tests provided this simple quick assessment. The Rockwell C test was used, and the results are shown in Table 2.5 below, from which one can see that 75% warm rolled TRIP steel is harder than hot-rolled 304 metastable stainless steel. This confirms the strengthening effect of the warm work put into those plates. The tensile stresses shown in the Table 2.5 are from the approximate hardness conversion table for steel [41].

Table 2.5 Hardness test for as-received experimental TRIP steel alloys for aircraft smart bolt

ID	HRC on the surface	HRC in core	Tensile stress (approximated in core, MPa)
1/2	37.2, 36.9	35.5	1172.0
2/2	40.9, 38.5	41.9, 40.5	1344.5
3/2	31.9, 33.7, 33.6	36.8, 38.0	1172.0
4/2	43.1, 35	41.9	1344.5
1/3	42	-	-
2/3	51.9	-	-
3/3	39.7	-	-
4/3	43.9	-	-

2.5.1 Conclusion

The estimated tensile stress from the tested hardness is not an exact value, but it gives an idea of the strength of the materials. Alloys 2/2 and 4/2 are promising from a strength standpoint, while Alloys 1/2 and 3/2 are less impressive.

2.6 Tensile Tests

Before the four identified alloys presented in Table 2.1 were melted for the purpose of complete testing, a preliminary melting was done in order to check the feasibility of warm working, and the level of strength that could successfully be imparted to the material using this method. To this end, Alloy 1 was chosen for experimental manufacturing. It was melted and tensile tested at Mintek as cited above, results of which follow in table 2.6.

Table 2.6 Mechanical properties of warm rolled Alloy 1/1

Specimen ID	% PDA	Proof stress MPa	UTS MPa	% Elongation
Plate A1	75	1334	1436	Broken outside gauge length
Plate A2*	75	1396	1396	24.5
Plate B1*	80	1321	1395	12.7

The specimens marked A2* and B1* were electro-polished in 20% perchloric acid solution to reduce the effect of machining marks. The material condition was warm rolled as indicated in Table 2.2. The specimens were tested in air at room temperature.

One of the characteristics of TRIP steel under tensile test is that the transformation from austenite (weaker) to martensite (stronger), which occurs when the gauge length is strained, causes a suspension of the necking process. By making a localized area stronger, the martensite effectively shifts the deformation to the weaker austenite region, which also transforms, and then shifts the deformation further. In this way, the whole gauge length transforms to martensite before a final brittle fracture occurs with little or no evidence of the necking phenomenon (see Figs 2.6 - 2.7). The fact that sample A1 broke out of the gauge section (see Fig 2.6) is evidence of martensite transformation during the tensile test, which is a requirement for a smart strain sensor.

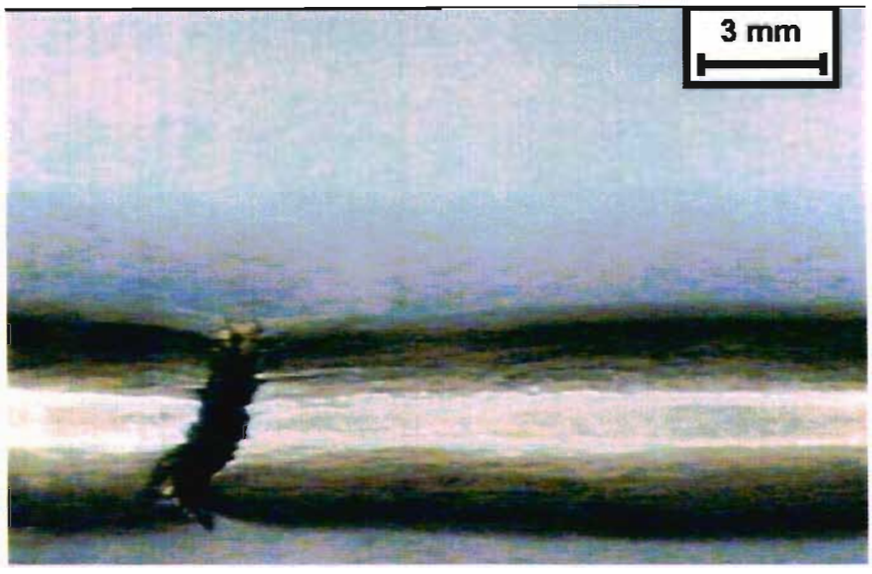

Figure 2.6 Broken out of gauge length 75% warm rolled sample A1 as reported on the test certificate

No localized necking occurred on sample marked B1*(see Fig 2.7) which indicates that transformation occurred during tensile testing.

Figure 2.7 Broken 80%Reduction warm rolled material samples B1*, showing brittle fracture, no necking is observed.

Sample A2* shows localized necking, which is an indication that strain induced martensite transformation did not occur sufficiently during tensile test (see Figure 2.8) to prevent necking.

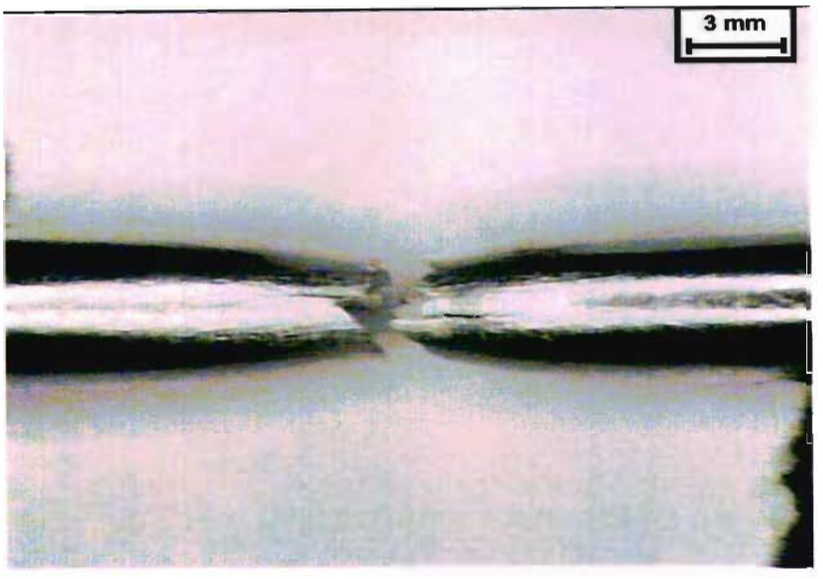

Figure 2.8 Broken warm rolled at 75% reduction and electro-polished sample A2*, showing ductile failure with localized necking

This first experiment showed promising results, especially in terms of the strength required for the smart aircraft bolt. Although the magnetic permeability of this material was not monitored during test, the suppression of the necking phenomenon in sample B1 (see Fig 2.7) is characteristic of TRIP steel.. This first experiment therefore shows that the processing is correct, and can be adopted in future experiments. It is also interesting to note that the greater amount of PDA (see Table 2.6) produced better transformation, although slightly less strength and significantly less ductility. But it is not clear why samples A1* and A2* behaved differently.

For the 2nd and 3rd experimental melts, tensile samples (see Figure 2.9-2.10) were machined (from laser cut strips) at DIT[2] Mechanical Engineering Department (2nd melting) and by an external company (3rd melting). Afterwards, they were sent back to UKZN for mechanical testing. Mechanical properties and strain induced phase transformation were determined by tensile testing, which was performed on an INSTRON tensile machine. Strain induced phase transformation was monitored by a magnetic susceptibility meter (see Fig 2.11), which was connected to a PC for data

[2] DIT is the Durban Institute of Technology.

capture (the reading on the meter varies with the distance between the meter and the sample). Although the same test set-up was used in the tensile test for the second and third meltings, the sample geometries differ as shown in figures 2.9 and 2.10. The difference in test specimen geometries is a consequence of attempts to move the magnetic susceptibility meter as close to the site of transformation as possible. Because an extensometer must be attached to the gauge area and not out of it as it was for the test of the second melted materials (elongation values on the stress strain graphs were not reliable), the length of the gauge section was enlarged from 25mm to 54mm (see Fig 2.10).

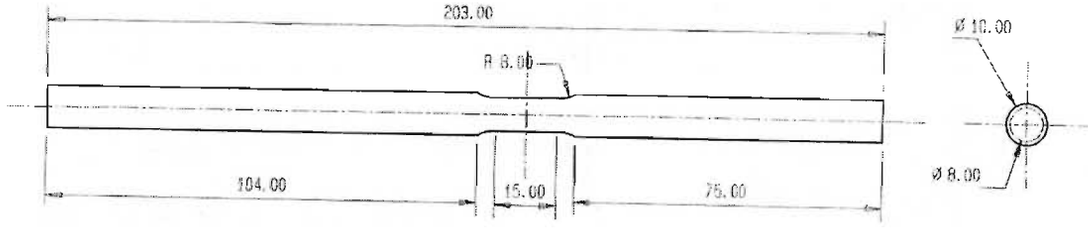

Figure 2.9 An offset tensile sample as phase transformation would occurs on small and precise zone

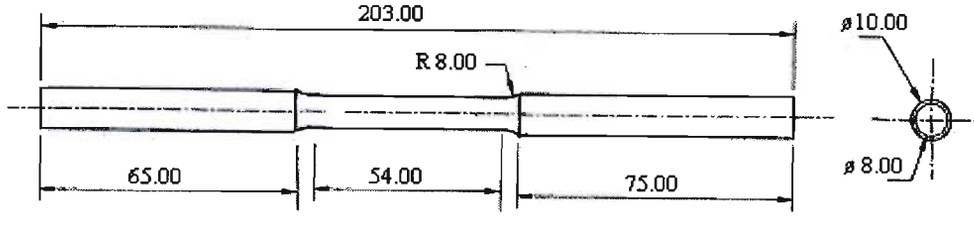

Figure 2.10 Offset modified 54mm gauge length tensile sample, as available extensometer will fit on the gauge section

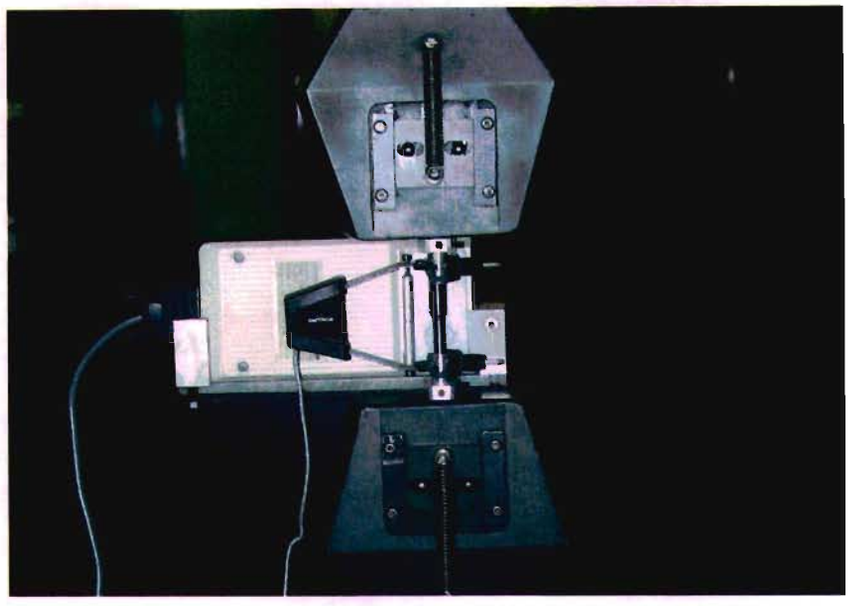

Figure 2.11 Back view of the test rig. An extensometer is used to record the strain.

The use of the extensometer and the magnetic susceptibility meter simultaneously during tensile testing on the Instron generated some problems; the extensometer fixing head was touching the meter. A device for attaching the extensometer to the sample was therefore constructed (see Figure 2.12). Tensile tests result are shown in Chapter 3.

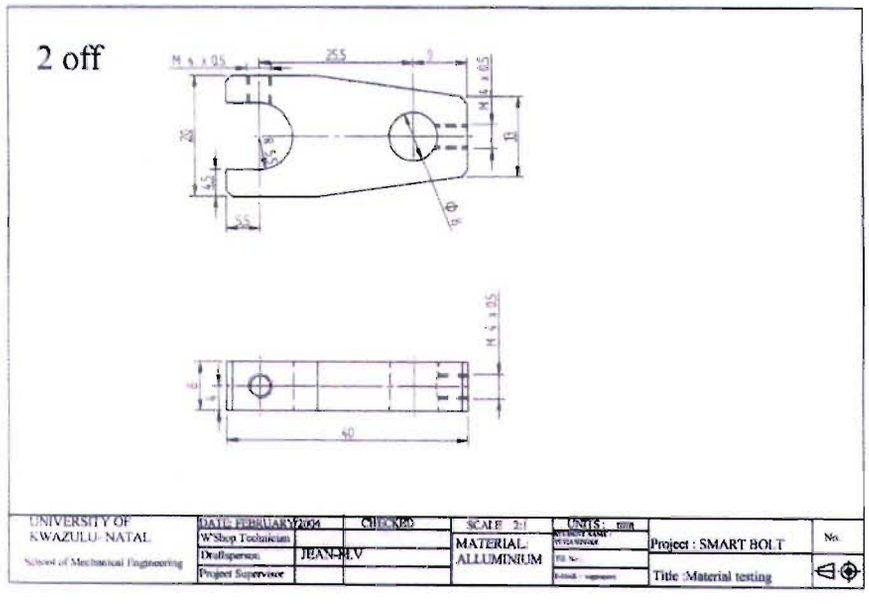

Figure 2.12 Accessory for attaching the extensometer to the tensile sample

2.7 Magnetic Sensors

Conventional magnetic measurement methods were reviewed in order to assess which would suit the aircraft smart wing bolt application. Different methods would be used during material testing of the kinetics of strain induced martensite phase transformation to check if they were compatible with testing equipment. Among the methods investigated were:

1. The ferrite scope is limited to a small depth of penetration.
2. A permanent magnet would give a qualitative appreciation rather than quantitative (more or less).
3. Magnetic balance requires the test to be stopped for measurement.
4. The Hall sensor reported to measure a localized area value rather than overall measurement and is directionally sensitive.
5. An electromagnetic inductance method offers sensitive results and the location of the coil is flexible as it may be placed near the highly stressed area of the structural element concerned.
6. An induction coil inserted in the washer used for the smart bolt prototype design in Chapter 4.

2.8 Magnetic Susceptibility Meter

A magnetic susceptibility meter (GMS-2) fixed in a permanent position in relation to the sample was used during tensile testing. The GMS-2 Magnetic Susceptibility Meter in Fig 2.13 is designed to measure the magnetic susceptibility of rock outcrops, rock samples and drilled cores. The functioning of the GMS-2 is based on electromagnetic induction. There are two coils placed orthogonally to each other in the detector head, which is mounted into the top of the unit's case. In the non-magnetic environment the voltage induced from the transmitter coil to the receiver coil is zero. When a rock is brought near the coils, a voltage which is proportional to the magnetic susceptibility of the sample is induced in the receiver coil. A phase-locked amplifier detects this signal and after rectification it is used to drive the circuitry for the display of the magnetic susceptibility readings. The reading is directly calibrated for susceptibility.

The capacity of the experimental alloys to monitor their own strain (damage detection), is estimated by measuring the magnetic susceptibility of the sample as the strain increases during tensile testing with a magnetic susceptibility GMS-2. The

GMS-2 has an optical accessory, an RS-232 port for downloading data to a PC computer either for memory or in real-time, via a serial interface adaptor (S.I.A.) and RS-232 data is supplied to a host computer.

Unfortunately, the meter was originally designed for geologic application (direct contact with the rock to be studied) and it was difficult to use it for measuring the magnetic permeability change during tensile test. It has been found that the reading on the meter decreases exponentially as the distance between the meter and the sample increases (see Fig 2.14). The orientations of the meter to the sample also affect the reading. In order to overcome this situation a rigid testing rig was designed and constructed (see Fig 2.15). The use of this rig allowed consistent and reliable readings, as the rig kept the meter at a permanent distance from the sample during all tests.

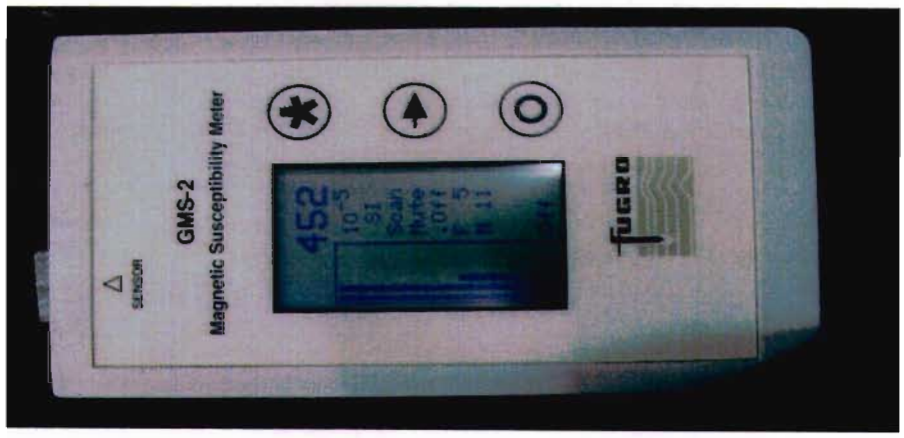

Figure 2.13Magnetic Susceptibility meters for monitoring TRIP steel element damage during tensile test

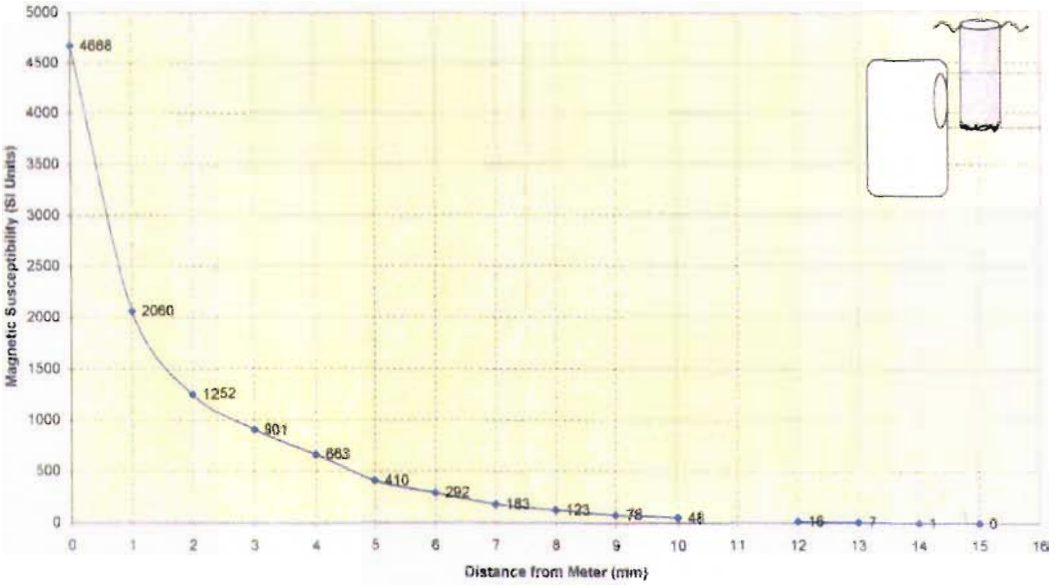

Fig 2.14 Graph of magnetic susceptibility versus distance between specimen and meter

Figure 2.15 Rigid test - rig which allows keeping the meter at a permanent position during all tests

Figure 2.16 Magnetic susceptibility meter mounted on the test-rig for monitoring magnetic changes during test

2.9 Compression Test

Pieces cut from all the different fully processed alloys were compressed on an Avery compression-tensile machine with different loads as functions of their cross-section size, to induce a stress of ± 2000MPa to make the material plastically yield. For the compression tests done on the second melting, the magnetic permeability of the samples was simply measured before and after compression testing by using a magnetic susceptibility meter, to check if martensite transformation had occurred during the compression test (see Table 2.7). For alloys 2/2 and 4/2 compression tests with carefully monitored strain-induced phase transformation were performed (see Fig 2.17). An inductance meter attached to a coil wrapped around a 116.33mm specimen was used during this testing. The applied force in kN and corresponding inductance reading were recorded (see Figs 3.16 and 3.38 Chapter 3)

Figure 2.17 Measurement of inductance of compression Specimen

Table 2.7 Strain-induced martensite transformation measured before and after compression test

ID	Magn. suscep. as-received μ (H/m)	Magn. suscep. before test μ (H/m)	Magn. suscep. after test. μ (H/m)	Comp. forces kN
1/2	0.54	0.072 0.055 0.035	0.178 0.13 0.158	160
2/2	0.24	0.049 0.011 0.055 0.052	0.083 0.029 0.087 0.11	160
3/2	0.018 0.045	0.0064 0.014 0.016	0.019 0.016 0.012 0.024	238
4/2	0	0.0085 0.0068 0.0028	0.010 0.011 0.0056	160 no yield
5/2 (304)	0	0.0013 0.0028	0.017 0.051	100
		0.0017 0.0035 0.0031	0.032 0.016 0.024	200

Note: Magnetic susceptibility measurements (in Table 2.7) were done at different locations and in different orientations (directions).

2.9.1 Conclusion

Compression tests show that all alloys which are investigated in this study exhibited strain-induced phase transformation (Table 2.7 and Figs 3.16, 3.38), giving further confirmation that all can be used as strain memory alloys. The testing also confirms that the transformation is induced either by tensile or compressive modes.

2.10 Impact test

For the smart aircraft bolt, it was important to evaluate the ability of TRIP steel to withstand impact load without fracturing during service. V-notch impact test samples were machined from alloys 2/2 and 4/2 at DIT Mech. Eng. Workshop (see Fig 2.18), in accordance with Table 3 in SABS 056-1973.

As the materials were too hard (42HRC) to be v-notched by the machine available at UKZN, the samples were sent to MET-LAB for v-notching and testing. An aircraft is supposed to operate in a $-50^{o}C$ to $+50^{o}C$ temperature window. Three samples of each material were struck at $-50^{o}C$ and 3 others samples at room temperature ($20^{o}C$). Magnetic permeability of impact samples was measured before (on sample) and after the impact test on the fractured area of the broken sample. Martensitic transformation occurred during the impact test in all tested samples at both temperatures, and results are presented in Chapter 3, sections 3.4.5 and 3.6.5.

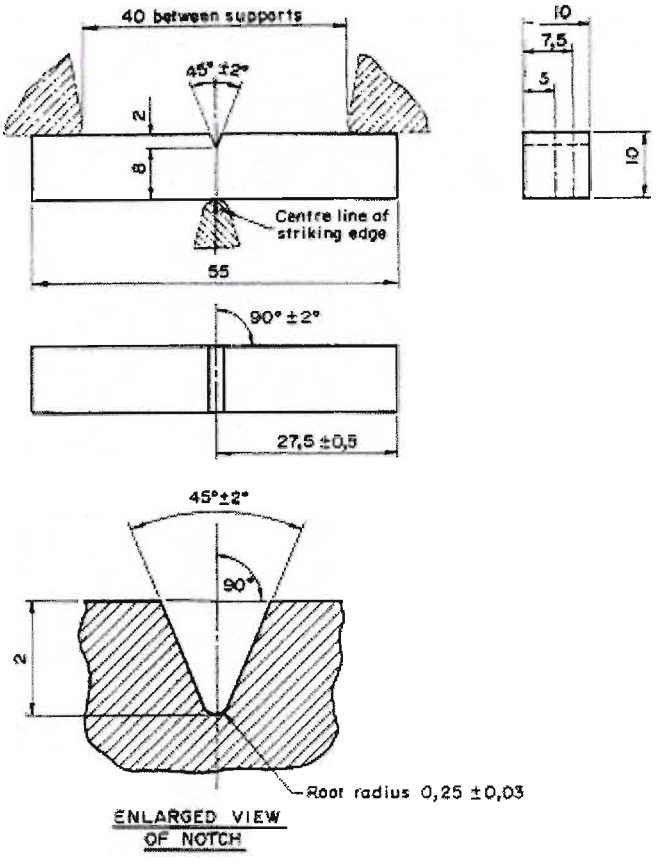

Figure 2.18 Impact sample drawing conforming to SABS 056-1973

2.11 Thermal Martensitic Formation Test

From impact test results, it was suspected that temperature induced phase transformation occurred within Alloys 2/2 and 4/2 during impact test (higher impact resistances were obtained at -50°C than at +20°C). For clarity, two specimens of each alloy were made and cooled from +20 down to –85°C by using dry ice. The magnetic susceptibility at different temperatures was recorded and summarized in Figures 3.22-3.23 and 3.44-3.45 where it was found that temperature-induced Phase transformation occurred in Alloy 2/2 but not in Alloy 4/2.

2.12 Metallography Analysis

As-received materials, and samples from specimens used in compression and tensile tests, were used to study the micro-structural change accompanying the deformation of the materials (strain induced phase transformation used for damage detection in strain memory smart sensors).

Sectioning: Cutting of metastable austenitic stainless steel must be done without excessive thermal or mechanical damage. The final cutting of the specimens to metallographic dimensions was performed using a soft silicon carbide abrasive wheel with fluid cooling at a slow feed rate. Metal saw cutting was not used due to the work -hardening property of these alloys (strain induced martinsitic transformation).

Mechanical polishing: After mounting and grinding, metallographical samples were polished in two steps:

- Rough polishing using 6 μm diamond paste on a napless nylon cloth, followed by 1μm diamond paste on a medium-nap nylon cloth.
- Fine polishing was carried out using colloidal silica or alumina (Al_2O_3) suspension and a medium nap cloth.

The specimens were always rotated in a direction opposite to that of the lapping wheel. Moderate pressure was applied. Between polishing, the specimens were washed with soap and running water, rinsed with alcohol, and dried in a blast of warm air. After fine polishing, specimens were rinsed in alcohol only to prevent staining by water.

Etching: The microstructure is usually visible only after etching. Only features that exhibit a 10% or greater difference in reflectivity can be viewed without etching. This is true of micro-structural features with strong colour differences or with large differences in hardness that cause relief formation: cracks, pores, pits, and non-metallic inclusions may be observed in the as-polished condition. The polished specimens were not exhibiting their microstructure, because light was uniformly reflected. The eye cannot discern small differences in reflectivity; therefore image contrast must be produced. Although this has become known as **etching**, it does not always refer to the selective chemical dissolution of various structural features.

Etchants: Kalling 1(1.5g $CuCl_2$, 33ml Ethanol, 33ml HCl and 33ml H_2O) or by a mixture of Vilella's reagent + picric acid 1g + nitric acid 1-2 drops, with an etching time of 10 sec. All samples were etched at room temperature.

2.13 Smart Bolt Prototype Test

Once the material development and testing was complete, a subscale prototype smart bolt was designed, manufactured and tensile tested (see Figures 2.19, 4.10, and 4.11(1)). This was done not only to show that the correct tensile yield strength could be achieved (as required by military specification) but also to attempt to integrate a means of measuring the transformation (induced by any type of damage) into a simulated wing bolt set-up. The principle of an induction coil inserted into a washer or nut was used See Figure 4.6 (2).

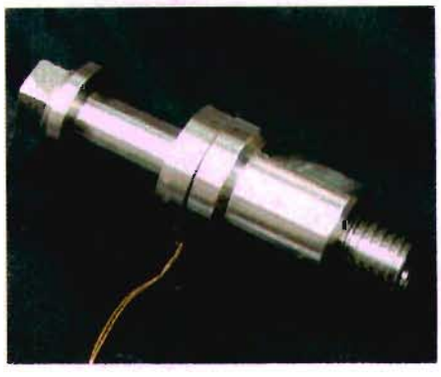

Figure 2.19 Smart aircraft bolt prototype

These were machined at DIT. The sensitivity of this prototype smart washer to stress and strain induced martensitic transformation was assessed. Two inductance meters, one connected to a coil located on the first engaged thread, and the other to a coil located under the bolt head were used concurrently. Both areas have been reported as critical (highly stressed). Results are presented in Figs 4.16-4.17, Chapter 4 section 4.3.

The concept of inductance is simplified by considering a toroidal coil connected to an AC source. As the alternating current passes through the coil, an alternating magnetic field is set up, in turn producing a voltage. Paramagnetic core materials like austenite have permeability higher or equal to that for a vacuum ($4\pi 10^{-7}$ H/m), while ferromagnetic materials (martensite) have permeability far greater than that of a vacuum. The above principle is used to monitor the health of a smart wing bolt prototype using an inductance meter during the test.

The inductance coil for the smart bolt prototype was wound using a coil winder machine. Miniature inductance coils were manufactured from a thin wire of diameter 0.091mm; about 140 turns were achieved on each 15mm diameter coil. Epoxy was

added to keep the wire together. A spindle type device (Figure 2.20) was manufactured to help in winding a coil with accurate dimensions and the maximum possible number of turns to increase the coil's magnetic sensitivity. Release wax was applied to the accessory part surface to make the coil easy to slide off when removing it from the spindle.

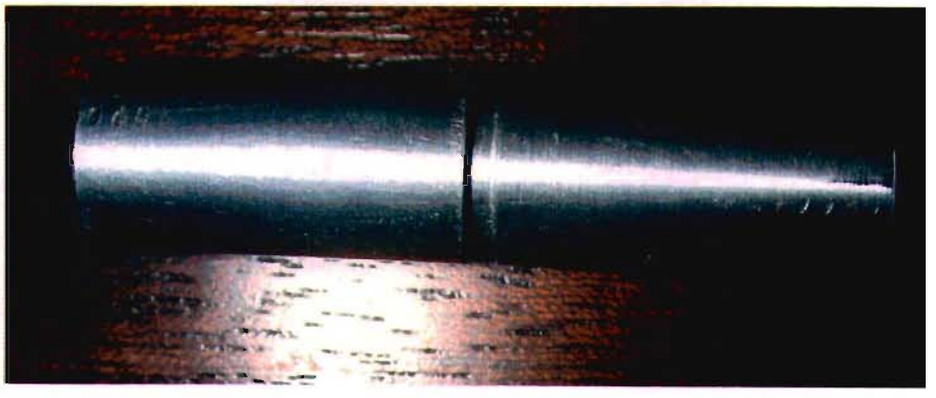

Figure 2.20 A spindle type device for making coils of the desired size with the maximum possible winding turns

CHAPTER 3

MATERIALS TESTING RESULTS

3.1 Experimental melting results

After the first experiment, all proposed alloy chemistries for this study were melted and thermo-mechanically processed as indicated in Chapter 2. Chemical analysis results after processing showed that the carbon content for all processed alloys was less than the expected carbon content (see Table 3.1) for the second melting.

Table 3.1 Actual chemical compositions (mass %) for Alloys 1, 2, 3, and 4 after processing (75 % warm reduction)

Elements	Alloy 1		Alloy 2		Alloy 3		Alloy 4	
	1/2	1/3	2/2	2/3	3/2	3/3	4/2	4/3
Carbon	0.16	0.30	0.21	0.33	0.19	0.20	0.29	0.35
Manganese	4.00	3.86	2.57	2.63	10.5	10.14	1.13	1.64
Sulphur	0.007	0.015	0.006	0.016	0.010	0.014	0.007	0.012
Phosphorus	0.005	0.011	0.005	0.013	0.005	0.011	0.005	0.011
Silicon	0.53	0.61	0.60	0.44	0.08	0.068	0.56	0.58
Chromium	8.14	9.09	8.0	8.75	11.6	9.66	11.6	11.95
Molybdenum	0.03	-	1.91	1.70	0.03	0.013	0.01	0.002
Nickel	8.31	6.30	8.91	8.49	1.33	1.86	9.48	8.89
Copper	0.01	-	0.01	-	0.01	-	0.01	-
Aluminium	0.01	-	0.01	-	0.01	-	0.033	-
Vanadium	0.014	-	0.015	-	0.031	-	0.005	-
Niobium	0.026	-	0.027	-	0.026	-	0.025	-
Boron	.0005	-	.0005	-	.0005	-	.0005	-
Iron	Bal.	Bal.	Bal.	Bal.	Bal.	Bal.	Bal.	Bal.

3.2 Introduction

Testing and analysis of the second melt of the four candidate alloys clearly reveals that most of the alloys manufactured were duplex phased (austenite and martensite). This is due to the shift in the chemistry (%C) occurring during alloying. Two alloys of the second melting were not strong enough for the aircraft wing bolt application. The same alloys were considered not qualified for smart sensor fabrication, as they did not transform to martensite during elastic deformation. A third experimental

alloy fabrication was designed to produce alloys with strict chemical compositions (see Table 3.1), with good transformation characteristics, and with high strength for the aircraft wing bolt.

3.3 Alloy 1 test results

3.3.1 Alloy 1 chemical analysis results

Alloy 1 was warm rolled to a 75 % reduction. A chemical composition analysis found that the carbon content was 0.16% for alloy 1/2 and 0.30 for alloy 1/3, both of which are less than the 0.35% expected (see Table 3.2).

Table 3.2 Alloy 1 chemical analysis result after processing

Element	C	Si	Mn	P	S	Cr	Mo	Ni	Fe
Target	0.35	0.50	3.5	-	-	9.00	-	8.00	Bal.
Alloy 1/2	0.16	0.53	4.00	0.005	0.007	8.14	0.03	8.31	Bal
Alloy 1/3	0.30	0.61	0.86	0.011	0.015	9.09	-	6.30	Bal.

3.3.2 Tensile test results

Several samples (of the form represented in Fig 2.9 and 2.10) were prepared and tensile tested at 0.5 mm/minute tensile speed, as cited in Chapter 2, section 2.6. The yield stress was found to be between 790 and 800 MPa (Alloy 1/2), and 1039 to 1072 MPa for Alloy 1/3. Tensile strains of 0.18 – 0.36 (Alloy 1/2) and 0.10 (Alloy 1/3) were measured (see Figs.3.1 – 3.5 and Table 3.3), respectively. The tensile tests indicate that this alloy does not meet the strength requirement of aircraft bolt material.

The magnetic susceptibility readings are marked on the same graphs as stress-strain data, and represented by B curves; and for reference a vertical line denoting the yield point of the material has also been inserted (in red). This is to enable the reader to easily differentiate transformation that occurs before plastic yield and that which occurs after plastic yield.

For alloy 1/2, the change in magnetic susceptibility before yield was in a negative direction only and the final reading was quite close to the first reading of the test. The overall change in magnetic susceptibility was therefore not sufficient to provide a reliable strain memory effect.

Alloy 1/3 showed initial magnetic susceptibility an order of magnitude less than alloy 1/2, which would imply that the crystal structure was FCC austenite. The percentage change or range of the magnetic susceptibility readings is greater than for alloy 1/2, but the transformation appears to occur after yield, which does not allow for early warning and time for replacement. (See Figures 3.4-3.5 and Table 3.3)

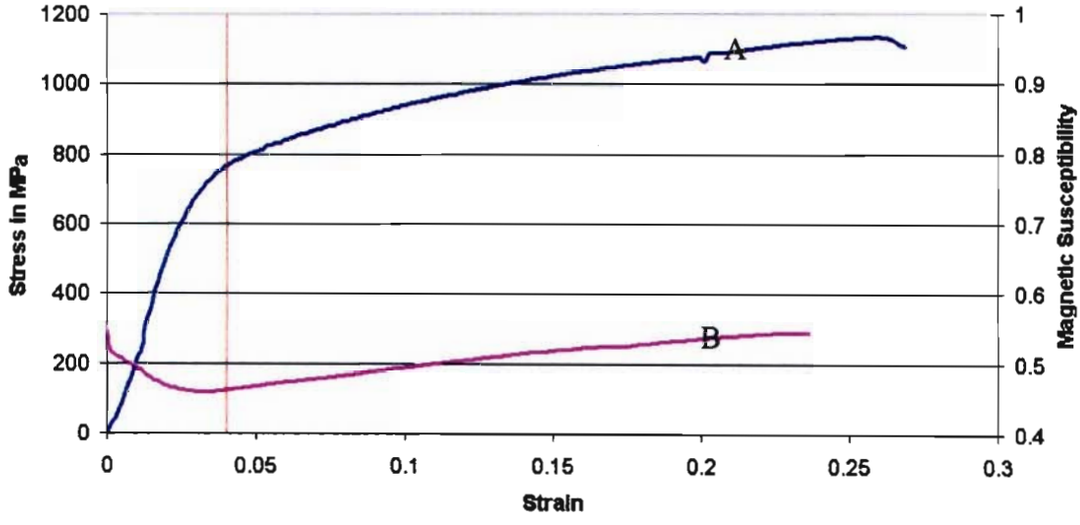

Figure 3.1 Stress-strain A and magnetic susceptibility - strain B curves for Alloy 1/2 Specimen 2(tensile test)

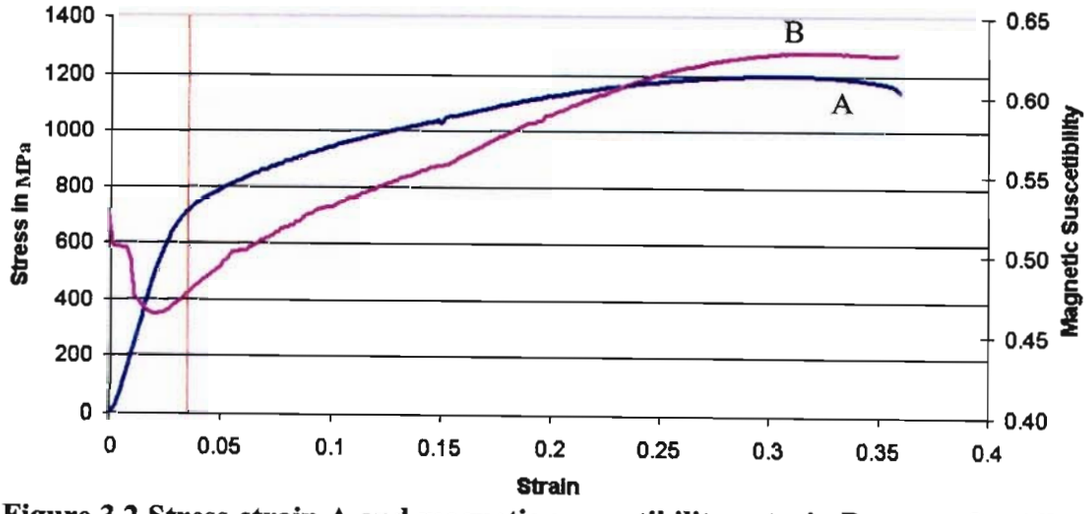

Figure 3.2 Stress-strain A and magnetic susceptibility - strain B curves for Alloy 1/2 Specimen 3 (tensile test)

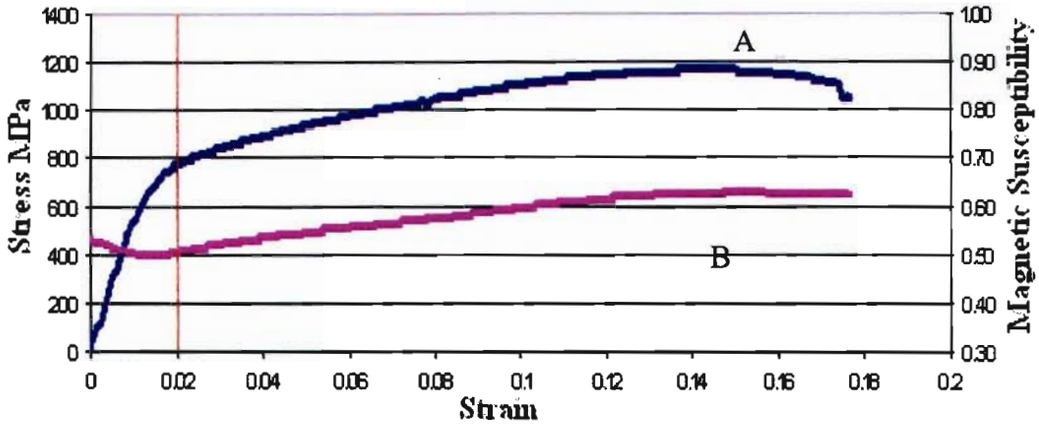

Figure 3.3 Stress-strain A and magnetic susceptibility - strain B curves for Alloy 1/2 Specimen 5 (tensile test)

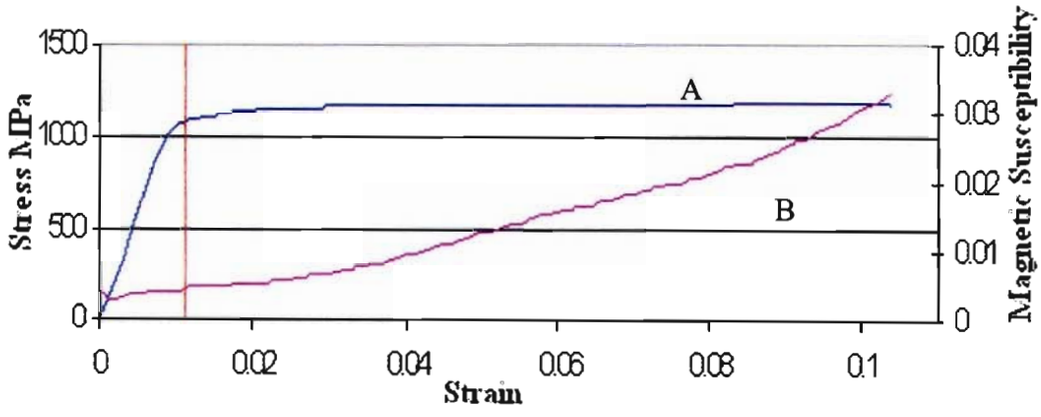

Figure 3.4 Stress-strain A and magnetic susceptibility - strain B curves for Alloy 1/3 Specimen 2 (tensile test)

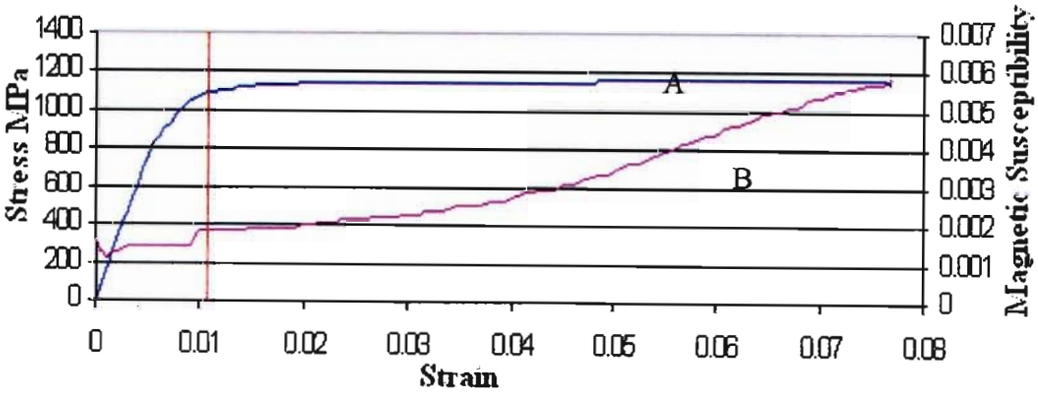

Figure 3.5 Stress-strain A and magnetic susceptibility - strain B curves for Alloy 1/3 Specimen 3 (tensile test)

Mechanical properties and transformation characteristics of the various samples of Alloy 1 are summarised in table 3.3 which follows.

Table 3.3 Room temperature tensile properties Alloy 1

Specimen ID	% PDA	Yield stress MPa	UTS MPa	Initial magn.	Final magn.	% Elongation
2 (1/2)	75	800	1150	0.575	0.575	26
3 (1/2)	75	790	1190	0.525	0.625	36
5 (1/2)	75	800	1100	0.525	0.625	18
2 (1/3)	75	1039	1120	0.005	0.035	8.0
3 (1/3)	75	1072	1181	0.001	0.006	10.5

Fractured Specimen 2 from Alloy 1/2 also shows localized necking, see Fig.3.6 (1/2), which indicates a lack of strain-induced martensite phase formation occurring during tensile testing. Broken tensile samples from Alloy 1/3 exhibited brittle fracture, with no localized necking or surface cracks along the gauge length can be seen in Fig 3.6(1/3).

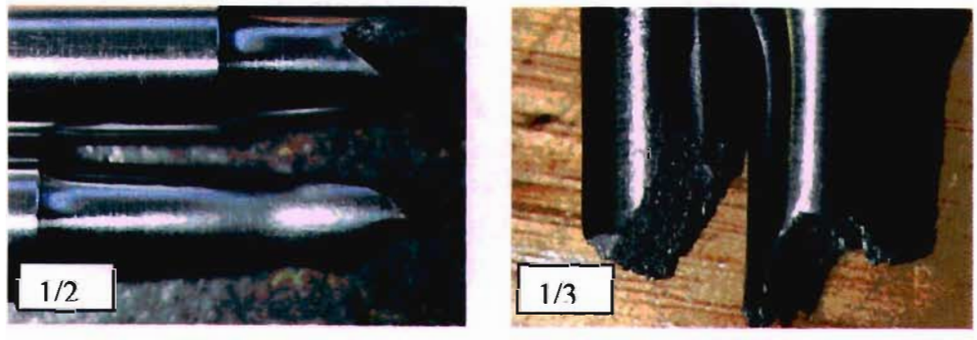

Figure 3.6 Alloy 1/2 Specimen 2 broken sample showing v-notch fracture (ductile shear mode failure), with localised necking and tensile tested samples from Alloy1/3 showing a brittle failure, no necking

3.3.3 Metallographic analysis

Microstructure analysis of as-received Alloy 1/2 and 1/3 material sample shows elongated austenitic and martensitic grains in the rolling direction, (see Figure 3.7); while analysis of samples from Alloy 1/2 after compression and tensile testing shows an increase in martensitic phase with strain induced martensite (dark) in the form of needles following the rolling direction, see Figures 3.8 – 3.9 (2).

An SEM image for a tensile tested sample at 1000 magnification shows a similar duplex microstructure, but the martensite is white while, the austenite is dark and both phases are elongated in the rolling direction, see Fig. 3.9 (1).

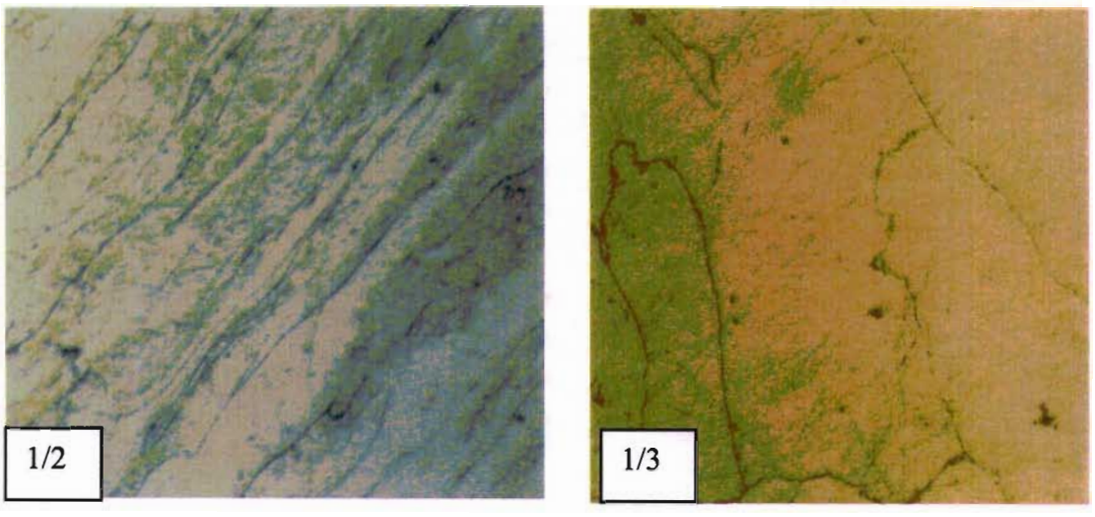

Figure 3.7 Heavy-worked microstructure showing elongated austenitic and martensitic grains in the rolling direction (slip band lines) for Alloy 1/2 (at 400X) and 1/3 (at 100X) with full elongated austenitic grains, both alloys before deformation.

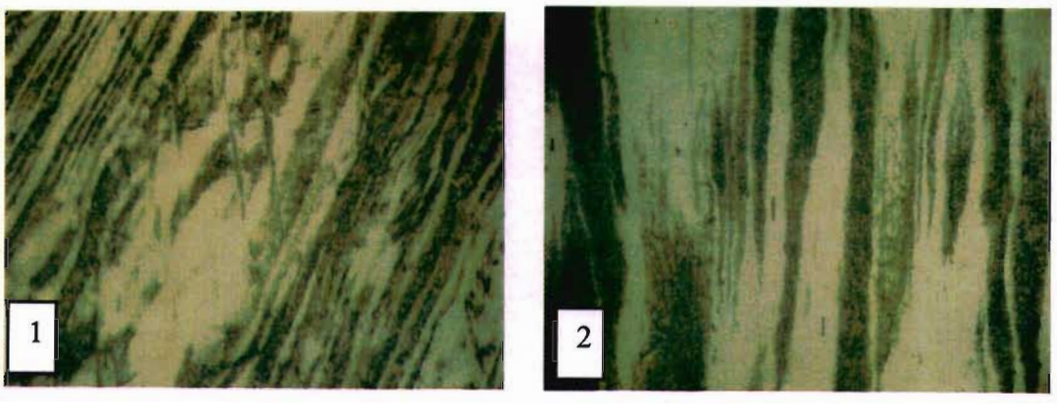

Figure 3.8 Microstructure of Alloy 1/2 after compression (1) and tensile (2) test showing an increase in martensite (strain induced= dark), at 400X

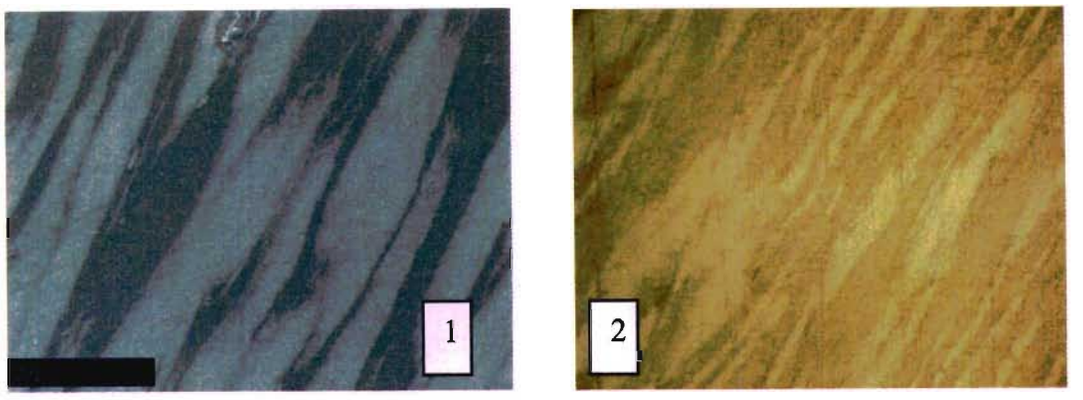

Figure 3.9 Microstructure of Alloy 1/2 after tensile test showing strain-induced martensite (= white) and retained austenite (dark), SEM image (1) at 1000X and Alloy 1/3 after tensile (2) test showing strain-induced martensite (dark) and retained austenite, at 400X

3.3.4 Conclusion

In summary, Alloy 1/2 has a low level of martensitic strain-induced transformation and lower tensile properties (yield strength) than those required for the aircraft wing bolt application (Figs 3.1- 3.5). This is probably due to the chemical modification that occurred during melting and processing, because the expected carbon content was 0.35% C, while the measured carbon content after melting and processing was only 0.16% C. A small amount of strain-induced martensitic transformation occurred after plastic deformation had started, which does not produce the desired early warning for a smart strain memory structural component. The necking observed in Sample 2, (Fig 3.6) testifies to the absence of strain-induced martensite transformation, as it is characteristic for TRIP steel to fail without necking [71]. Alloy 1/2 was ferromagnetic after processing which means that it had a ferrite, semi-ferrite or duplex microstructure Fig 3.7(1/2), with less austenite left for transformation during straining, even though microstructure analysis on samples after compression and tensile testing showed a slight increase in the martensitic phase proportion (see Fig. 3.7- 3.9).

Alloy 1/3 has a stress-strain induced martensite transformation starting directly with the application of stress on the material, and this material is strong enough for the aircraft bolt application σ_y =1039MPa (see Figs 3.4-3.5 and Table 3.3). The stress-strain tensile curves show no work hardening which is characteristic for strain

memory alloys. However the greatest portion of the transformation occurs after yield, with only a small discernable change in magnetic susceptibility in the pre-yield region. Evidence of the strain-induced phase transformation is assessed by metallographic analysis (compare Figs 3.8 with Fig 3.9). Figure 3.9 (Alloy 1/3) shows a greater percentage martensite than Alloy 1/2 (Figure 3.8), testifying to the better transformation properties.

3.4 Alloy 2 test results

3.4.1 Chemical analysis results

The chemical composition of Alloy 2/2 (tested by spectro-chemical analysis) shows a carbon content of 0.21%, which is lower than the 0.30% C that was expected. The Mo, Ni, Si, Mn, content were, however, acceptable (see Table 3.4). Alloy 2/3 has a carbon content of 0.33% which is more than the expected value of 0.30% C (see Table 3.4).

Table 3.4 Alloy 2 chemical analysis result after processing

Element	C	Si	Mn	P	S	Cr	Mo	Ni	Fe
Target	0.30	0.50	2.10	-	-	8.50	2.00	8.40	Bal.
Alloy 2/2	0.21	0.60	2.57	0.005	0.006	8.00	1.91	8.91	Bal
Alloy 2/3	0.33	0.44	2.63	0.013	0.016	8.75	1.70	8.49	Bal.

3.4.2 Tensile test results

Tensile tests for all Alloy 2/2 samples produced a yield stress of 900 MPa and a tensile strain of 25-26% (see Figs 3.10-3.12 and Table 3.5), and the magnetic susceptibility varied from 0.175 - 0.375 (see Fig. 3.10-3.12). This is a very marked difference in the magnetic susceptibility characteristic, when compared with Alloy 1/2. These samples were too strong for the tensile machine and tests were stopped before the specimen failed, so the ultimate tensile strengths were not recorded. Figure 3.15 shows the tested samples (that are clearly not fractured), which show no signs of necking.

For alloy 2/3 a yield stress of 1100 MPa was achieved, and strain varied from 14.5 to 15%, with magnetic susceptibility varying from 0 to 0.25 (see Figs 3.13-3.14 and Table 3.5). The reduction in elongation is consistent with the higher percentage carbon present in Alloy 2/3.

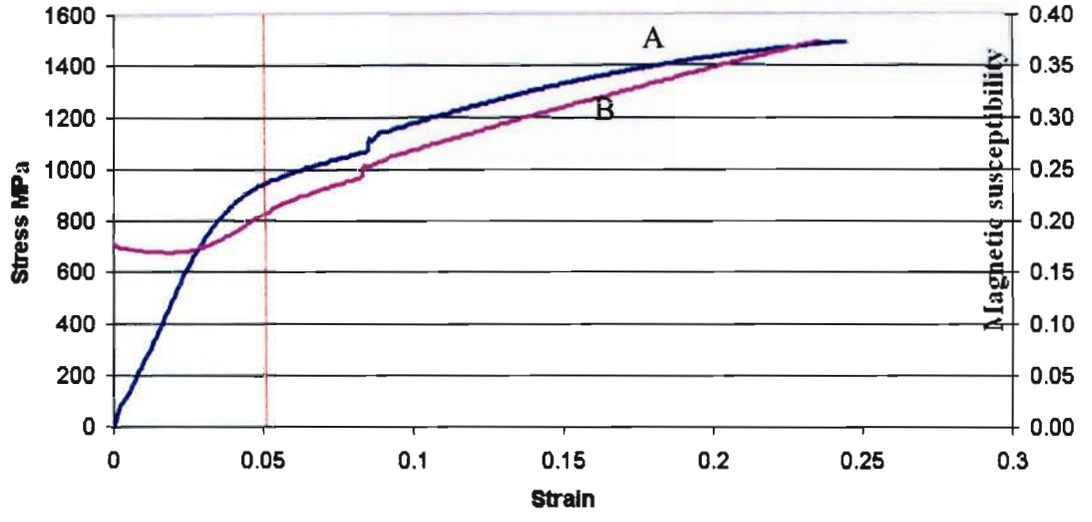

Figure 3.10 Stress-strain A and magnetic susceptibility-strain B curves for alloy 2/2 Specimen 1 (tensile test)

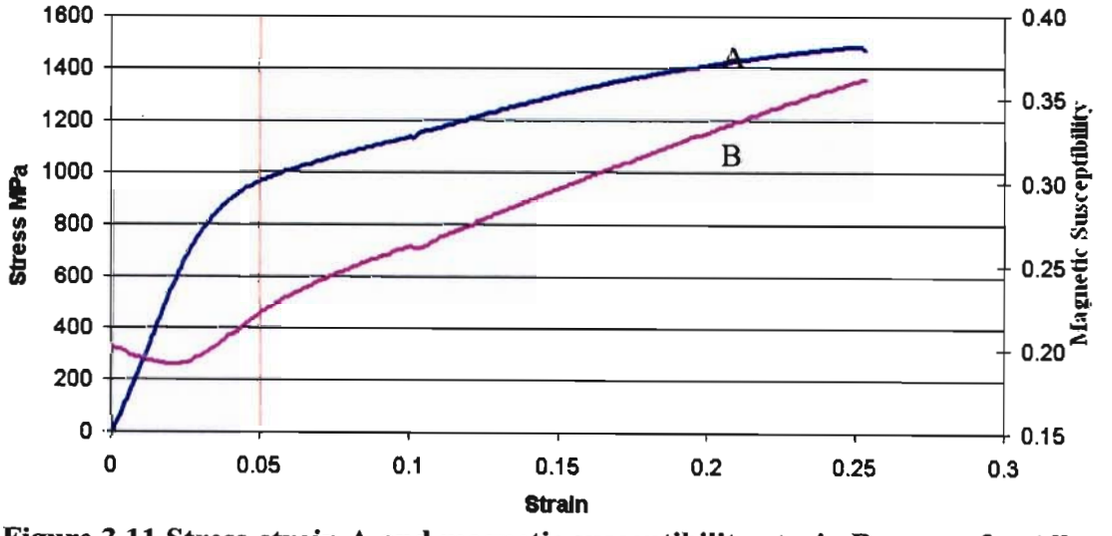

Figure 3.11 Stress-strain A and magnetic susceptibility-strain B curves for Alloy 2/2 Specimen 2 (tensile test)

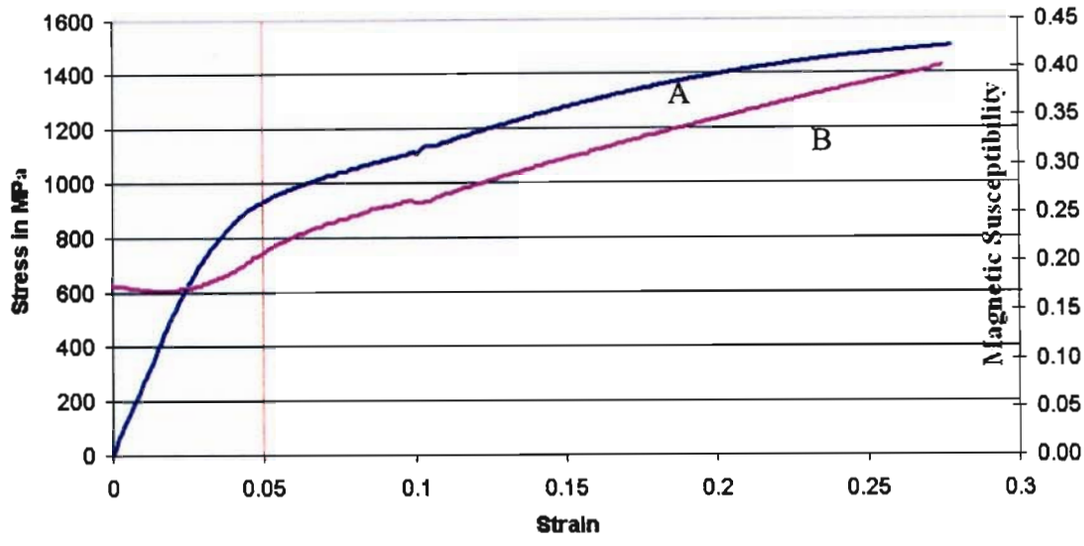

Figure 3.12 Stress-strain A and magnetic susceptibility-strain B curves for Alloy 2/2 Specimen 3 (tensile test)

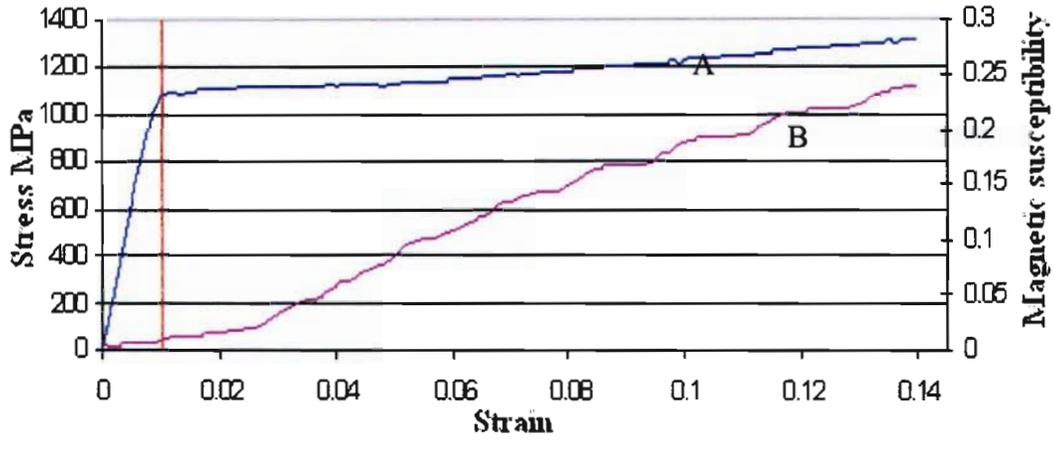

Figure 3.13 Stress-strain A and magnetic susceptibility-strain B curves for Alloy 2/3 Specimen 1 (tensile test)

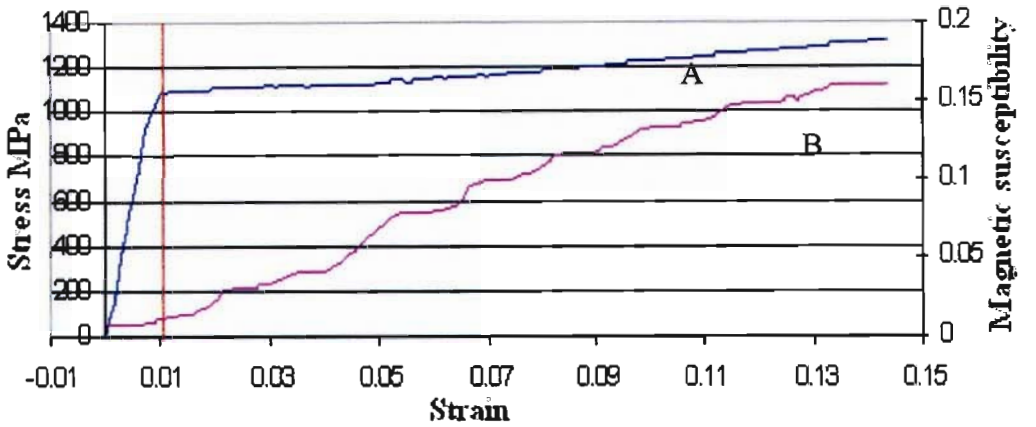

Figure 3.14 Stress-strain A and magnetic susceptibility-strain B curves for Alloy 2/3 Specimen 3 (tensile test)

A summary of mechanical and transformation characteristics of Alloys 2 are shown in Table 3.5 below. This summary together with the pictures of the tested samples (in Figure 3.5) indicate much better transformation properties for Alloy 2 than Alloy 1. The difference in carbon content between Alloys 2/2 and 2/3 (0.21 and 0.33% C respectively) produces a lower yield strength in Alloy 2/2 than in Alloy 2/3, but the reduction in elongation consequent of the higher carbon content in Alloy 2/3, produced a lower UTS in this Alloy than in alloy 2/2.

Table 3.5 Room temperature tensile properties for Alloy 2

Specimen ID	% PDA	Yield stress MPa	Final stress MPa	Initial magn.	Final magn.	% Elongation
1 (2/2)	75	900	1500	0.175	0.375	25
2 (2/2)	75	900	1490	0.200	0.350	25
3 (2/2)	75	900	1500	0.175	0.410	27
1 (2/3)	75	1100	1315	0.00	0.25	14.5
2 (2/3)	75	1117	1320	-	-	17.5
3 (2/3)	75	1050	1320	0.00	0.16	15

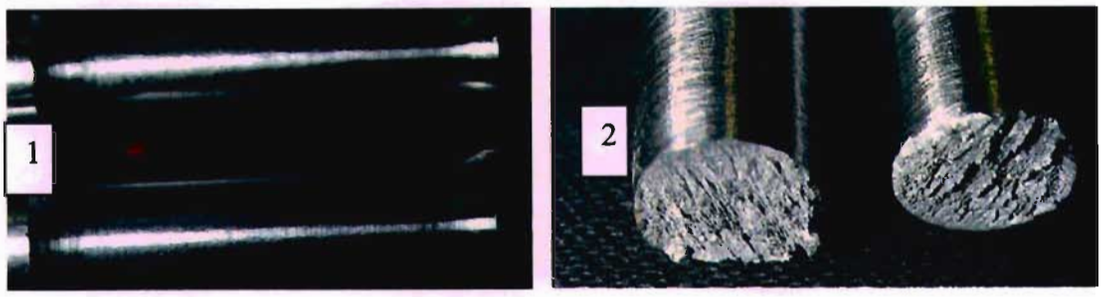

Figure 3.15 Tensile tested specimen Alloy 2/2(1), and failed Specimens from Alloy 2/3 showing a brittle failure. Neither show localized necking; only the gauge length is showing slip lines.

3.4.3 Compression test results

Samples for compression testing were also prepared and tested (as indicated in Chapter 2 section 2.9) and the magnetic inductance was measured and recorded for different loads (stresses). The strain-induced martensite transformation occurred before the material plastically yielded (see Fig 3.16) as happened during tensile test of Alloy 2/2, which is more promising than Alloy 1/2.

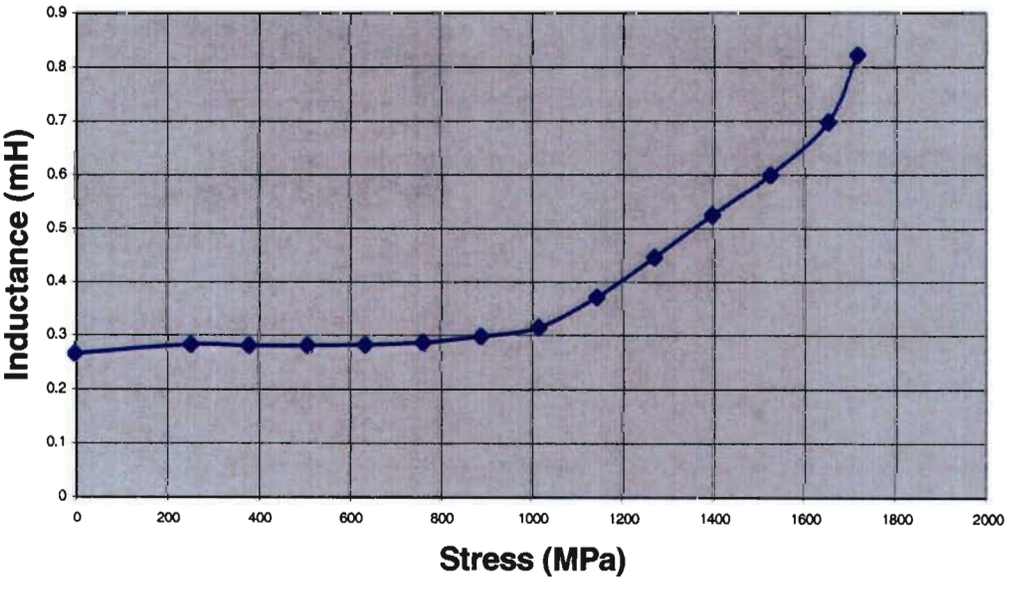

Figure 3.16 Stress versus Magnetic Inductance as evidence of strain-induced phase transformation (compression test), Alloy 2/2

3.4.4 Metallographic analysis

The microstructure analysis results of Alloy 2/2 and 2/3 material samples are shown in Figs 3.17-3.19 for as-received, compression tested and tensile tested samples. Figure 3.17 presents similar microstructure to the corresponding microstructures of Alloy 1/2. There is a significant increase in the martensitic phase after tensile and

compression testing (See Figures 3.18- 3.19 for SEM image and optical images respectively). After tensile testing the microstructure is similar to that of Alloy 1/3 after tensile testing, but the martensite seems present in greater proportion.

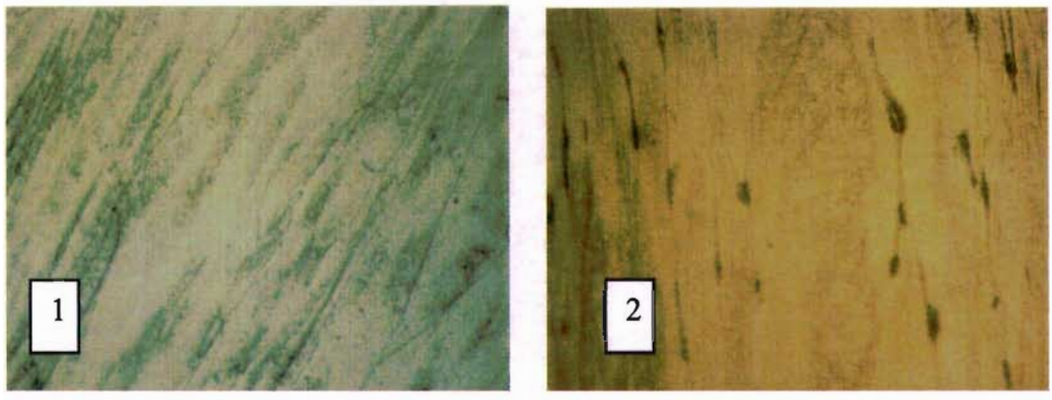

Figure 3.17 Heavy-worked microstructure showing elongated austenitic grains and martensite, as-received Alloy 2/2 (1) and 2/3 (2) at 400X

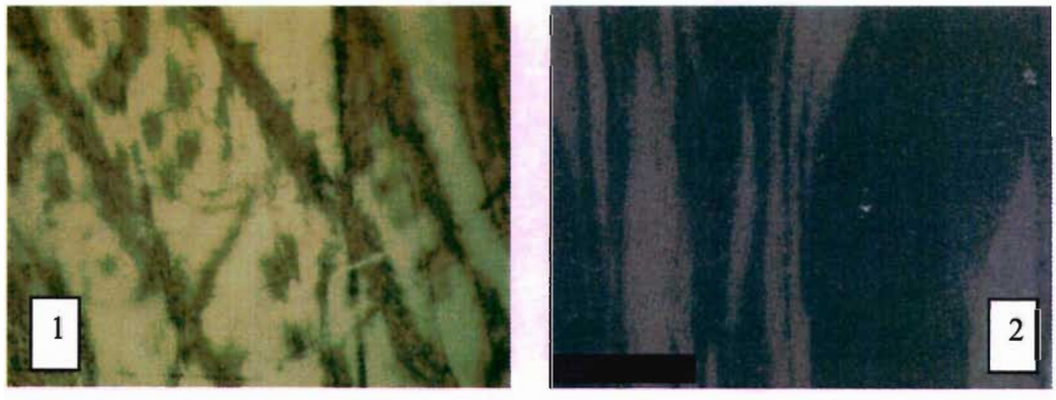

Figure 3.18 Microstructure of Alloy 2/2(1) at 400X after compression test and 2/3(2) tensile tested both showing an increase in martensite on slip bands (strain induced= dark), SEM image (2)

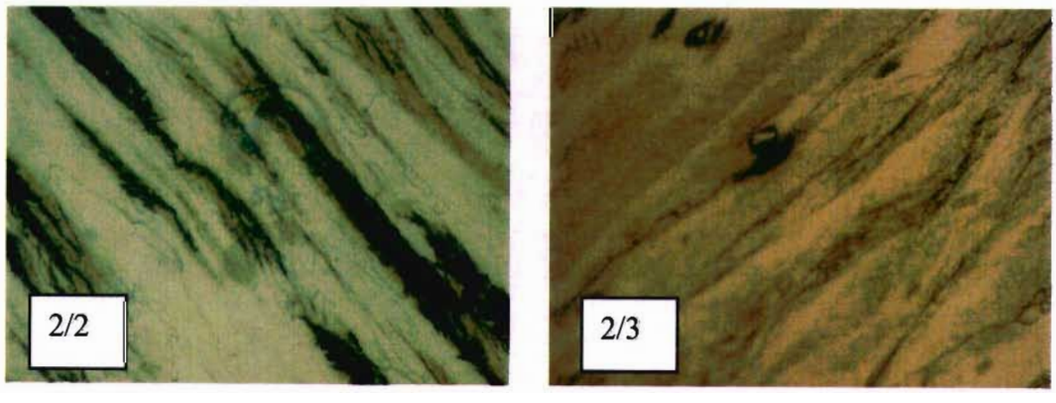

Figure 3.19 Microstructure of Alloy 2 after tensile test showing martensite (strain-induced=dark) and retained austenite, at 400 X

3.4.5 Impact test results

Because the strength and transformation characteristic of this composition were promising an impact test was also conducted. Charpy v-notch impact Specimens machined from Alloy 2/2 were struck at room temperature to give about 60 Joules impact resistance, while samples struck at -50°C give about 80 Joules (see Table 3.6 below). The magnetic susceptibility measured on impact specimens before and after impact shows that, the magnetic susceptibility increases after impact testing for samples at both temperatures (see Fig. 3.20 and Table 3.7).

Table 3.6 Impact test results Alloy 2/2

ID	Lateral expansion		Shear %		Impact resistance(Joules)	
	20°C	-50°C	20°C	-50°C	At 20°C	At -50°C
Alloy 2/2	0.43	0.18	100	100	50	88
	0.48	0.27	100	100	60	78
	0.61	0.33	100	100	62	87

Magnetic susceptibility for each sample was recorded for different temperatures, and the effect of lowering the temperature quantified in table 3.7 which presents the magnetic susceptibility data that confirms that strain-induced martensite transformation occurred within Alloy 2/2 during the impact test (see Table 3.7 and Fig 3.20).

Table 3.7 Magnetic susceptibility measurement before and after impact test Alloy 2/2

ID	Sample's magnetic susceptibility before impact test		Sample's magnetic susceptibility after impact test on fracture area	
	At room temperature	At –50°C	At room temperature	At –50°C
Alloy 2/2	0.009298 0.006360 0.003970		0.01484 0.01010 0.008876	
		0.01883 0.02260 0.02212		0.02545 0.02929 0.03006

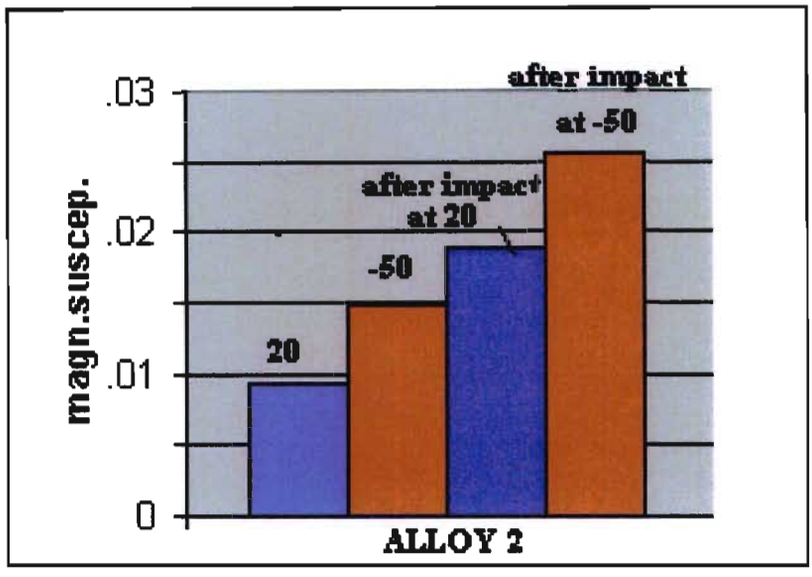

Figure 3.20 Magnetic susceptibility changes with temperature and impact testing temperature of Alloy 2/2

Broken impact specimens were fractured predominantly in shear mode at room temperature, see Fig.3.21 (1), while those tested at –50°C show a brittle fracture, see Fig.3.21 (2).

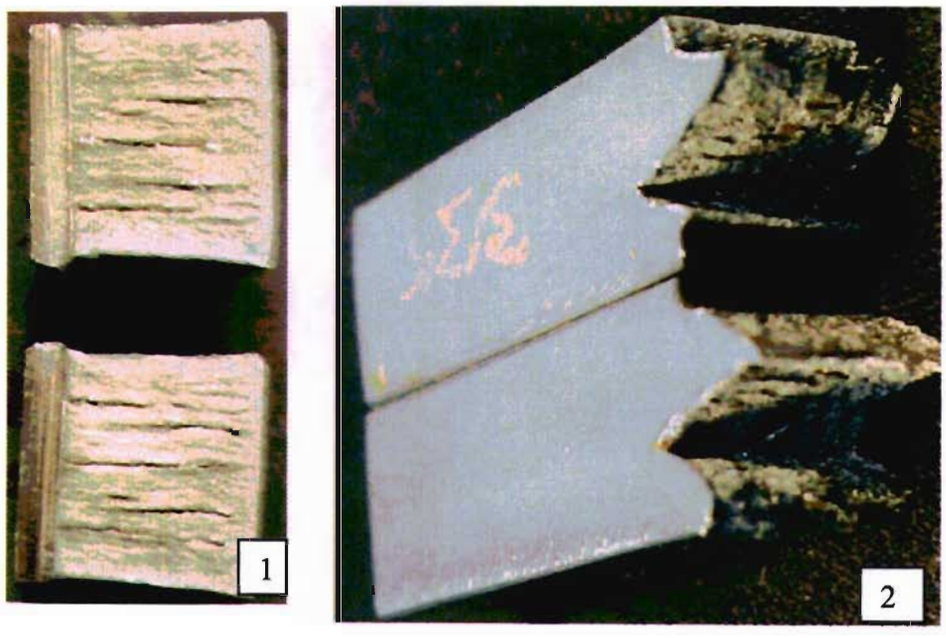

Figure 3.21 Impact fracture (shear) Alloy 2/2 at room temperature (1) and Impact v-notch fracture Alloy 2/2 at -50 degree Celsius (2)

Alloy 2/2 shows elevated impact resistance at -50°C. The fact that impact resistance increases with the temperature decrease could be associated with thermal martensite phase transformation occurring in the vicinity of –50°C (M_S temperature). This

hypothesis is tested by quenching Alloy 2/2 samples in methanol below zero degrees Celsius cooled using dry ice (see Fig 3.22 and 3.23).

3.4.6 Spontaneous martensite formation by cooling

Further testing to determine the spontaneous transformation characteristic at temperatures less than 0°C, was conducted as this is obviously of interest for the operating temperatures of "in flight" bolts. Two specimens A and B cut from Alloy 2/2 plates were cooled to different temperatures using dry ice. The magnetic susceptibility within those samples increased with temperature decrease (see Fig 3.22 and 3.23). The difference in the two curves below is due to the orientation of the probe measuring the martensitic susceptibility **by different orientation**. One can clearly deduce from these two graphs that a substantial portion of martensite is formed spontaneously between 0°C and – 95°C. This is a disadvantage because, should this material be used in an aircraft bolt, this thermal effect would have to be "calibrated" out, requiring substantial data manipulation to obtain a correct damage assessment.

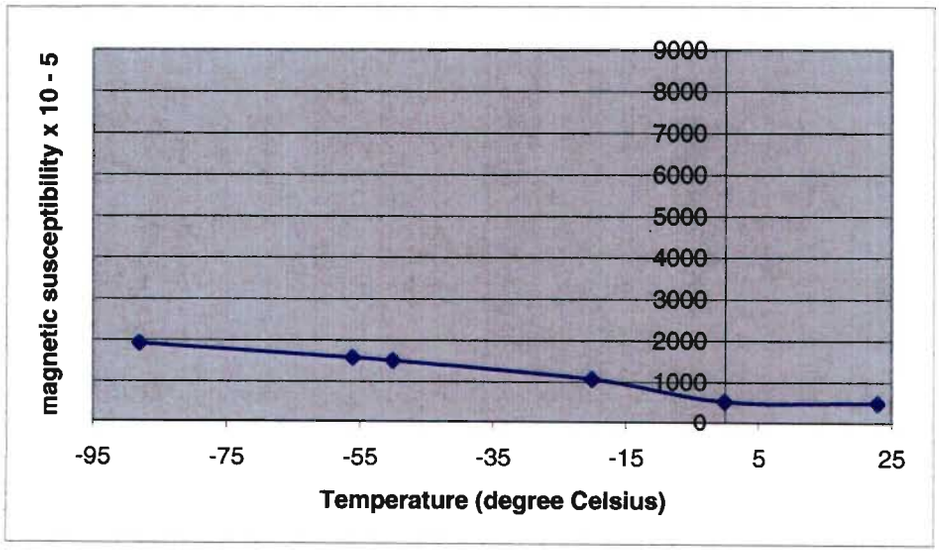

Figure 3.22 Magnetic susceptibility at different temperatures Alloy 2/2 SampleA

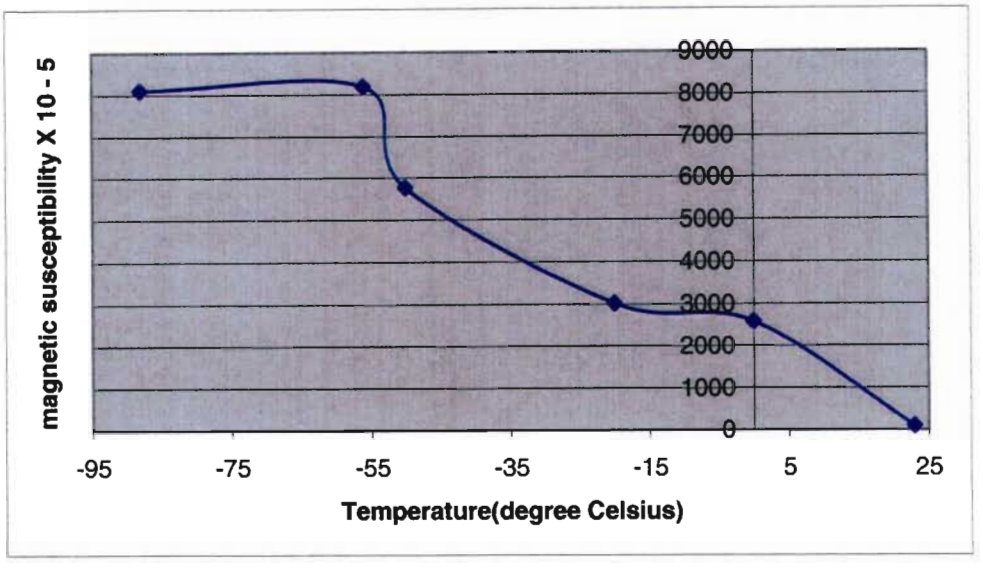

Figure 3.23 Magnetic susceptibility at different temperatures Alloy2/2 Sample B

3.4.7 Conclusion

Even Alloy 2/2 has a duplex microstructure after thermo-mechanical processing as revealed by magnetic measurement and metallographic analysis in Fig 3.17 (1). It did however demonstrate good strain sensing ability with low incubation strain and a stress-strain martensite transformation that started before the material plastically yielded (see Figs 3.10-3.12 and Fig 3.16). This is very good for a smart damage detector component, as it must be able to pick up the damage before the structural element fails. This alloy has acceptable mechanical properties for the aircraft bolt application (see Figs 3.10-3.12 and 3.16) and it also has good work hardening; but this good combination of strain-induced phase transformation and high strength is marred by spontaneous martensitic phase precipitation on cooling, (see Fig 3.22-3.23). Alloy 2/2 would therefore be a good high strength smart strain sensor element for a structure operating upwards of $0^{o}C$ (see Fig 3.23).

Alloy 2/3 has a stress-strain induced martensite transformation starting directly with application of stress to the material; this phase transformation is also revealed in the by microstructures shown in Figs 3.18 (2)-3.19 (2/3). This material with 1.7% Mo is strong enough for the aircraft bolt application having achieved a yield strength σ_y =1100 MPa (see Fig 3.13-3.14 and Table 3.5).

3.5 Alloy 3 test results

The expected and actual (received) chemistries for Alloy 3/2 are presented in table 3.8. Most of the chemistry is within acceptable limits, but the received carbon content of 0.19% C is again significantly lower than the 0.25% C expected.

The chemical analysis of Alloy 3/3 (Mn based TRIP steel) after thermo-mechanical processing gives a 0.20% C content, and is still less than the expected value of 0.25%. But the manganese content is similar to the expected 10% Mn (see Table 3.8).

Table 3.8 Alloys 3 chemical analysis results after processing

Element	C	Si	Mn	P	S	Cr	Mo	Ni	Fe
Target	0.25	-	10.0	-	-	12.0	-	1.50	Bal.
Alloy 3/2	0.19	0.08	10.5	0.005	0.010	11.6	0.03	1.33	Bal
Alloy 3/3	0.20	0.068	10.2	0.011	0.014	9.66	0.13	1.86	Bal.

3.5.1 Tensile test results

Again the same tensile testing procedure (as Alloy 1/2 and 2/2) was used, and the yield stress was found to be 800 MPa. The magnetic susceptibility varied from 0.04 to 0.11 units as summarised in Table 3.9 below. Figures 3.24-3.26 show the tensile test and magnetic susceptibility curves. For Alloy 3/3 a yield stress of 850MPa was achieved, and a strain of 21% produced, while magnetic susceptibility varied from 0 to 0.09 (see Fig 3.27 and Table 3.9).

Table 3.9 Alloy 3 room temperature tensile properties

Specimen ID	% PDA	Yield stress MPa	Final stress MPa	Initial magn.	Final magn.	% Elongation
1 (3/2)	75	800	950	0.05	0.11	15
2 (3/2)	75	800	1000	0.04	0.14	24
3 (3/2)	75	800	1027	0.04	0.14	25
1 (3/3)	75	850	1071	-	-	24
2 (3/3)	75	850	1000	0.00	0.09	21

As was the case for Alloy 1, the transformation characteristic is samewhat disappointing: although transformation does occur (and produces a far greater change

in susceptibility units than Alloy 1) there is no significant change before the yield point of the material.

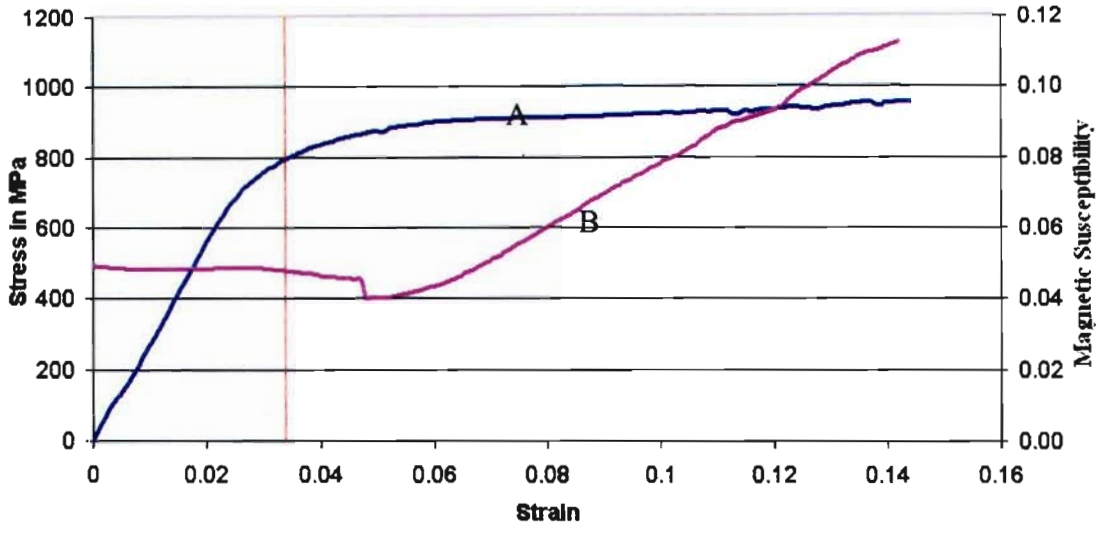

Figure 3.24 Stress-strain A and magnetic susceptibility - strain B curves for Alloy 3/2 Specimen 1 (tensile test)

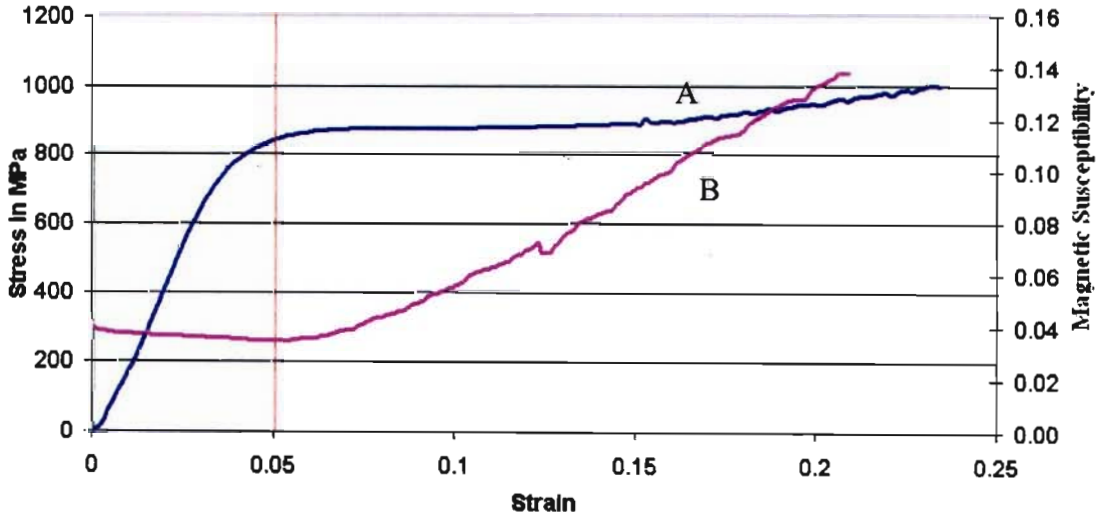

Figure 3.25 Stress-strain A and magnetic susceptibility - strain B curves for Alloy 3/2 Specimen 2 (tensile test)

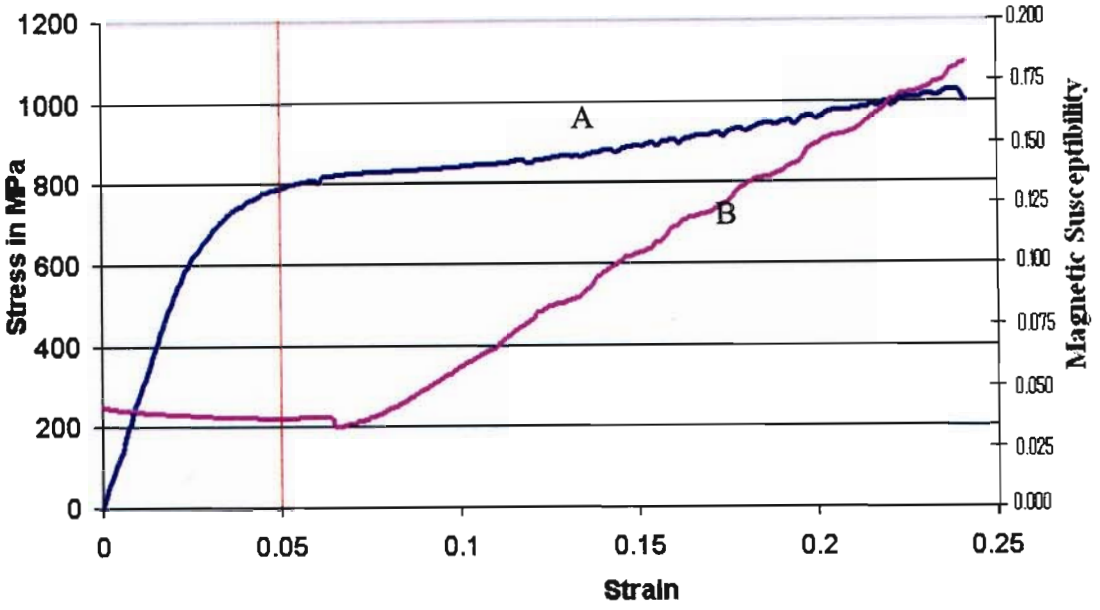

Figure 4.26 Stress-strain A and magnetic susceptibility - strain B curves for Alloy 3/2 Specimen 3 (tensile test)

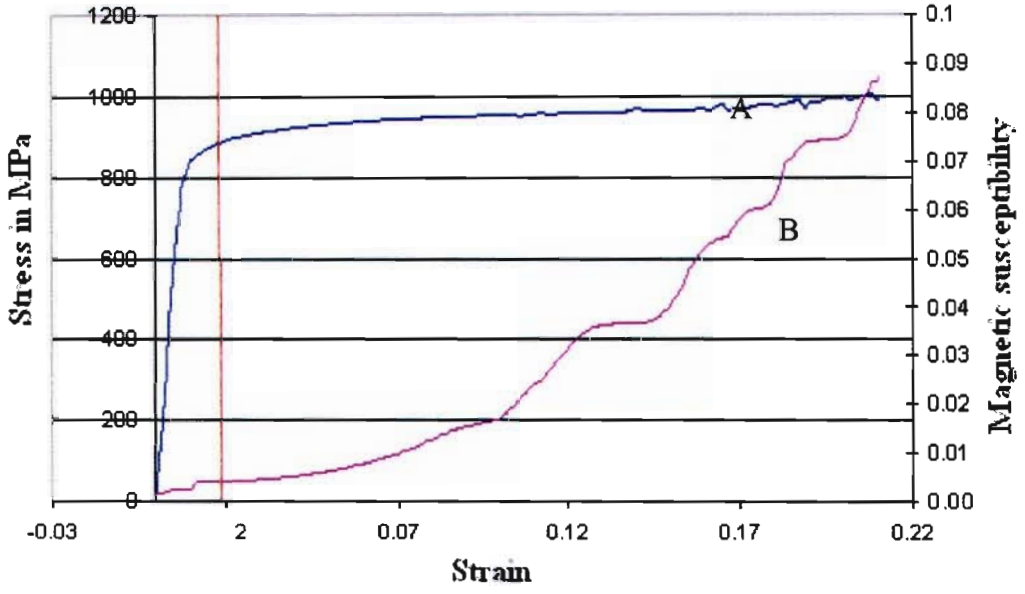

Figure 4.27 Stress-strain A and magnetic susceptibility - strain B curves for Alloy 3/3 Specimen 2 (tensile test)

Broken specimens 1 and 4 (by tensile test) show primarily brittle fractures with cracks along the gauge length (see Fig 3.28), but Specimen 3 shows a brittle-shear fracture, see Fig 3.28 (2 and 3). None of the specimens from Alloy 3 display localized mechanical necking; this implies that they have undergone the transformation to martensite during tests.

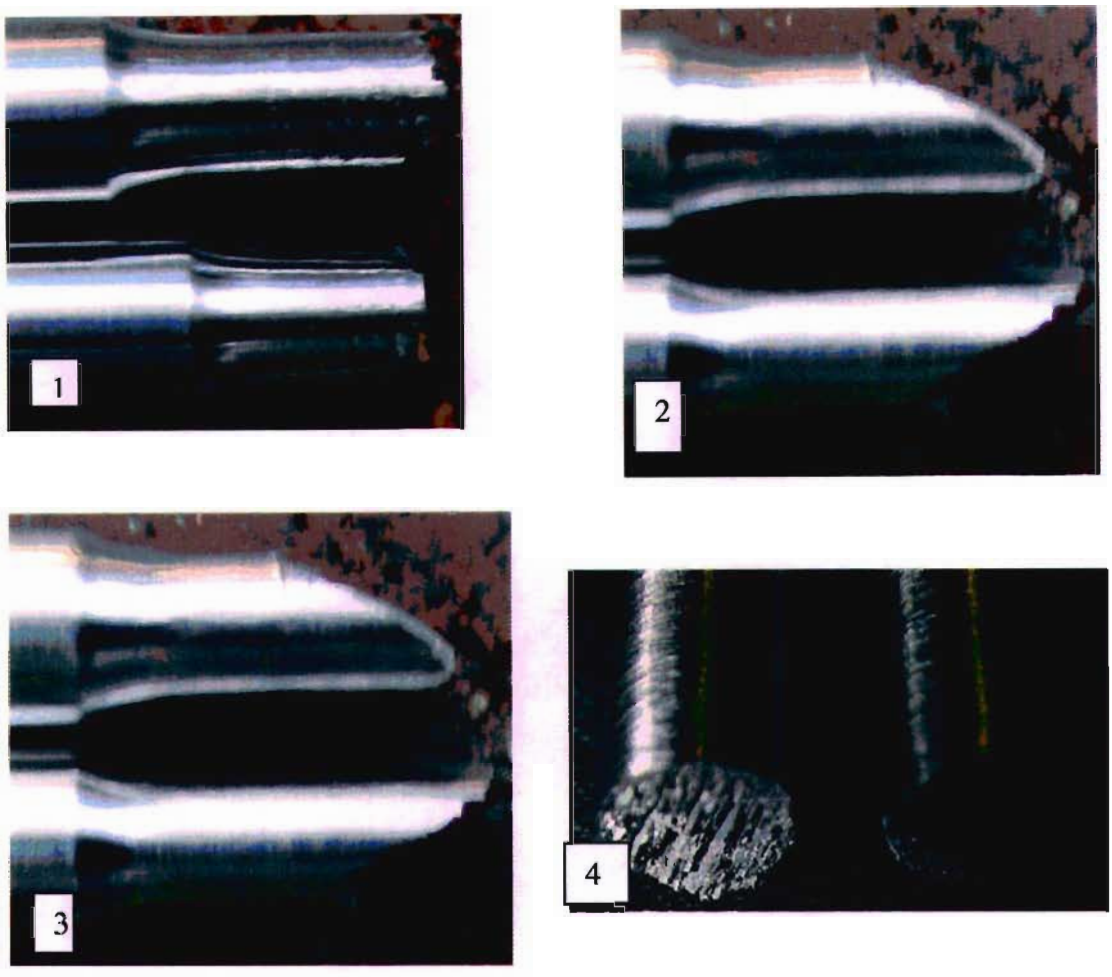

Figure 3.28 Alloy 3/2 (1) and Alloy 3/3 (4) display brittle failure with circumferential cracks along entire gauge length, while Alloy 3/2 (2 and 3) have a shear failure at 45 °. All samples failed with no localised necking.

3.5.2 Metallographic analysis

Microstructural study of **as-received** Alloy 3/3 (before tensile testing) shows elongated austenitic grains with more martensite than alloys 1/3 and 2/3 (see Fig 3.29). The percentage strain-induced martensite (dark) present after tensile testing increased; but retained austenite is also present. (see Fig 3.30-3.31).

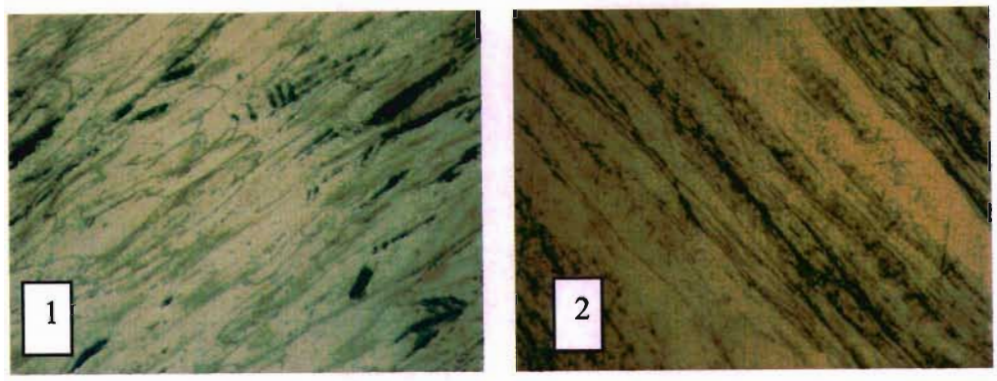

Figure 3 .29 Heavy-worked microstructure showing elongated austenitic grains and martensite, Alloy 3/2 (1) and 3/3 (2) before deformation, at 400X

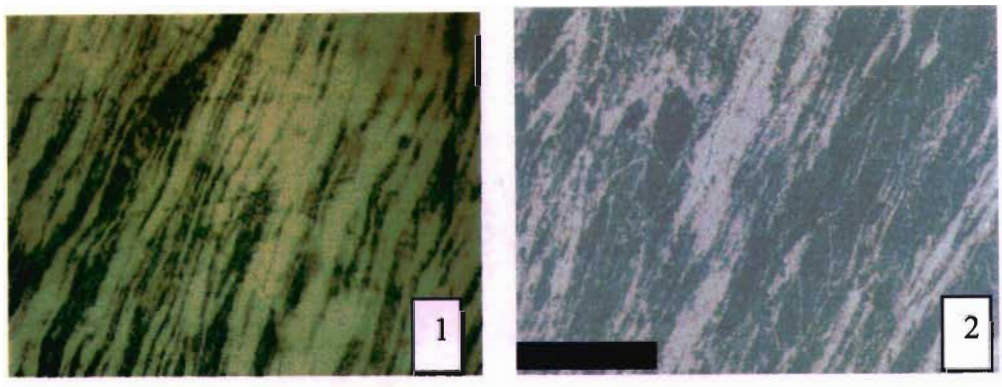

Figure 3.30 Microstructure of Alloy 3/2 at 400X after compression test (1) and tensile test (2) showing an increase in martensite on slip bands (strain induced= dark), SEM image (2) strain induced=white and retained austenite =dark

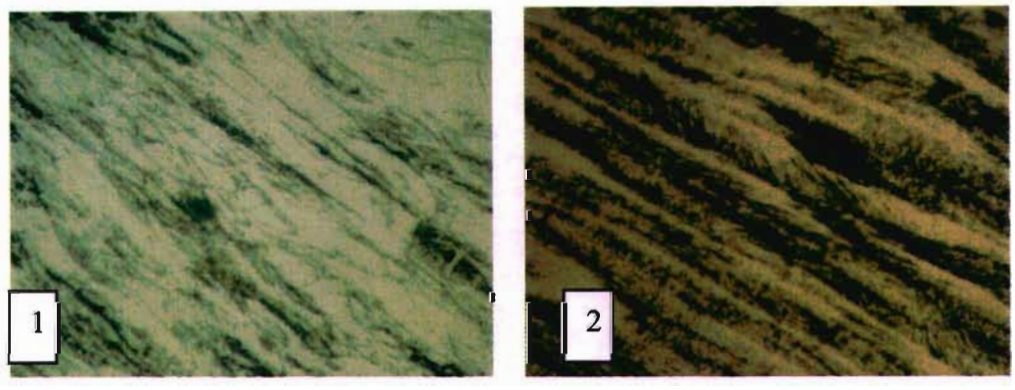

Figure 3.31 Microstructure of Alloy 3/2 (1) and 3/3 (2) after tensile test showing martensite (strain induced = dark) and retained austenite, 400 X

The metallographic analysis of Alloys 3/2 and 3/3 shows the same characteristic elongated grains as Alloys 1 and 2, with a satisfactory increase in the martensitic phase after any kind of plastic testing, as seen in figures 3.20 and 3.31. There is however not a completely austenitic structure after material processing (warm rolling) as seen in Figures 3.29 (1 and 2).

3.5.3 Conclusion

Alloy 3/2, which is a Mn based alloy, has a large incubation strain period and no stress induced martensite transformation. The strain induced martenstic phase transformation starts only after the material plastically yields (see Figs 3.24-3.26). As before this is unacceptable for the application in question. This same alloy also has lower mechanical properties than required for the aircraft wing bolt application (see Figs 3.24-3.26 and Table 3.9). The ferromagnetism apparent after thermo-mechanical processing means that the ferrite phase must have precipitated during alloy manufacturing, therefore reducing the quantity of metastable austenite available for transformation during deformation (see Fig. 3.29). It is however interesting to note that the Mn base TRIP steel responded well to the PDA, since this type of alloy has not been warm worked before. The yield stress of Alloy 3/2 increased to 800MPa with PDA, even though the plate started cracking at 75% warm reduction.

Alloy 3/3 (Mn base) has a stress-strain induced martensitic transformation starting directly with application of stress to the material, but this material is not strong enough for the aircraft bolt application with the yield stress σ_y = 850 MPa only (see Fig 3.27 and Table 3.9). It may however be considered for other smart structural applications.

3.6 Alloy 4 test results

3.6.1 Chemical analysis results

After warm rolling (at 550°C) to 75 % reduction, the chemical composition of Alloys 4/2 had a 0.29 % C content, while the expected carbon content is 0.35% C. Alloy 4/3 achieved the expected carbon content of 0.35%, (see Table 3.10). Expected Ni and Cr contents were also achieved.

Table 3.10 Alloys 4 chemical analysis results after processing

Element	C	Si	Mn	P	S	Cr	Mo	Ni	Fe
Target	0.35	0.50	1.00	-	-	12.0	-	9.00	Bal.
Alloy 4/2	0.29	0.56	1.13	0.005	.007	11.6	0.01	9.48	Bal
Alloy 4/3	0.35	0.58	1.64	0.11	.012	12.0	-	8.89	Bal.

3.6.2 Tensile test results

Samples for tensile testing were prepared in a similar manner to previously tested Alloys 1/3-3/3 of this experimental melting (Chapter 2 section 2.6). Two offset Samples 4/2 (see Fig 2.9 and 2.10) were tensile tested and the average yield stress was 1100 MPa, while the tensile strain varied from 17 to 23%. The magnetic susceptibility varied from 0.05 (from the surrounding material during tensile test) to 0.175 units (see Fig 3.32-3.33 and Table 3.11), and the strain induced phase transformation started before the material plastically yielded (see Figs 3.32-3.33). For the 54 mm gauge length sample, which was tested without magnetic change monitoring, a yield stress of 1150 MPa (see Fig 3.34 and Table 3.11) was achieved. This suggests that the Alloy 4 chemistry is extremely promising for the aircraft bolt application.

Tensile tested samples Alloy 4/3 yield at a stress of 1050 MPa, with a strain of 7.7% and the magnetic susceptibility varied from 0.02 - 0.11 (see Fig 3.35 and Table 3.11).

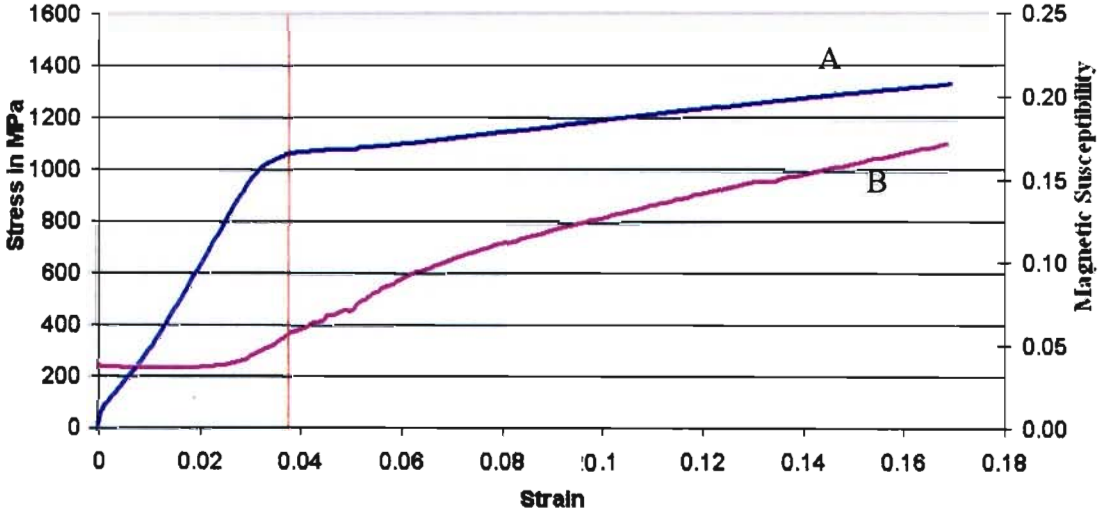

Figure 3.32 Stress-strain A and magnetic susceptibility - strain B curves for Alloy 4/2 Specimen 1 (tensile test)

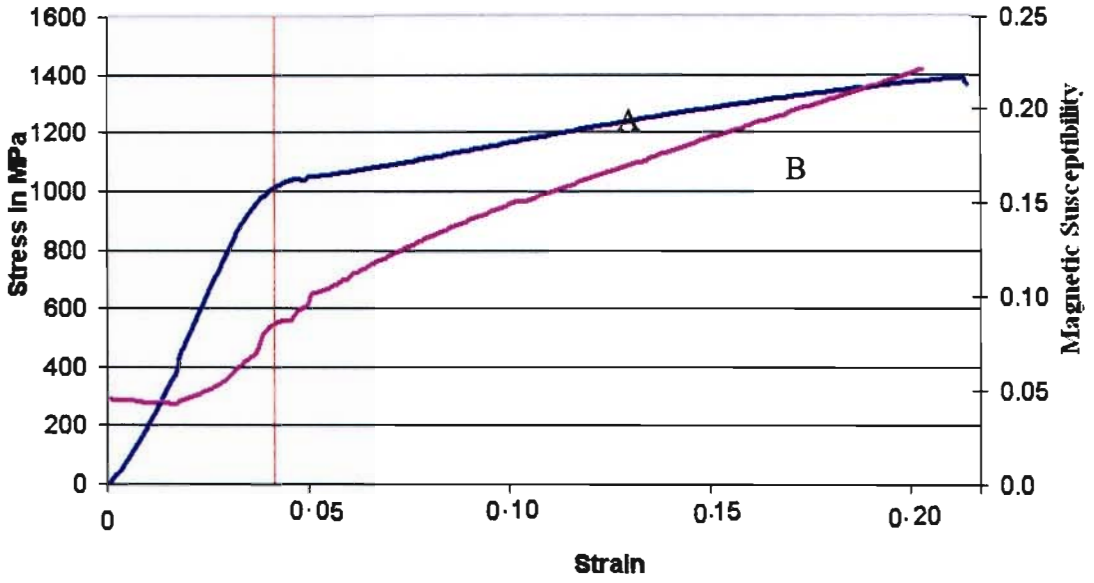

Figure 3.33 Stress-strain A and magnetic susceptibility - strain B curves for Alloy 4/2 Specimen 2 (tensile test)

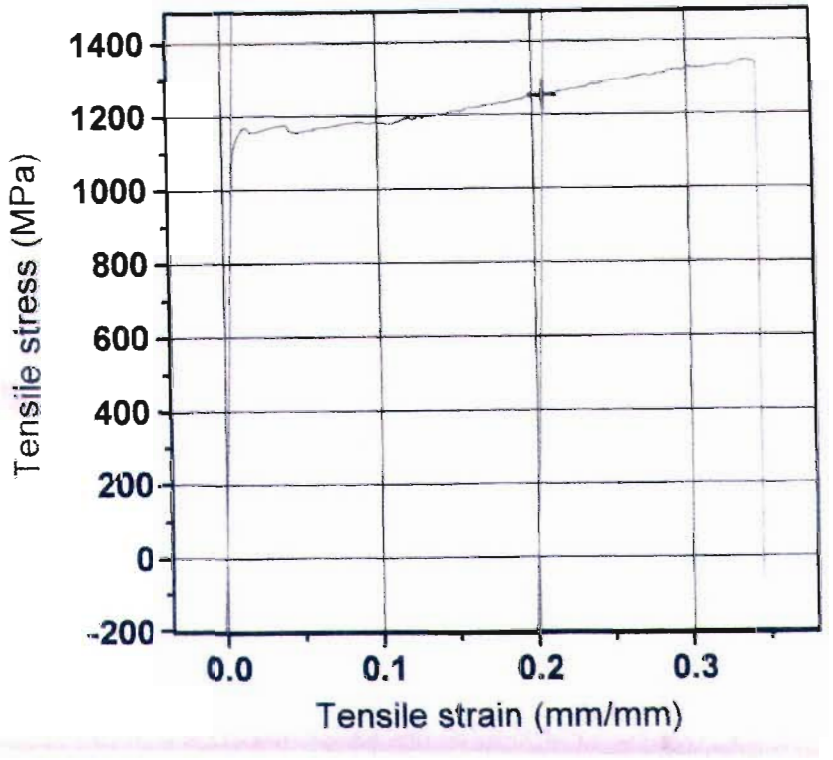

Figure 3.34 Mechanical properties, Alloy 4/2 (54 mm gauge length sample)

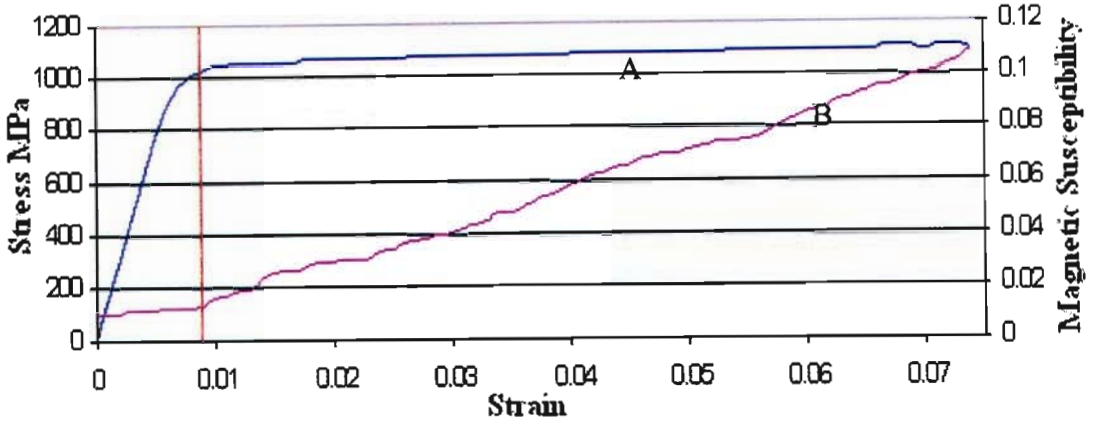

Figure 3.35 Stress-strain A and magnetic susceptibility - strain B curves for Alloy 4/3 Specimen 2 (tensile test)

Table 3.11 Room temperature tensile properties for Alloy 4

Specimen ID	% PDA	Yield stress MPa	Final stress MPa	Initial Ind.	Final Ind.	% Elongation
1 (4/2)	75	1100	1350	0.05	0.175	17
2 (4/2)	75	1050	1400	0.05	0.22	23
3 (4/2)	75	1150	1340	0.0007 (MS)	0.018 (MS)	35 (54mm G.L.)
1 (4/3)	75	1061	1075	-	-	11
1 (4/3)	75	1050	1103	0.02	0.11	7.7

Tensile Specimen 1 of Alloy 4/2 failed at 45° in a brittle fashion with no cracks and no localised necking, see Fig 3.36 (1), while specimen 2 shows a v-notch with a brittle failure out of gauge length see Fig.3.36 (2). The specimen with 54 mm gauge length shows a brittle v-notch fracture and V-cracks are present along the gauge length, see Fig.3.36 (3). The lack of localized necking is consistent with a high level of martensitic transformation.

The broken tensile sample Alloy 4/3 shows a 100% brittle failure without cracks along the gauge length and no localized necking, Fig 3.36 (4).

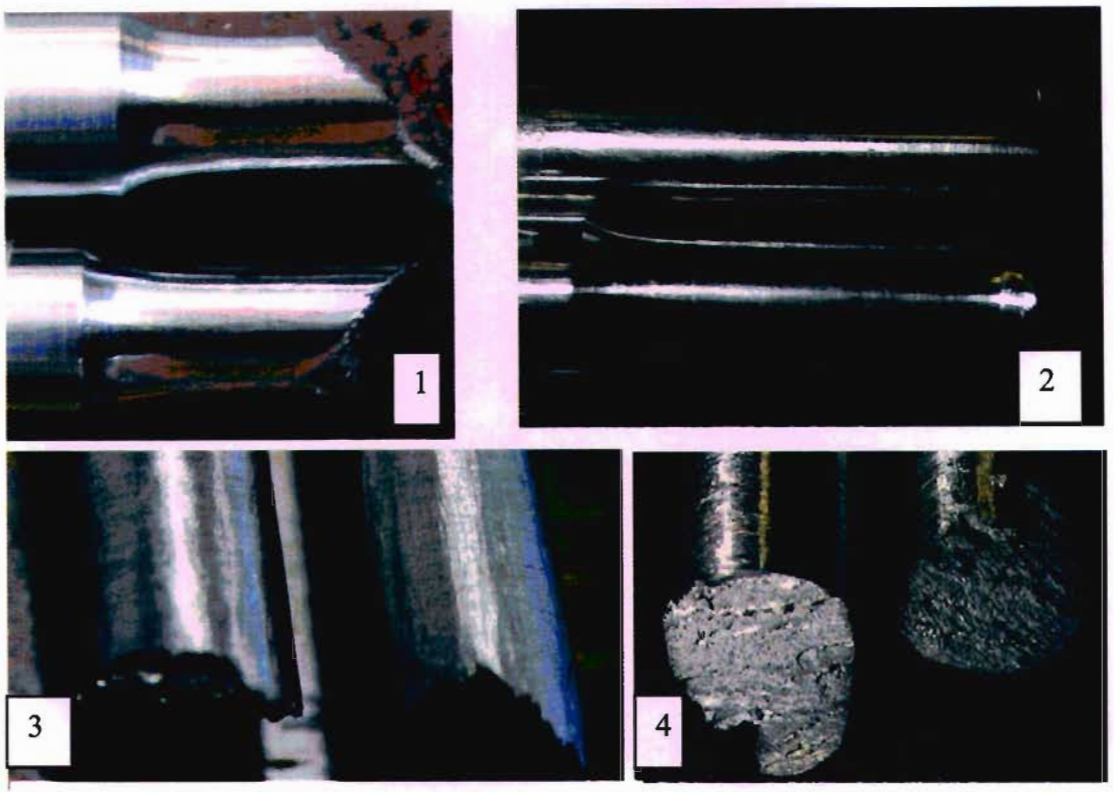

Figure 3.36 Specimen 1 and 3 (4/2) brittle failed at 45° while 2 (4/2) brittle failed with a V-notch, 3 (4/2) and 4 (4/3) is showing a 100% brittle failure. All specimens present no localized necking

3.6.3 Compression test results

The compression tests of alloy 4/2 followed the same procedure. Again the strain induced martensite transformation occurred before the material plastically yielded as had happened for the tensile test of this Alloy 4/2 (see Fig.3.38). The tested compression samples showed definite slip band lines (see Figure 3.37).

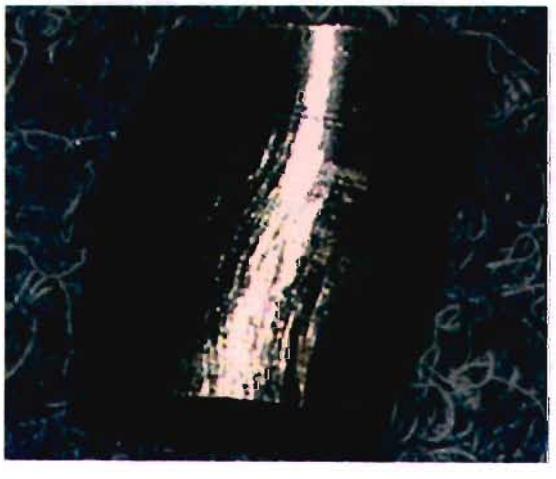

Figure 3.37 compressed tested sample showing definite slip band lines, Alloy 4/2

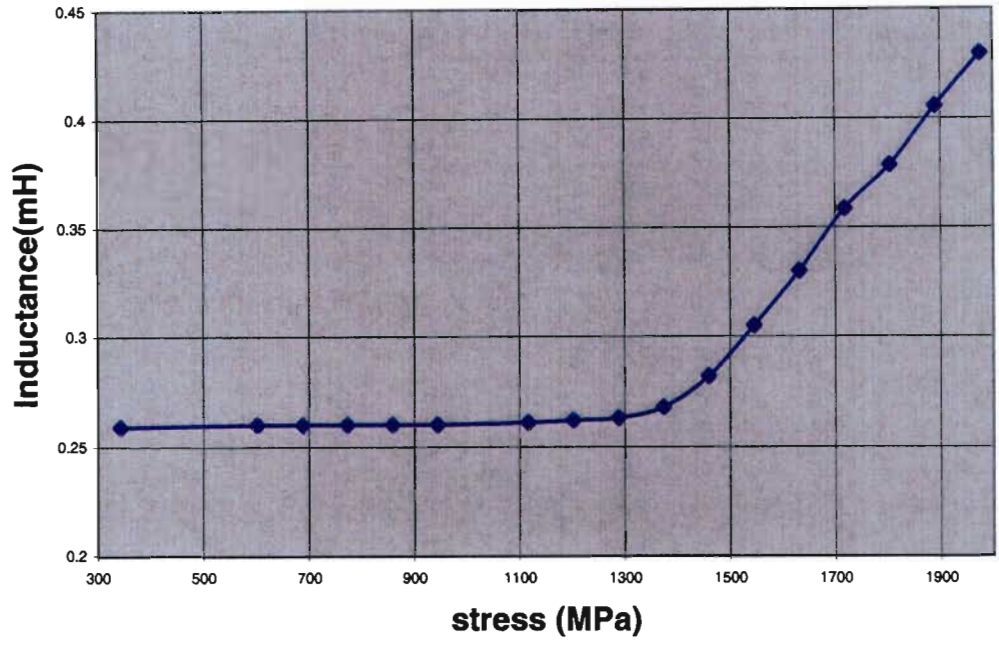

Figure 3.38 Stress versus magnetic susceptibility as evidence of strain induced phase transformation (compression test), Alloy 4/2

3.6.4 Metallographic analysis results

The microstructure analysis of as-received Alloy 4/2 and 4/3 shows the same microstructure as was found in Alloys 1/2, 2/2, and 3/2, and similar results for similar tests, as presented in Figs 3.39-3.41. There is a difference in the amount of martensite evident in figure 3.41 (1 and 2), as it seems to be greater than for alloys 1/2, 2/2 and 3/2.

Microstructure study on an as-received Alloy 4/3 (2) (before tensile testing) shows elongated austenitic grains with a small amount of martensite as seen in Fig 3.39 (2). Tensile tested Alloy 4/3 presents a microstructure comparable with those observed in previous tensile tested Alloys 1/3-3/3, consisting of strain induced martensite (dark) which increased after tensile testing and retained austenite, see Fig 3.41 (2).

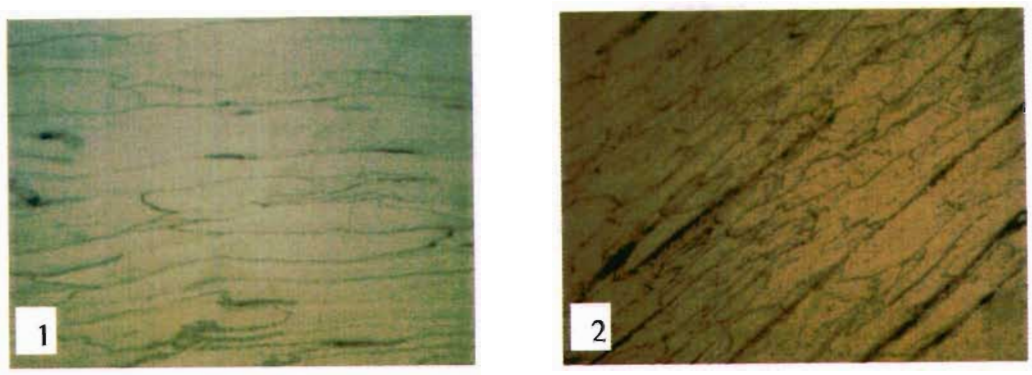

Figure 3.39 Heavy-worked microstructure showing elongated austenitic grains and Alloy 4/2 (1) and 4/3 (2) before deformation 400X

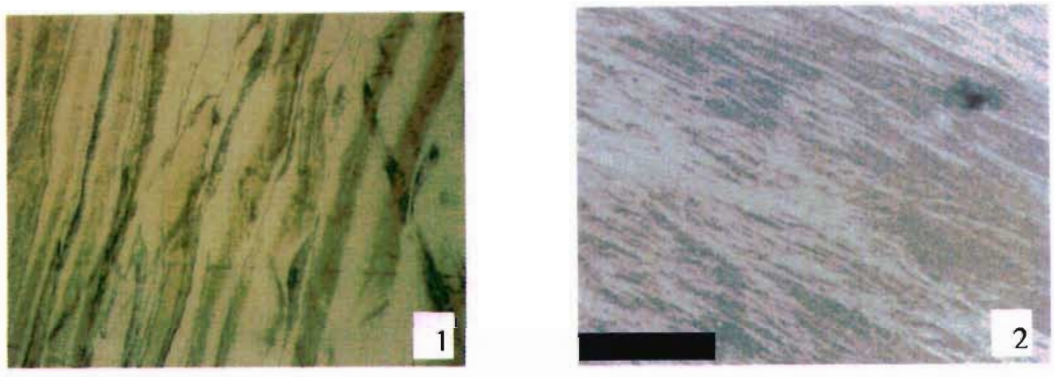

Figure 3.40 Microstructure of Alloy 4/2 after compression test (1) at 400X and tensile test (2) SEM image, both showing martensite appearing on slip bands (strain induced=dark in (1) and white in (2)

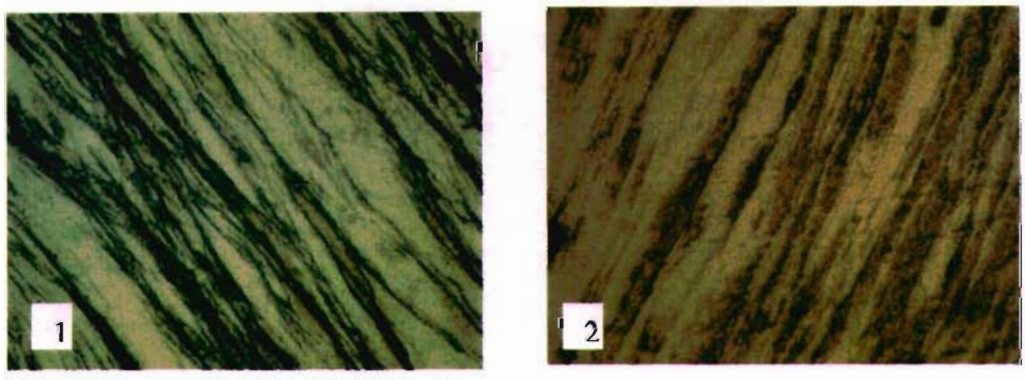

Figure 3.41 Microstructure of Alloy 4/2 (1) and 4/3 9 (2) after tensile test showing martensite (strain induced=dark) and retained austenite, 400 X

3.6.5 Impact test results

The promising results of tensile and compression testing prompted both impact testing and further cooling tests. Impact samples from Alloy 4/2 struck at room

temperature display impact resistance from 70 to 90 Joules, and those struck at -50°C display higher impact resistance from 106 to 144 Joules, (see Table 3.12).

Table 3.12 Impact test results Alloy 4/2

ID	Lateral expansion		Shear %		Impact resistance (Joules)	
	20°C	-50°C	20°C	-50°C	At 20°C	At -50°C
Alloy 4/2	0.24	0.22	100	100	90	106
	0.21	0.12	100	100	98	144
	0.16	0.28	100	100	70	118

This material shows elevated impact resistance, which is very good. The fact that impact resistance increases with a temperature decrease is associated with the thermal martensite phase transformation occurring in the vicinity of –50°C (M_S temperature). This was verified by cooling using dry ice (in contrast to alloy 2/2) as was done for Alloy 4/2 and results are seen in Figs 3.44-3.45 where Samples A and B show no change in the magnetic susceptibility with the temperature decrease.

The Impact samples broke with brittle v-fracture at room temperature, see Figure 3.43 (1), and with shear v-fracture at –50°C see Figure 3.43 (2)

Broken specimens were attracted by a permanent magnet after impact test, which confirms that strain induced martensite transformation occurred during the impact test, (see Table 3.13 and Fig 3.42).

Table 3.13 Magnetic susceptibility measurement before and after impact test

ID	Sample's magnetic susceptibility before impact test		Sample's magnetic susceptibility after impact test on fracture area	
	At room temperature	At –50°C	At room temperature	At –50°C
Alloy 4/2	0.000362 0.000393 0.000218		0.003468 0.007124 0.005650	
		0.001446 0.000432 0.000541		0.01215 0.01489 0.01113

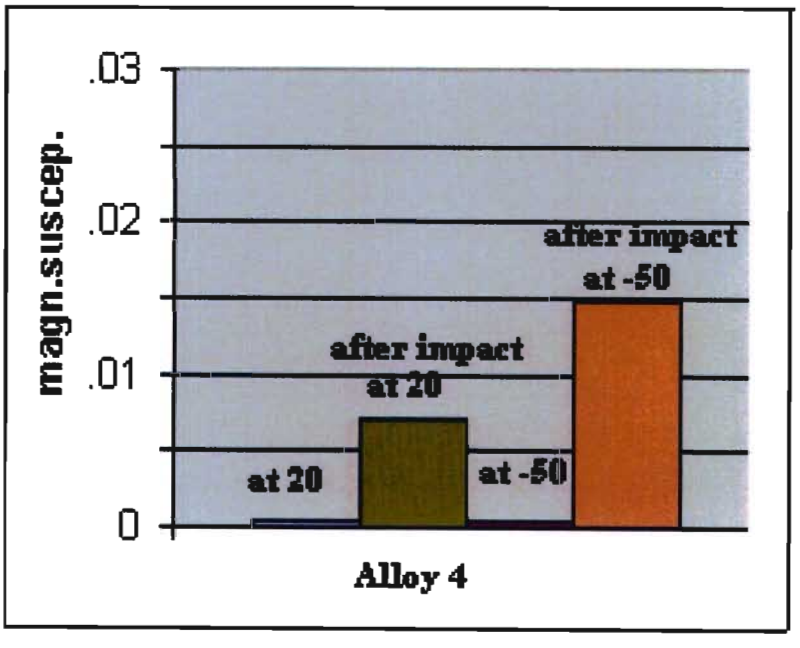

Figure 3.42 Magnetic susceptibility changes with temperature and impact testing temperature Alloy 4/2

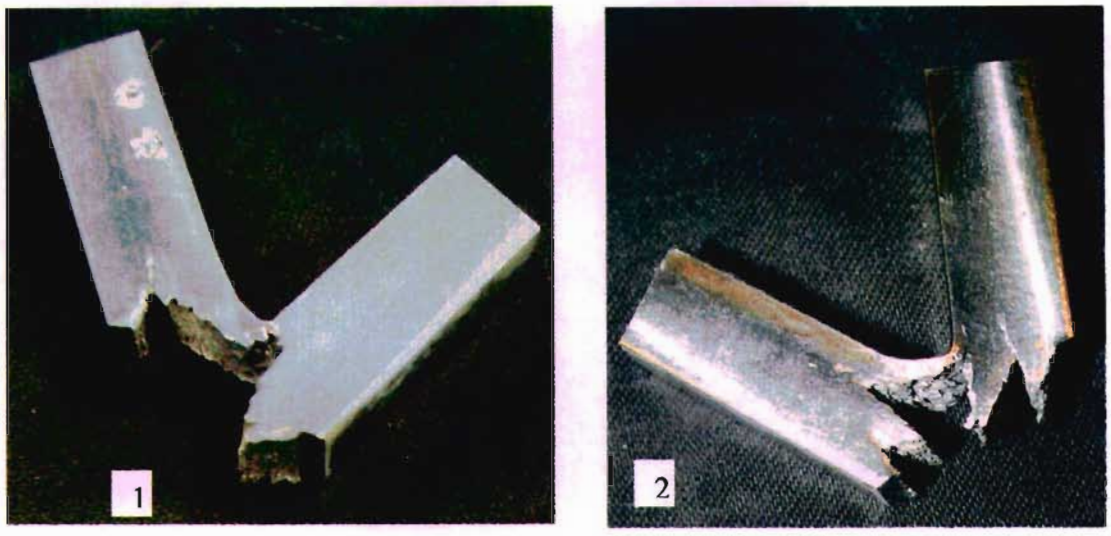

Figure 3.43 Impact v- notch fracture Alloy 4/2(1) at room temperature and (2) at -50°C

3.6.6 Spontaneous martensite formation by cooling

Specimens (Alloy 4/2) were cooled to subzero temperatures using dry ice. There was no measurable change in the magnetic susceptibility right down to -80°C for samples A and B (see Figs 3.44-3.45), from which it can be inferred that there was no thermally induced transformation.

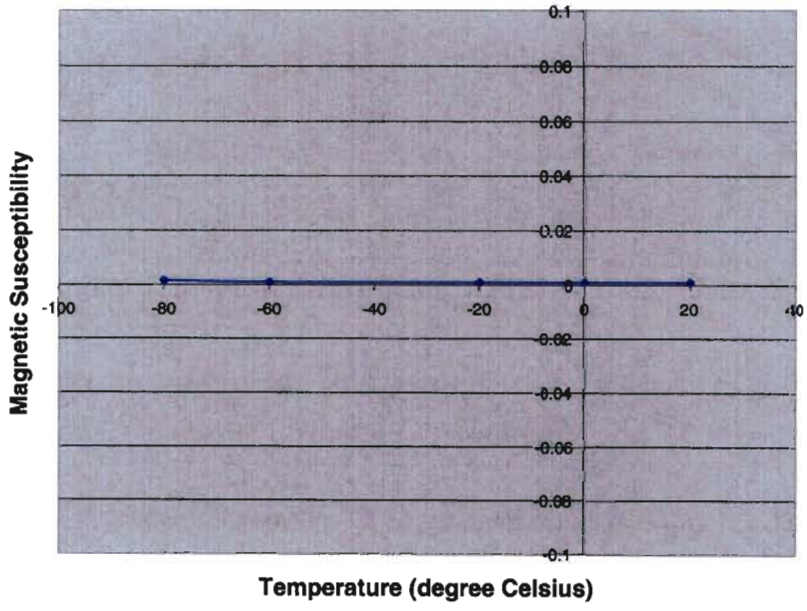

Figure 3.44 Magnetic susceptibility at different temperatures Alloy4/2 Sample A

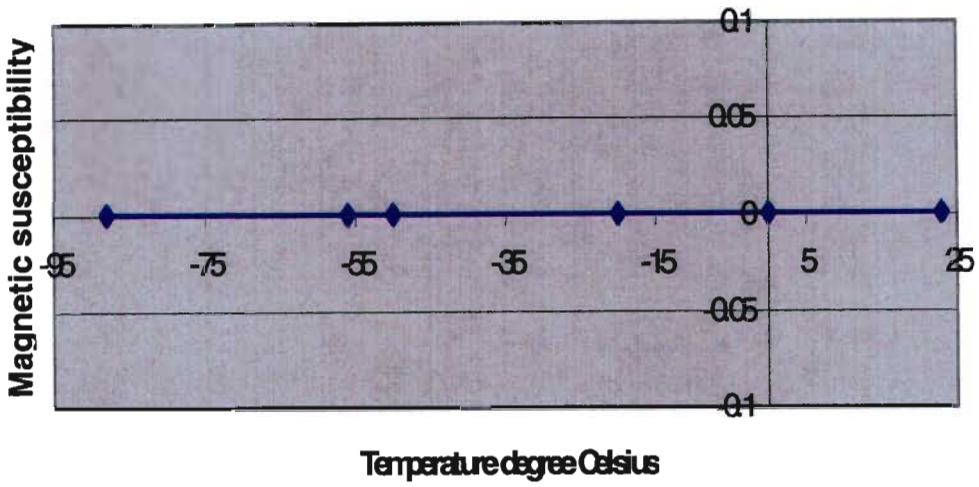

Figure 3.45 Magnetic susceptibility at different temperatures Alloy4/2 Sample B

3.6.7 Conclusion

Extensive testing of Alloy 4/2 shows that the material displays stress - strain induced martensite transformation with a small incubation strain. Stress induced martensitic phase formation started before the material plastically yielded (see Figs 3.32-3.33 and 3.38), which is very good for a smart strain sensor, as the structural element will give warning before it fails. It has the requisite mechanical properties required for the aircraft wing bolt application (see table 3. 14 where is compared to AISI 4340) and it has some work hardening ability. Alloy 4/2 was also non-ferromagnetic after thermo-mechanical processing (see table 2.2), which means that the austenitic phase is stable during alloy processing. This composition is therefore a good strain memory alloy as it transforms during deformation, and is thermally stable above –80°C (see Figs 3.44 and 3.45), meaning that it will not give false warning while in service as an aircraft bolt where temperature changes are bound to happen.

Alloy 4/3 has been melted with the same chemical composition as was selected in the beginning of this study. It has no incubation strain as strain (or stress) induced martensite transformation starts directly with application of stress to the material, (see Fig 3.35). The presence of the strain-induced matrensite formation is also proved by metallographic study (see Figs 3.39-3.41) but no apparent work hardening in Figure 3.35. Furthermore this material is strong enough for the aircraft bolt application with σ_Y =1050 MPa.

Table3.14 Mechanical properties of quenched and tempered nickel-chromium-molybdenum alloy steel (AISI 4340) compared to Alloy 4/2 of this study

Alloy ID	Tempering T ° C	Yield strength MPa	Tensile strength MPa	Elongation %
Alloy 4/2	-	1050	1400	10
AISI 4340	427	1368	1468	10

All TRIP steel manufactured experimentally during this study, was produced in the form of 13 mm plate. This plate is insufficient for manufacturing a real aircraft wing bolt with 37 mm bolt-head diameter. The processing of a warm rolled TRIP steel plate of such thickness is expensive because it cannot be done in any laboratory in South Africa. For this reason a scaled-down prototype was manufactured from some available 22 mm thick, low strength TRIP steel. It is clear that this bolt prototype will not respond mechanically as a bolt that will be manufactured from the proper high strength material of this study, also the phase transformation will be different, but it will help us to design and test the **electronic device** which will be used on the future bona fide smart aircraft bolt. The design of this subscale bolt prototype is shown in Chapter 4; it was tensile tested, and results are presented in Section 4.

CHAPTER 4

SMART BOLT PROTOTYPE DESIGN

A photograph of a C-130 aircraft is shown below (see Fig 4.1). The arrows depict the position of the wing bolts that are the subject of this study.

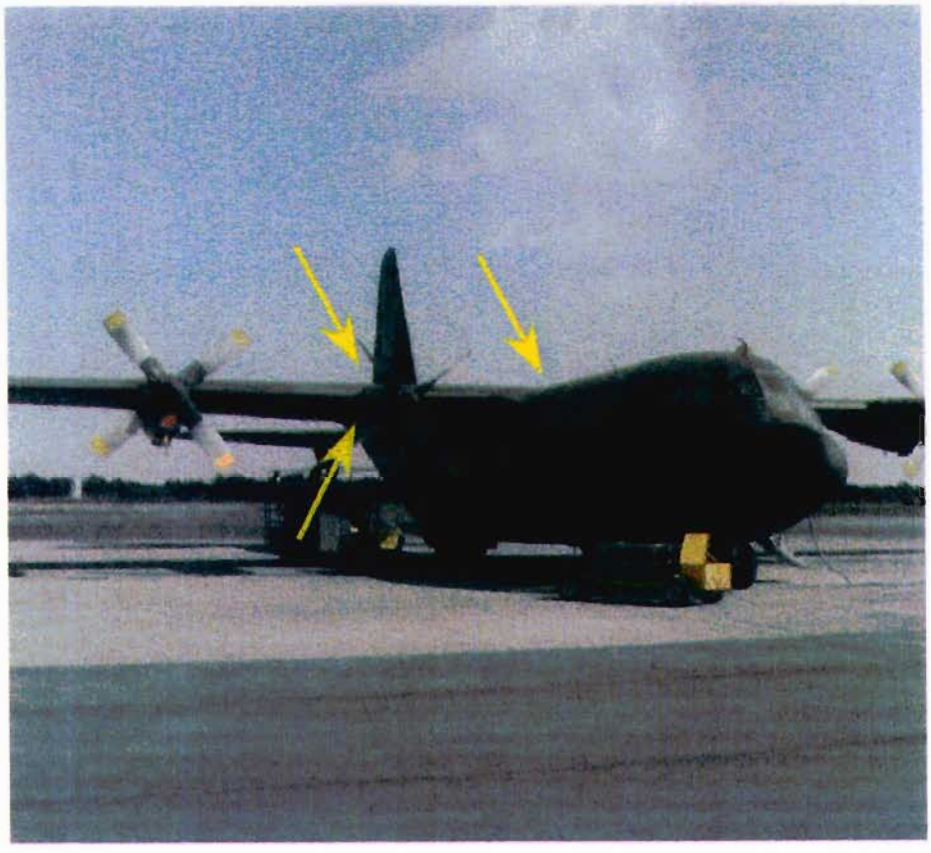

Figure 4.1 Location of high stressed wing bolt on C130 aircraft [94]

A wing bolt clamps the wing to the fuselage (see Fig 4.2). The bolts are designed to operate in tension [89]. In reality, the bolts do not experience a static tensile failure, but rather a fatigue failure that initiates at the first thread of the bolt. In order for this typical crack to initiate however, a small damage zone ahead of the site must plastically yield. Thus, because of the damage mechanisms at work, the strain memory alloy will transform and give the warning. Care will also be taken to select alloys that transform before the yield (stress-assisted) point. The scope of this work therefore revolves around producing the requisite tensile strength (for the military

specification requirement) and the correct transformation characteristics for the smart aircraft bolt. The fatigue response of the candidate alloys is under investigation and forms the focus of a different study.

When a bolt is put in service, it experiences one or more working loads which are applied to the bolt in any combination of static and cyclic tension and shear loads. The military specification sets a required tensile load as well as ductility. Ordinary aircraft bolts for a C-130 cargo plane are shown in Figure 4.3. These aircraft bolts are simple threaded fasteners with geometry as shown in Figure 4.3. Currently bolts are manufactured from high strength steel. The bolts operate in highly stressed conditions and they must periodically be inspected for wear and fatigue.

This inspection is a time consuming and expensive procedure. The replacement of these bolts by smart bolts capable of being investigated in situ (regarding of their level of damage) is the reason for the development of a high strain memory alloy, which forms the topic of this study. While investigating the processing of high strength TRIP steel materials with similar or better mechanical properties than AISI 4340 (normally used for manufacturing these bolts), a smart aircraft bolt prototype made from low strength TRIP steel with strain–induced transformation properties was also designed for the testing of various smart monitoring concepts. Those concepts include various off-the-shelf monitoring devices as well as custom-designed electronic circuitry.

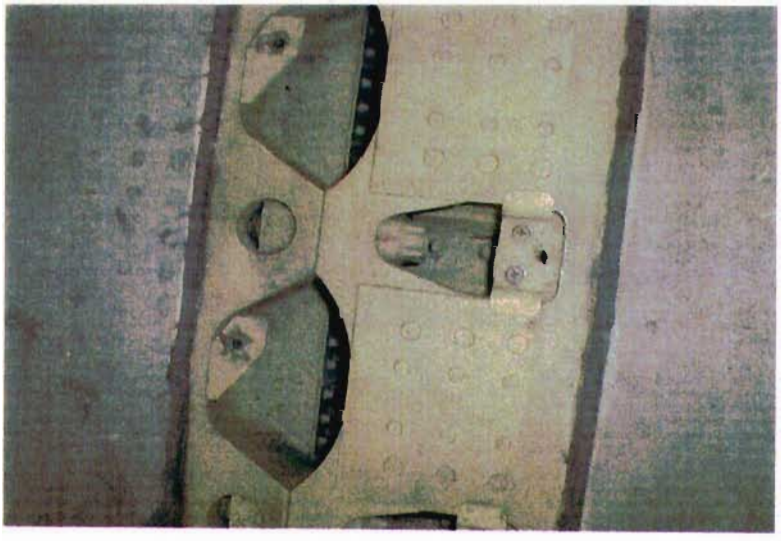

Figure 4.2 Bolt located in the wing structure, close up view [94]

Figure 4.3 Top and bottom aircraft wing bolts [94]

4.1 Calculations of Design Data

A number of 13 mm thick high strength smart material plates were manufactured. This material was the largest size that could be experimentally produced with 80% warm work, but it is too small for full-size aircraft bolt fabrication. The only material available for prototype manufacture is 22 mm diameter low strength TRIP steel with σ_y=450 MPa, σ_{UTS}=750 – 800 MPa and 25% elongation. The biggest bolt (with machined head) that can be manufactured in this material is M11x1.5 [90].

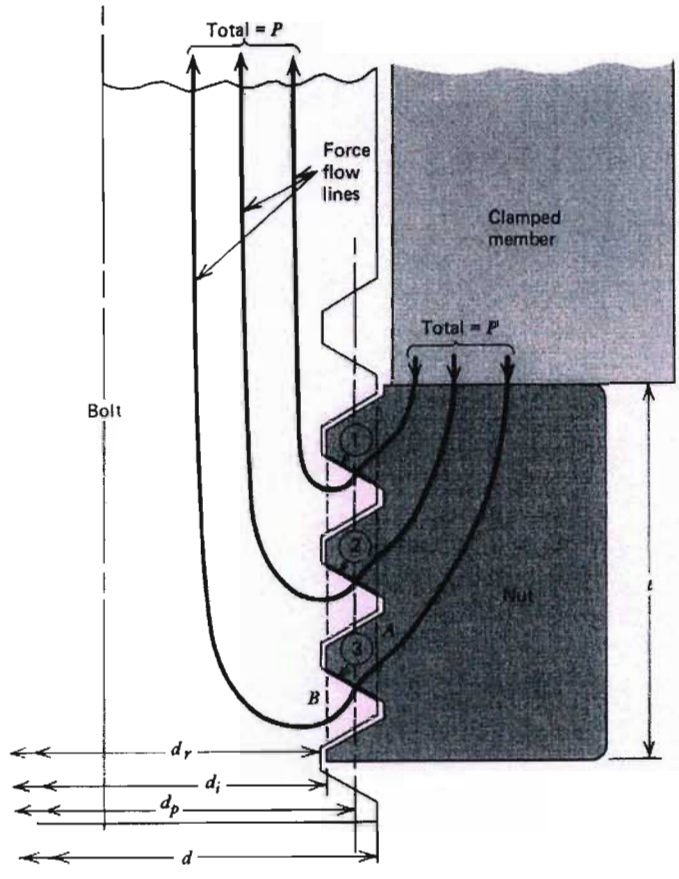

Figure 4.4 Bolt in tension, A is the shear fracture line for nut thread stripping and B is the shear fracture line for bolt thread stripping [91]

The threaded section is

$A_t = d_r^2 \times \Pi/4 = (9.5\ mm)^2 \times 3.14/4 = 70.88\ mm^2 = 71 mm^2$ (12)

Where d_r is the thread root diameter (see Fig 4.4)

A certain load level required to stretch the bolt while making the joint clamped is called preload force, it is designated by P. It is slightly more than the force required to cause plastic yield of the bolt, which is equal to the yield stress of the bolt material times the bolt thread section (σ_y A). This force is applied on the bolt joint by turning the bolt nut.

$P > \sigma_y \times A_t = 450\ MPa \times 71\ mm^2 = 31950\ N$ (13)

A sufficient overload would strip the threads from the nut along the cylindrical surface. From a geometric point view, the shear area is equal to $\Pi\ d_p\ (0.75\ t)$. The nut thickness needs to provide a balance between bolt tensile strength and thread stripping

strength if both members are made of the same material. The bolt tensile force required to yield the entire threaded cross section is:

$$F = A_t S_y \cong (\Pi/4)(0.9\ d)^2 S_y = 34639.59\ N \quad (14)$$

Where d is the major diameter of the thread. The bolt tensile load required to yield the entire thread-stripping failure surface of the nut is

$$F = \Pi d\ (0.75t) \quad (15)$$

$$S_{SY} \cong \Pi\ d\ (0.75t)\ x\ (0.58\sigma_y)$$

Where, t is the thickness of the nut (see Fig 4.4).

From the two equations for F, bolt tensile and stripping strengths are balanced when t is approximately 0.47d. [91]

Since the material for the aircraft bolt is ultra-high strength material, the nut is softer than the bolt so that the highly loaded first thread of the nut will deform, thereby transferring more of the load to other threads. This situation is preferred and the load is distributed along the threads [91]. The standard nut thickness is approximately 7/8d. Nut thickness is approximately $t \cong 10$ mm.

The nut material is 316 steel, with a yield strength of σ_y=206 MPa. The calculated thickness was found to be 11.18mm but for safety allowance, the nut thickness adopted is 20 mm. (see Fig 4.7)

Thus the geometrical dimension of the bolt was defined according to the available TRIP steel material (22 mm diameter bar used for other applications). An electronic sensor to measure the damage occurring in the bolt must be incorporated in it. The smart aircraft bolt will thus give information about the level of damage while interrogated in situ. An inductor was identified as the best method for measuring the magnetic permeability change accompanying the strain-induced martensitic phase transformation, which means that an inductor (coil) must be inserted somewhere within or around the bolt, without affecting the physical geometry of the bolt. The coil must also be protected while the bolt is stretched. It must have an inductance strong

enough to pick up small magnetic permeability changes occurring during the deformation of the bolt, and it must thus be located as near as possible to the highly stressed area of the bolt, where strain-induced phase transformation may occur. The use of a grooved smart bolt, with the sensor coil inserted in the groove would be the simple option, but the coil was not fully protected and may stretch or break when the bolt is stretching. Aviation authorities also had reservations about the use of a grooved smart bolt. In order to resolve this problem a smart washer and smart nut have been introduced, in which an inductor is inserted (see Figs 4.7 - 4.8).

4.2 Smart Washer

4.2.1 Principle of action

The smart aircraft bolt designed is shown in Figs 4.11 - 4.12. By using the principle of an inductor inserted into a washer or nut (smart washer and smart nut from Fig 4.5 - 4.8) as the strain sensors, the strain (damage) can be recorded by reading an inductance meter connected to the washer or nut coil, located on an approved area of the bolt identified to have the highest stress concentration.

The concept of inductor is simplified by considering an inductor connected to an AC source. As the alternating current passes through the coil, an alternating magnetic field is set up, in turn producing a voltage. The relationship between these quantities may be expressed as:

$$v = -L\frac{di}{dt} \qquad (16)$$

Where v is the voltage

i is current (Amps)

t is time (sec) and

L is inductance (Henry)

The inductance $L = \frac{d\phi}{dt}$, and if the coil has N windings $L = N\frac{d\phi}{di}$. (17)

One can then add a constant C_1 related to the dimension of the core of the coil, and the field configuration and the equation (17) in the above expression becomes:

$L = \frac{N^2}{C_1} x \frac{B}{H}$ where $\frac{B}{H}$ is the permeability of the core. (18)

Paramagnetic core materials like austenite have permeability higher or equal to that for a vacuum ($4\pi x10^{-7}$H/m), while ferromagnetic materials (martensite) have permeability far greater than a vacuum. The above principle is used to monitor the health of smart wing bolts using an inductance meter reading.

In Figures 4.5- 4.7 one can see the designed smart washer and nut drawings which show clearly the small groove that houses the inductor, which is now fully protected (see Fig 4.6 (2)).

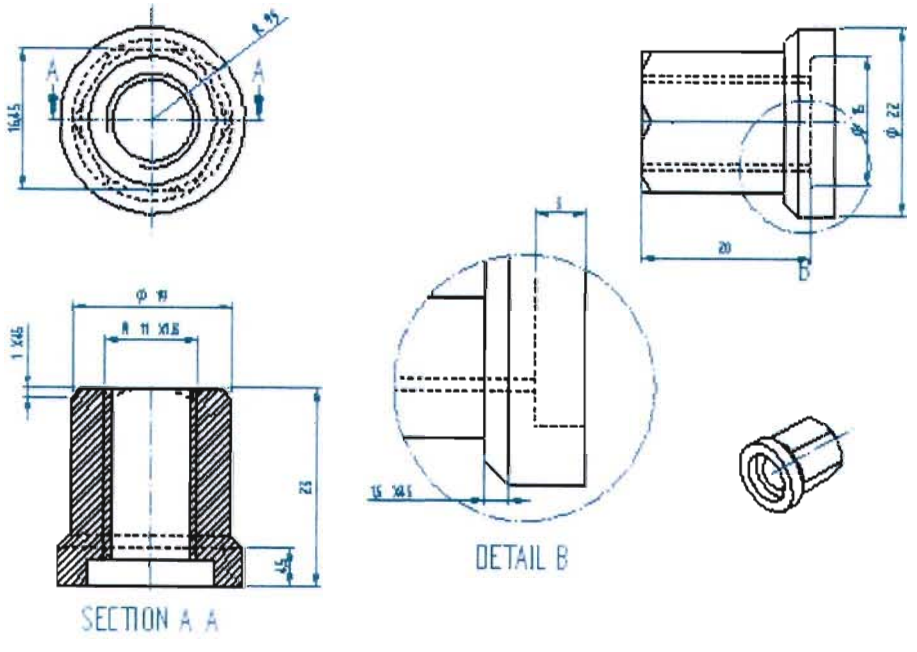

Figure 4.5 Smart nut drawing

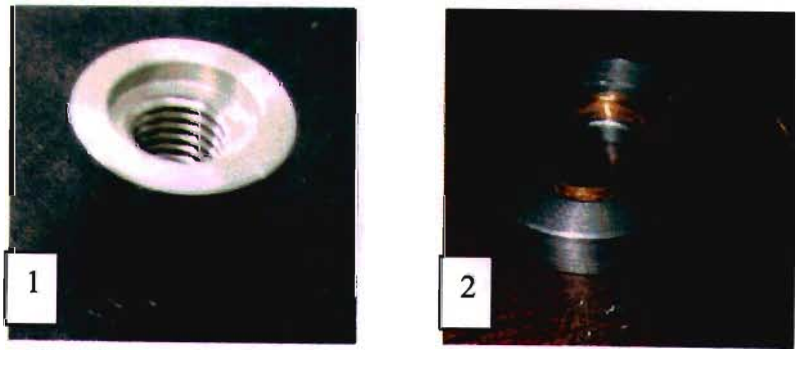

Figure 4.6 Smart nuts (1) and Smart washer (2) (with inserted coil: 149 turn, Φ_{wire}= 0.019 mm) for smart aircraft bolt prototype

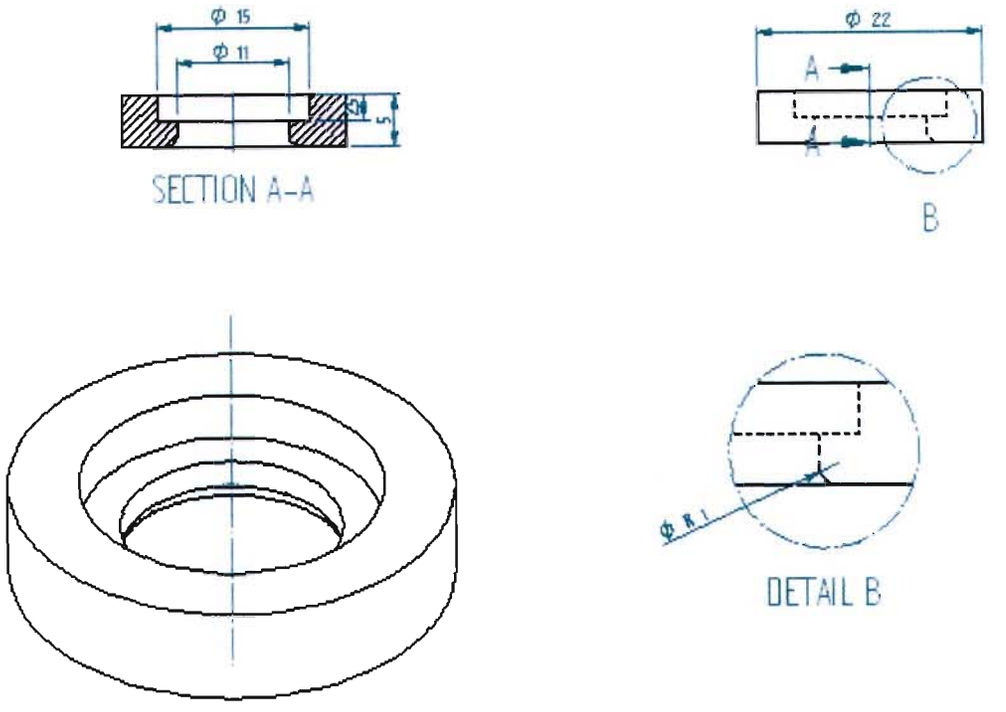

Figure 4.7 Smart washers drawing

The introduction of a smart washer or a smart nut permits the use of a wing bolt with the same geometry as before. Smart wing bolts with grooves were also tested in order to demonstrate the effectiveness of damage sensing and for comparison of the grooved and un-grooved bolts. The location of the strain sensor coil was a challenging matter, as the coil must be placed at a high stress concentration location. This has been addressed by using Finite Element Analysis data [92-94] and service data from an Aircraft Company.

4.2.2 Inductor Location

Various model prototypes were considered when investigating the correct location for the inductor:

1. Simple bolt without any stress concentrator
2. Bolt with groove under bolt head
3. Bolt with groove on the first thread

The analysis is complex as bolts are subject to cyclic loading service (take off and landing), the actual tensile strength of the body of the bolt would be much smaller

than the required load for simple tensile failure. Fatigue failure is anticipated at stress concentrations. Stress concentrations are expected at:

1. The root of the first engaged thread
2. The thread run out point
3. The fillet between the shank and the head

The Air Force workshop and inspection personnel report that failure occurs at the first engaged thread [94]. Finite Element Analysis for a bolt with a centrally drilled hole shows a high stress area on the first engaged thread.

In order to verify the stress distribution through the bolt, Finite Element Analyses performed by Johnson [93], and Francis [94] for a bolt with centre drilled hole Fig 4.8, and [92] a fully solid bolt with 3 mm radius at head to shank transition, Fig 4.9, were used. Both above cited cases (see Fig 4.8-4.9) show higher stresses at the first engaged thread.

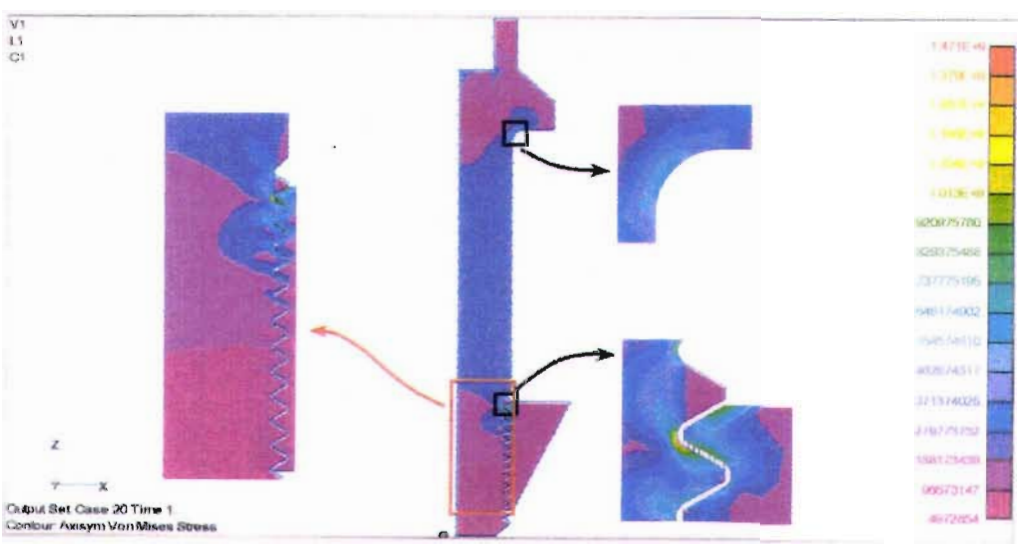

Figure 4.8 Stress distributions on bolt and nut model with 5mm drilled hole through the centre of the bolt [94]

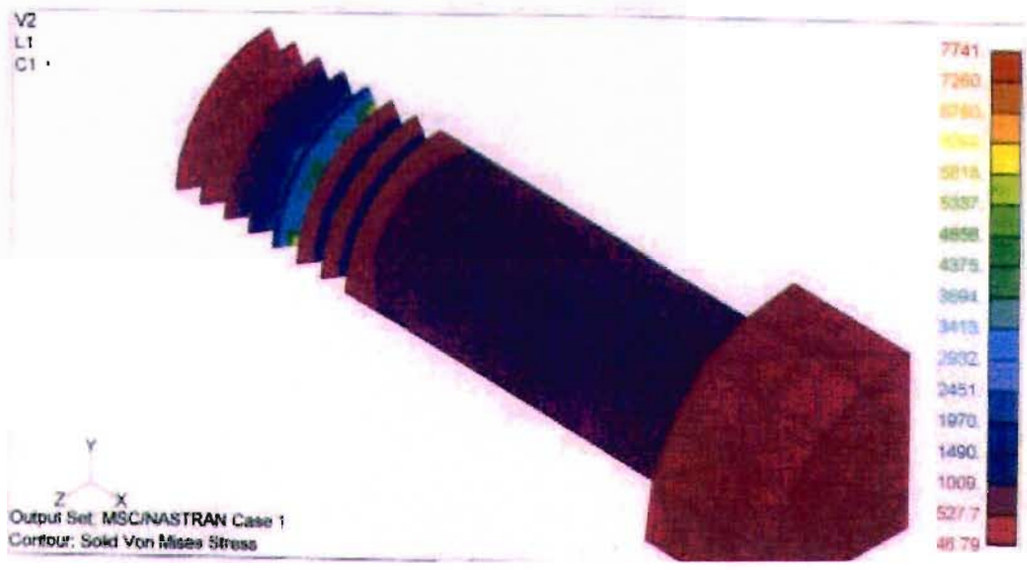

Figure 4.9 Stress distributions on a full solid bolt with 3 mm fillet radius at head to shank transition [92]

The final smart aircraft bolt is shown in Figures 4.10 and 4.11 (1) with coil wire ends to pick up the strain state of the bolt. The sensor coil is located at the first engaged thread. As was confirmed by previous work on bolt stress analysis, the bolt fails at that thread. A smart bar (without the usual bolt head) was manufactured from alloys developed in this study (Figs. 4.11 (1) - 4.12). The test results for these are presented below in Section 4.3.

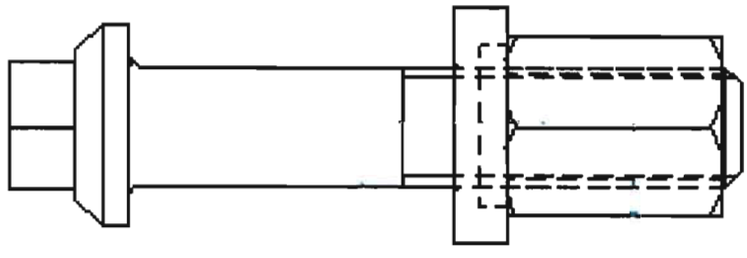

Figure 4.10 Smart aircraft bolt prototype

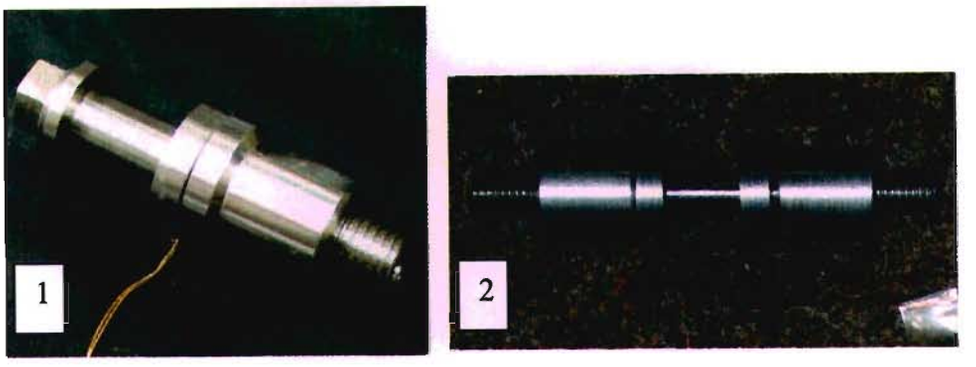

Figure 4.11 Subscale smart aircraft bolt prototype in assembly with visible coil ends (1) and Smart-bar manufactured from high strength TRIP steel (2)

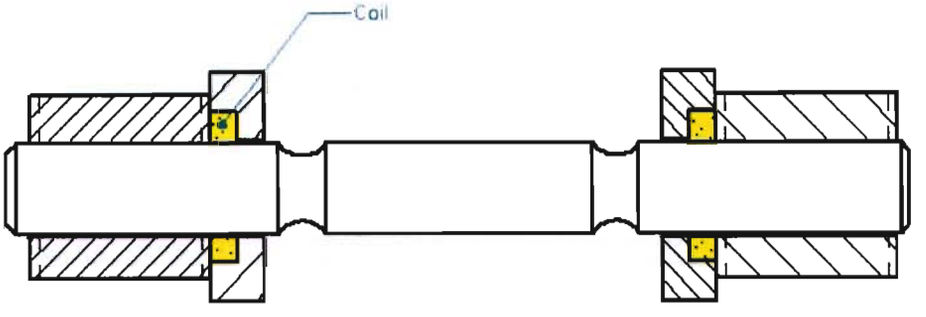

Figure 4.12 Schematic illustrations of smart bars in assembly showing the coil inserted in the smart washer

4.3 Smart Bolt Prototype Test Results

Two smart bolt prototypes one with a groove under the bolt head (see Figure 4.13), the other bolt without any groove (see Figure 4.14), were both tensile tested and strain induced phase transformation monitored during the test as it is described this section. Results can be seen in Figs 4.15-4.17, where it can be seen that substantial change in inductance (magnetic susceptibility) happens at the first engaged thread where both bolts failed (see Figs 4.15- 4.18). The strain was measured by cross-head of the tensile machine; no extensometer was used, which explain the high exaggerated value obtained during the bolt tensile test.

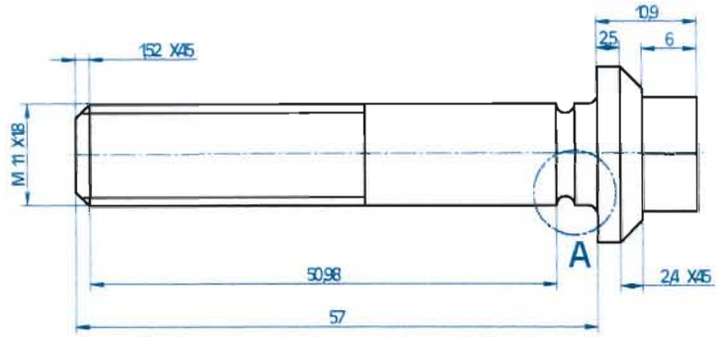

Figure 4.13 Bolt prototypes with under-head groove

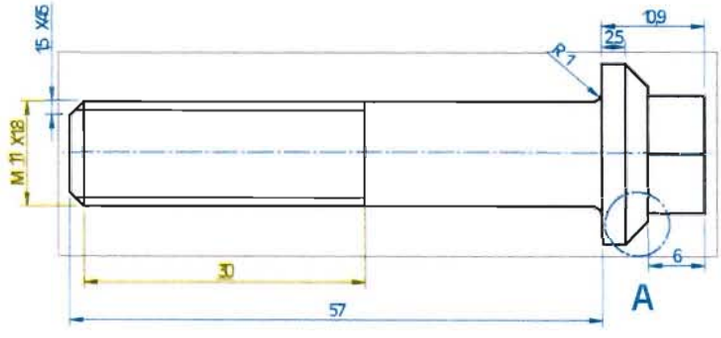

Figure 4.14 Bolt prototypes without any groove

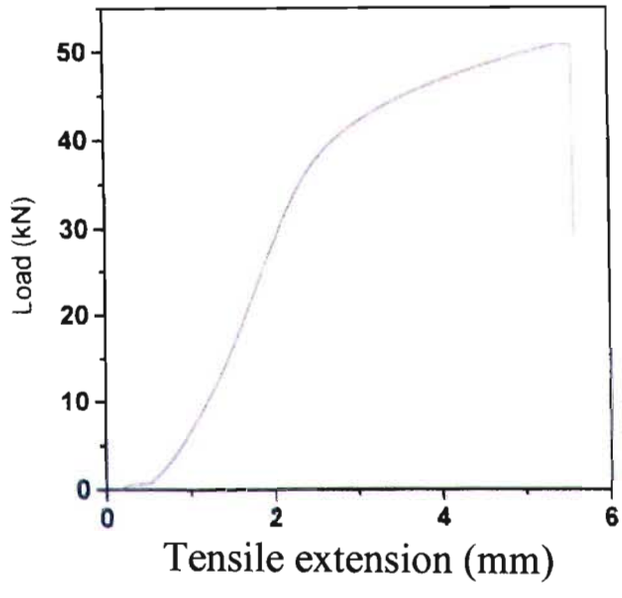

Figure 4.15 Load-cross head strain curves of the bolt tensile test

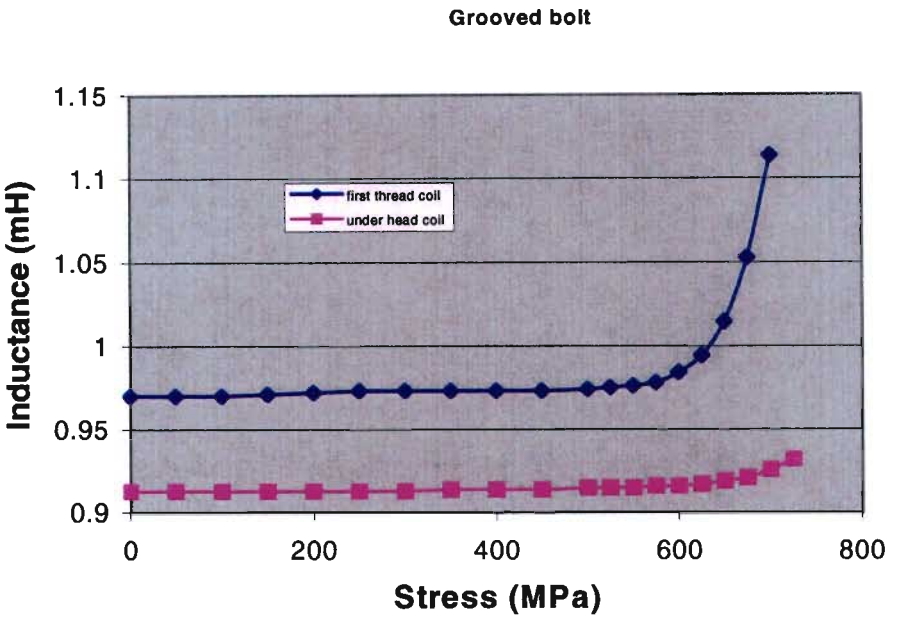

Figure 4.16 Inductance readings from the thread and under-bolt head, bolt with 1mm groove under the head (tensile test)

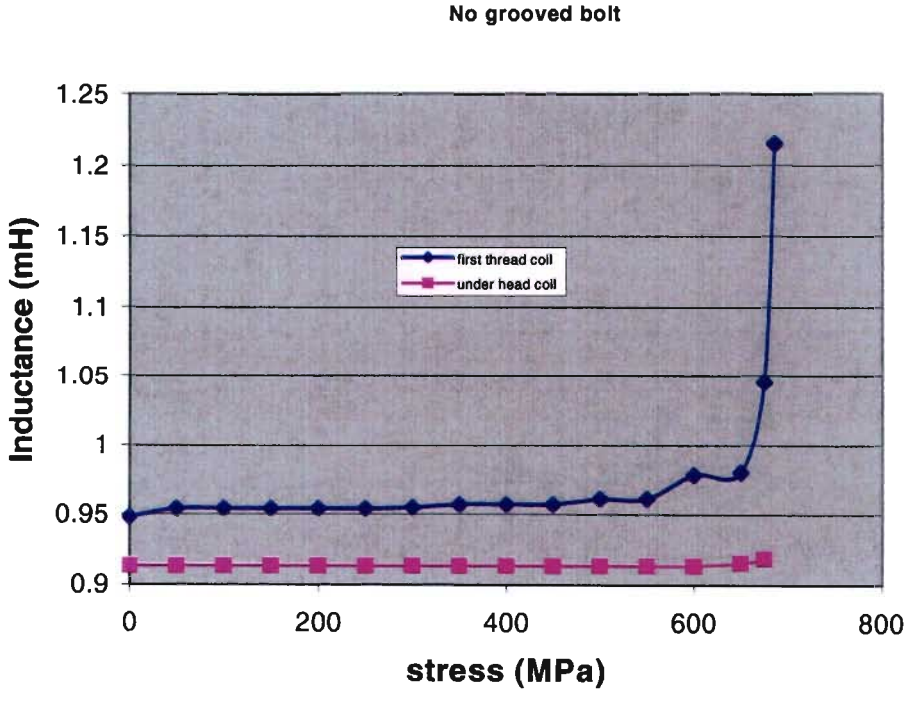

Figure 4.17 Inductance readings from the thread and under-bolt head (no-grooved bolt, tensile test)

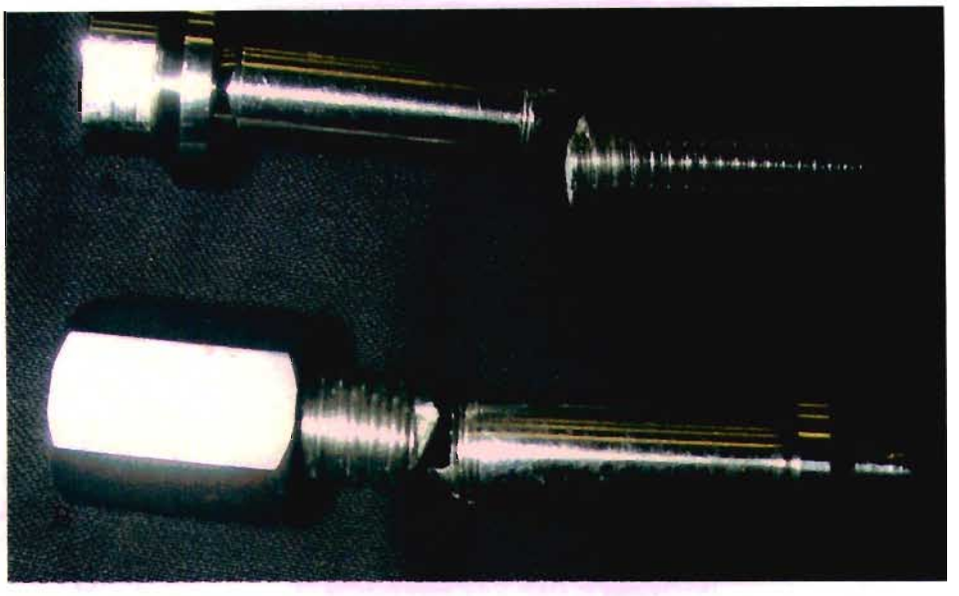

Figure 4.18 Tensile tested subscale smart bolts both failed at the first thread

4.4 Conclusion

For convenience the material used for manufacturing these smart bolt prototypes was a low strength TRIP steel, which transformed to martensite after plastic deformation had started (see Figs 4.18- 4.19).

A coil located under the bolt head would be easily accessible, but the higher stress concentration region is located at the first thread, where the bolt fails (see Fig 4.20).
The coil and washers both at the head and the thread were not damaged during tensile tests, and were even re-used for a second set of tests without breaking. The smart bolt prototype was manufactured from low strength TRIP steel only to experiment with the smart washer and bolt design to check strain sensitivity of the electronic sensing device (see Fig 4.17).

A miniature coil inserted within the washer is sensitive to the magnetic permeability changes accompanying the strain induced martensite transformation. see Figs 4.18-4.19.

And this electronic device will be used for measuring damage on an authentic smart aircraft bolt.

CHAPTER 5

DISCUSSION

The four candidate alloys for the smart aircraft bolt prototype were melted in small quantities using research laboratory facilities, and processed (also using laboratory equipment) by warm rolling to a 75% reduction in thickness. The difficulties experienced in the first attempt to produce accurate melting of alloys prompted another melting of each of the alloys with closer control on melt atmosphere and processing parameters. These closer control parameters resulted in a significant improvement. The problems that arose with the accuracy of the melt chemistry were in part due to the fact that the melting was performed under laboratory conditions with no facility available to check or alter melt chemistry before casting; and theoretically one could expect that an industrial melt, which allows for chemistry checks and alterations before casting, should produce better results. It should however be noted that industrial melts with extremely tight operating windows (or tight chemical tolerances) are expensive and not particularly easy to acquire. This implies that an alloying chemistry which is fairly tolerant of slight chemistry mismatches (or perhaps one should say chemistry that has a decent operating window for foundries to work with) is preferable to one that only works in a very narrow bandwidth.

Of the four candidate alloys tested, only Alloy 4 produced a fully austenitic structure in the as-received (or untested) condition. The second melt of the other three alloys (even though the chemistries were quite close to the ordered chemistry) all produced a duplex structure in the as-received state. The carbon concentration in most cases was lower than the expected content, which caused a lack of austenitic stability at room temperature, hence the duplex microstructure and the presence of martensitic phase after thermo-mechanical processing (Alloys 1, 2, and 3). This means that they were slightly ferromagnetic. This affected the strain-induced phase transformation, as there was less austenite left for transformation to martensite during deformation. Carbon is also a general strengthening element for steel and the shortage of carbon was reflected in lower yield strengths for Alloys 1 and 3 (2^{nd} melting). Additions of molybdenum (2% by

weight) however, showed an ability to increase the strength of TRIP steel of Alloy 2. This would have been due to the fact that molybdenum carbides are effective barriers to slip band movement.

The four candidate steels were all processed at 550°C (warm rolled to 75% reduction in thickness). The ability of warm work or PDA to impart strength to the material is self-evident. Literature suggests that different warm working temperatures produce different levels of strength and slightly different transformation characteristics. It is also suggested that lower temperature PDA produces more martensitic nucleation sites, and would therefore produce better transformation properties. The processing temperature of 550°C chosen for this work was a result of laboratory equipment constraints. An optimum temperature (minimum) at which warm work must be performed without producing strain-induced phase transformation in the alloys deserves further investigation.

The PDA produced no transformation during warm working in Alloy 4, but did most definitely increase the dislocation density, thereby providing martensitic nucleation sites; which effectively destabilized the austenite to allow easier stress-strain induced transformation below the M_D temperature. Also noteworthy is the fact that the warm rolling is performed within the sensitization temperature interval (400 to 950°C) which means that carbides are formed at grain boundaries thereby consuming carbon. Carbon is an austenitic stabilizer; and the alloy therefore became chemically destabilized, making the material easily transformable by small lattice perturbation. In addition carbides also raise the yield strength of the material as they act as slip band barriers, thereby making the alloy stronger. The effect of carbides on fatigue performance was not established during this study and should form part of further investigation.

Observations during the warm working of the material also revealed that there is a limit to the warm work (PDA) which can be induced in these TRIP steels. This force is equal to a force which produces a stress equal to the breaking stress of a material. In this study a warm rolled plate started cracking at an 80% reduction in thickness. It was also interesting to note that TRIP steel based on manganese as main austenite stabilizer

element responds well to the warm deformation, as this type of material has not previously been thermo-mechanically processed. Alloys 3/2 and 3/3, which started cracking at 75% warm reduction, had their yield strength raised from 450MPa (for a similar hot rolled material) to 850MPa.

All four alloys were tensile tested with magnetic susceptibility monitoring added to assess transformation characteristics simultaneously, and microstructural observation was used to confirm this transformation. When the magnetic susceptibility data was superimposed on the tensile stress-strain data, it was easy to identify which alloys began to transform before the yield point. The results of this first round of testing indicated that there were two alloys (namely 1 and 3) that produced unacceptably low yield strengths for this particular application, and that the transformation characteristics of Alloys 1 and 3 were also not suitable. The other two alloys, namely 2 and 4 displayed acceptable mechanical properties with strain induced phase transformation starting before the material plastically yielded (stress induced), which is imperative for a smart damage monitoring structural element, such as an aircraft bolt, which must be replaced before it yields. These alloys were then further tested to verify their "acceptable" behaviour.

The compression tests provided similar transformation results as for the tensile tests in terms of the total change in susceptibility, but due to difficulties in the actual physical measurement of the magnetic susceptibility **during** the test, the exact form of the transformation curve was not established for Alloys 2 or 4. It is important to realize that both tensile and compression tests used here to determine basic mechanical properties, do not constitute curves from which to tune or calibrate the monitoring circuitry for the final commercial bolt prototype. In order to correlate levels of damage (which will be a combination of tensile, compressive, shear and in particular fatigue loading) with levels of martensite or magnetic susceptibility, scaled bolts will need to be tested with a fatigue spectrum of loading typical of aircraft bolt loading. The transformation characteristic would then be monitored by the actual monitoring equipment already developed as part of this study, i.e.: the smart washer/nut. From the data of these tests, it would then be

possible to pre-determine levels of magnetic susceptibility that would correspond to bolt replacement.

When the notion of the sub-scale bolt prototype was considered, there were several options that could provide a completely integrated structural health monitoring system, i.e.: one where the damage monitor became part of the bolt assembly. The first of those options was to drill a hole down the centre of the bolt to allow a magnetic susceptibility probe to be inserted during periodic maintenance. The second concept involved placing a damage concentrator (or groove) under the head of the bolt. And, the third involved the location of a coil close to the site of the first thread, which is where fatigue failure initiates. Apart from the extreme resistance of aircraft maintenance personnel to the notion of any kind of geometry change, the option of drilling a centre hole to insert a probe was found not to allow accurate magnetic susceptibility measurement. The damage concentrator under the head of the bolt was a workable solution, but not a desirable solution, and the washer/smart nut solution was found to achieve the best results in terms of sensitivity as well as desirability. The smart washer/nut concept provides a fully-protected sensor coil, is simple, user-friendly and therefore an acceptable option for smart aircraft bolts. Tests of this circuitry (coil embedded within a smart washer/nut connected to inductance meter only when necessary to interrogate) proved that it is viable and sensitive enough to monitor damage.

CHAPTER 6

CONCLUSION

Following an in-depth literature study of previous work on TRIP steels, austenitic stainless steels, strain memory alloys, as well as the individual effects of various alloying elements; fours high strength TRIP steel alloys were melted, thermo-mechanically processed, and mechanically tested to ascertain suitability for the smart aircraft bolt application.

The material processing technique used to impart strength as well as de-stabilise the austenite, was warm rolling at 550°C to a 75% reduction in thickness. At this temperature (which was chosen to fit within the constraints of laboratory equipment) the maximum reduction in thickness that could be achieved was 75%, thereafter cracking of the material surface became evident. This working temperature was not however optimized in any way, and it may be possible to improve the strength levels achieved by lowering the working temperature.

All of the four candidate alloys displayed a strain-induced transformation, confirmed by a suppression of the necking phenomenon in tensile fractured samples and evidence of generous proportions of the martensitic phase in microstructural observations. However, only Alloys 2 and 4 displayed a high enough yield strength to satisfy the military specification for aircraft bolt material. These alloys were then further tested, and both displayed good transformation in compressive loading, as well as heightened impact resistance due to the phase transformation. Further tests involving cooling, to ascertain the influence of low temperatures on martensitic formation revealed that alloy 2 suffers thermal instability below 0°C; that is: thermal martensite is produced inside the operating temperature window. This means that there would be no way to determine whether strain (damage) or a drop in temperature below 0°C had produced the martensite. Alloy 2 will therefore be unsuitable for an aircraft application.

Alloy 4 (Fe + 0.29%C + 0.56%Si + 1.13%Mn + 11.6%Cr + 9.48%Ni) however produced far better results when subjected to the same cooling tests, with no thermal martensite presenting inside of the operating temperature window, from which it could be inferred that the M_S temperature is suppressed sufficiently by the carbon content not to interfere with the strain-induced transformation. Alloy 4 also achieved a stress-induced transformation, meaning that the transformation began before the yield point of the material was reached. This alloy was therefore the only one of the four candidate alloys to achieve suitable yield strength (1000 to 1100 MPa), tensile strength (1270 to 1500 MPa) as well as transformation characteristics with 0.06 - 0.08 unit of magnetic susceptibility at the yield point, and is the alloy that will be further tested for fatigue properties in the form of prototype sub-scale bolts.

In parallel with the materials development presented above, the concept of the smart aircraft bolt and its associated monitoring equipment was further developed in terms of design and magnetic susceptibility measurement technique. In this work, a tested prototype smart bolt made from low strength TRIP steel gave following results: 1) a miniature coil was sensitive to the magnetic permeability changes occurring within the bolt during the tensile testing. 2) A coil located on the first engaged thread picked up more phase transformation than that located under the bolt head, even for a bolt with a groove under the head. 3) Both bolts, one with 1mm groove under the head and the other without any groove failed at the first engaged thread. It is again confirmed that the bolt is most highly stressed on the first engaged thread where a sensing coil inserted in the washer (smart washer) will be located. In terms of bolt design, the addition of a smart washer or nut allowed the bolt geometry to remain unchanged (without centre drilled hole or damage concentrating groove under the bolt head) by locating the sensing coil at the site of the first thread, which is the location of failure.

Future work in related areas includes:

1) A study of a thermal processing method to replace the expensive thermo-mechanical method used in this study.

2) A study of the fatigue characteristics of the candidate alloys is already in progress and forms the basis for a separate thesis. Scaled testing of the bolts in fatigue will also be conducted.
3) Further investigations into the sensitivity of the electronic circuitry comprising the monitoring device.
4) In addition to the above, the relations between combination loading (cyclic tensile and shear) and the strain induced martensite transformation (kinetic), mainly for Alloy 4 need to be clarified.

GLOSSARY

TRIP- Transformed Induced Plasticity

Yield strength- is stress at which material exhibits a specified limit of 0.2 per cent permanent deformed (stress at which a material start to be permanently deformed)

UTS- Ultimate Tensile Stress which is the maximum stress experienced by a material during a tensile test prior to breaking

PDA- Prior deformation of austenite

$\mathbf{M_S}$ – Temperature at which thermal induced martensite begins to form

$\mathbf{M_F}$ – Temperature below which thermal induced martensite no more forms even in the presence of retained austenite

$\mathbf{M_D}$ – The higher temperature at which strain induced martensite may occur; it is above the M_S temperature.

$\mathbf{V_{FM}}$ – transformed volume fraction of martensite

TTT - curve or diagram- Diagram on which Time Temperature and phase Transformation are represented

CE - Chromium Equivalent

NE – Nickel Equivalent

REFERENCES

1. L D Thompson, B Westermo and M Tominaga, "Monitoring Based Maintenance for Civil Engineering Structures", International conference on structural safety and reliability, Newport Beach , June 2001
2. V Zackay, E Parker, D Fahr and R Bush, "The Enhancement of Ductility in High-Strength Steels", Transaction of ASM, 60, 1967, pp 252-259
3. G B Olson, R Chair, M Azrin and R A Gagne, "Fatigue Strength of TRIP Steel", Metallurgical Transaction, 11A, pp. 1069-1071, 1980
4. V F Zakay, M D Bhandarkar, and E R Parker, " The Role of Deformation-Induced Phase Transformation in the Plasticity of Some Iron Base Alloys", Metallurgical Transactions, vol. 41, 1978, pp. 351-403
5. D Stephen, S D Antolovich and D Fahr, " An Experimental Investigation of the Fracture Characteristics of TRIP Alloys", Engineering Fracture Mechanics, Vol.4, 1972, PP 133-144
6. B L Verijenko, " Smart Materials for Structural Health Monitoring", PhD Thesis, University of Natal, Durban, January 2003
7. V Verijenko, B Burton, " Smart materials for structural health monitoring" ESDA, July 2002, Istanbul, Turkey
8. F Lecroisey and A Pineau, "Martensitic Transformation Induced by Plastic Deformation in the Fe-Ni-Cr-C System", Metallurgical Transactions, Vol. 3, February 1972, pp 387-396
9. G R Chanani, S D Antolovich, W W Gerberich, Metallurgical Transaction, vol. 3, 1972, pp 2661-2672.
10. A Hall James, V F Zackay and R E Parker, "Structural Observation in a Metastable Austenitic Steel", Transactions of the ASM, vol. 62,1969, pp. 965-976
11. D Webster, " Devlopment of a high strength stainless steel with improved toughness and ductility", Metallurgical Transactions, vol. 2 1971, pp 2097-2104
12. G R Chanani, S D Antolovich, Metallurgical Transactions, 1974, pp 217-229.
13. P C Maxwel, A Goldberg, J C Shyne, Metallurgical Transactions, vol. 5, 1974, pp 1305-1318

14. J R C Guimarares, R J De Angelis, Metallurgical Transactions, vol. 4, 1973, pp 2379-2381
15. U Krupp, P Luezuo, R G Teteruk, and H J Christ, "Deformation-induced Martensite Formation in Metastable Austenitic Steel in Dependence on the Carbon Content", Institut fur Werkstofftechnik, Universitat Siegen Fed. Rep. Germany, 2002.
16. F A Grossley and R W Lindberg, "Microstructure Analysis of a High Strength Martensite-Beta Titanium Alloy", Metallurgical transactions vol.13, 1970, pp. 841-883
17. F Abrassart, F Lecroisey, A Pineau, " Martensitic Transformation and Plasticity in the Fe-Ni-Cr-C System", Metallurgical Transactions, vol. 16, 1970, pp-905-909
18. G B Olson And M Cohen, "Kinetics of Strain-Induced Martensitic Nucleation", Metallurgical Transactions A, vol 6A, April 1975, pp 791-795
19. R G Stringfellow, D M Parks and G B Olson, "A Constitutive Model for Transformed Plasticity Accompanying Strain- Induced Martensitic Transformation in Metastable Austenitic Steels", Acta Metallurgica, 1992,vol.40, 7, pp 1703-1716
20. V I Leivitas, A Idesman and G B Olson, "Continuum Modeling of Strain-Induced Martensitic Transformation at Shear-band Intersections", Acta Metallurgica, vol.47, 1, 1999, pp 219-233
21. W B Morrison, " Plastic Instability During Luders Deformation in Ultrafine-Grained Low- Carbon Ferritic Steel", Transaction of the ASM, 1970, pp.879-893
22. J S Dunning, L D Thomson. "Development of Smart Solid-State Structural Damage Assessment Systems for Underground Facilities", North-American conference on smart structures and materials, San Diego 1995
23. G B Olson, M Azrin, "Transformation Behavior of TRIP Steels", Metallurgical Transactions, Vol. 9A, 1978, pp 713-721.
24. E H R Wade and C M Preece, "Cavitation Erosion of Iron and Steel", Metallurgical Transactions, A.,1978, vol. 9A, pp 1299-1309
25. E Arnold, "Steels: Microstructures and Properties", Metallurgy and Materials Science Series, R W K Honeycomb, 1981, pp 55-56.

26. W F Smith, "Structure and Properties of Engineering Alloys", McGraw-Hill, New York, 1993
27. A G Pineau, R M Pelloux, Metallurgical Transactions, vol. 5, 1974, pp1103-1112
28. E R Parker and V F Zackay, "Enhancement of Fracture Toughness in High Strength Steel by Microstructural Control", Engineering Fracture Mechanics, Vol.5, 1973, pp 147-165
29. W Gerberich, P L Hemmings, and V F Zackay, 'Fracture and Fractography of Metastable Austenites", Metallurgical Transactions, vol.2 August 1971, PP 2243-2253
30. D Bhandarkar, V F Zackay, E R Parker, Metallurgical Transactions, vol. 3, 1972, pp 2619-2631
31. Y Tomita, Y Shibutani, "Estimation of deformation behavior of TRIP Steels", International journal of Plasticity 16 (2000), pp.769-789.
32. F Abrassart, Metallurgical Transactions, vol. 4, 1973, pp 2205-2216.
33. C J Guntner and R P Reed, " The Effect of Experimental Variables Including the Martensitic Transformation on the Low-Temperature Mechanical Properties of Austenitic Stainless Steels", Transactions of ASM, Vol.55, 1962, pp.399-419
34. Tamura, T Maki, H Hato, Y Tomota and M Okada, "Strength and Ductility of Austenitic Iron Alloys Accompanying Strain- Induced Martensitic Transformation", Transactions of the ASM, 1970, pp 900-904
35. D Goodchild, W T Roberts and D V Wilson, "Plastic Deformation and Phase Transformation in Textured Austenitic Stainless Steel", Acta Metallurgica, vol.18, November 1970, pp1137-1144
36. J M Drapier, P Viatour, D Contsanradis, L Habraken, " Hardening Mechanism in Multiphase Alloys", Paper 11.4, 1970, PP 830-834
37. R D Knutsen, M Sbanda, " Evaluation of the Formability Properties of Nitrogen Alloyed Meetastable Austenitic Stainless Steels", Proceedings of Stainless Steels, 93 Processes and Material Innovation, vol. 3, Florence, AIM, 1993, pp 3.333-3.342.
38. T Biggs, R D Knutsen, Journal de Physique 4, vol. 5, 1995, pp C8-515- C8-520.
39. M Sibanda, S L Vismer, R D Knutsen, Materials Letters 21, 1994, pp 203-207.

40. R Paton, J S Moema, C J Fletcher and D Adams, "The Use of Smart Bolt Technology to Assess the Condition of Mining Roof Support Systems", 6th International Colloquium, Ageing of Materials and Methods for the Assessment and Extension of Lifetime of Engineering Plant. Cape 2001
41. D S Clark and W R Varney, "Physical Metallurgy for Engineers", New York 1962
42. E W Pages, P Mangamon, G Thomas and V F Zackay, "Structure and Dynamically Strain Aged Fe-Cr-C and Fe-Mo-C Alloys", Transactions of the ASM vol.62, 1969, pp 45-54
43. D J Drobujak, J G Parr, Metallurgical Transactions, vol, 1 1970, pp 759-765.
44. T Angel, Journal of the Iron and Steel Institute, May 1954, pp 165-174
45. J Lefevre, R Tricot, A Gueussier, R Castro, Metallurgical Transactions, vol. 5, 1974, pp 2277-2285.
46. D A Woodford, "Cavitations Erosion-Induced Phase", Metallurgical Transactions, Vol 3, May 1972, pp 1137-1145
47. S O Walter, " Strengthening by Transformation", Transaction of the ASM, 1970, pp. 795-814
48. W W Gerberich, G. Thomas, E. R. Parker and V F Zackay, "Metastable Austenite Decomposition and Strength", Paper 13.6, 1970, pp 894-899
49. J C Shyne, V F Zackay, D J Schamtz, Transactions of the ASM, vol. 52, 1960, pp 347-361.
50. G Thomas, D Schmatz, and W Gerberich, "Structure and Strength of Some Ausformed Steels", MT-74, 1964, pp 251-296
51. T J Koppenaal, Metallurgical Transactions, vol. 3, 1972, pp 1549-1554
52. G R Chanani, V F Zachay, E R Parker, Metallurgical Transactions, vol.2, 1971, pp 133-139.
53. G F Bolling and R H Richman, "The Plastic Deformation – Transformation of Paramagnetic FCC. F-Ni-C Alloys", Acta Metallurgica, vol.18, June 1970, pp 673-681
54. R G Davies and C L Magee, " On the Occurrence of the Various Martensite Morphologies", 1970, paper 11.2, pp 817-821

55. C Altstetter and M Rashid, "Defects and Strengthening in Transformed Crystals", paper 11.7, 1970, pp 846-849
56. H Smith and D R F West, "The Strengthening of Stainless Steels by the Reverse Martensite Transformation", paper 13.5, 1970, pp 892-893
57. V F Zackay, E R Parker, D Farh, and R Bush, Trans. ASM, 1967, vol. 60, pp 252
58. G Krauss, and M Cohen, Trans. TMS-AIME, 1962, vol. 224, pp 1212
59. G Krauss, Acta Metallurgica, 1963, vol.11, pp 499
60. D Fahr, "Stress and Strain- Induced Formation of Martensite and it Effect on Strength and Ductility of Metastable Austenitic Steels", Metallurgical Transactions, Vol. 2, July 1971, pp 1883-1892
61. V F Zackay and E R Parker, "Some Fundamental considerations in Design of High-Strength Metallic Material", High Strength Design, 1964, pp 130-153
62. A R Marder and G Krauss, " The Effect of Morphology on the Strength of Lath Martensite", 1970, paper 11.2, pp-822-829
63. D P Roberts, "Testing of Mining Tunnel support Elements and Systems for Hard Rock Mines", M Sc. Thesis, University of Natal, 1995.
64. B G Orson, M Azrin, and H E Band, "AC-permeability measurement of strain-induced martensite during tensile deformation of TRIP steels", AMMRC TR 77-10, Massachusetts, March 1977.
65. L D Thompson, "The FCC to HCP to BCC phase transformation sequence in metastable Fe-Mn-Cr alloy", Department of Mechanical Engineering San Diego State University, CA 92182-0191.
66. M Fisher and E Hill, "Neural network burst pressure prediction in fiberglass/epoxy vessels using acoustic emission", Proceedings of the 6th International Symposium on Acoustic Emission from Composite Materials, San Antonio, Texas, June, 1998.
67. C Shakeri, M Noori, and Z Hou, "Smart material and structures. A review." Tech. Report of Worcester Polytechnic Institute, 1998.
68. G Mook, J Phol, F Michel, T Benziger, "Damage Evaluation of Smart CFRP-Piezoelectric Materials Using Non-destructive Methods". Proceeding of the 12th International Conference on Composite Materials, Paris, 1999.

69. B Cina "Transitional HCP. Phase in Fe-base Alloys", Acta Metallurgica, vol. 6 1958.
70. P C De Vera, and G Guemes, "Embedded Self-Sensing Piezoelectric for Damage Detection." J. International Systems and Structures 11, 1999.
71. M Azrin, G B Olson and R A Gagne, "Inhomogeneous Deformation and Strain Rate Effects in High-Strength TRIP Steels", Materials Science and Engineering, vol.23, 1976, pp 33-41.
72. E Gold and T J Koppenaal, "Anomalous Ductility of TRIP Steel", Transactions of the ASM, Vol.62, 1969, pp 607- 610
73. G W Form and W M Baldwin, "The Influence of Temperature on the Ductility of Austenitic Stainless Steel", Transactions of the ASM, vol. 48, 1956, pp 474-485
74. R A Lincoln and W H Mather, " Effect of Temperature on Cold Rolling, Temperature of Testing and Rate of Pulling on Tensile Properties of Austenitic Stainless Steels with Low Nickel Content", Regional Technical Meeting, Iron and steel Inst. 57, 1948
75. V N Krivobok and A M Jalbot, " Effect of Temperature on the Mechanical Properties, Characteristics, and Processing of Austenitic Stainless Steel", Proc ASTM, 50,1950, pp 895
76. J F Waston and J L Christian, "A Study of Austenite Decomposition at Cryogenic Temperature", Transactions AIME, 224, 1962, pp 998
77. K M Carlsen and K C Thomas, "Effect of Composition, Heat Treatment and Cold Rolling on Mechanical Properties of Cr-Ni Stainless Steels", Transactions Quart, 55, 1962, pp 462
78. G W Powell, E R Marshal and W A Backofen, "Strain Hardening of Austenitic Stainless Steels", Transactions of the ASM, 50, 1958, p 478
79. J F Breedis and W D Roberton, "The Martensitic Transformation in Single Cristals of Iron-Chromium-Nickel Alloys", Acta Metallurgica, 10, 1962, p 1077
80. J P Bressanelli and A Moskowitz, "Effect of Strain Rate, Temperature, and Composition on Tensile Properties of Metastable Austenitic Stainless Steel, Transactions of the ASM, volume 59, 1966 pp 223-235

81. D C Ludvigson, J A Berger, Journal of the Iron and Steel Institute, Jan 1969, pp 413-419.
82. A Z Hanzaki, P D Hodgson and S Yue, "Hot deformation characteristics of Si-Mn TRIP Steel with and without Nb additions", ISI international, vol.35 (1995) N° 3 pp 324-331
83. S D Antolovich, B Singh, Metallurgical Transactions, vol.2, 1971, pp 2135-2141.
84. P C Maxwell, A Goldberg, J C Shyne, Metallurgical Transactions, vol. 5, 1974, pp 1319-1332.
85. E Schmid, R D Knutsen, " Reducing the Nickel content in metastable Austenitic Stainless steel", Proceedings of the 1st International Chromium Steel and Alloys Congress, Cape Town, vol. 2, 1992, pp 151-156.
86. G Chanani, and S Antolovich, "Low Cycle Fatigue of a High Strength Metastable Austenitic Steel", Metallurgical Transactions, vol. 2, 1974 PP 217-229
87. D Hennessy, G Steckel and C Alstetter, " Phase Transformation of Stainless Steel During Fatigue", Metallurgical Transactions, Vol.7A, March 1976, pp 415-424
88. S S Hecker, M G Stout, K P Staudhammer, J L Smith, "Effect of Strain State and Strain Rate on Deformation- Induced Transformation in 304 Stainless Steel: Part 1, Magnetic Measurements and Mechanical Behaviour", Metallurgical Transactions, vol. 13A, 1982, pp 619-626.
89. J H Bickford, An Introduction to the Design and Behaviour of Bolted Joints, Marcel Dekker, 1990
90. Unified Inch Screw Threads, ANSI Standard B1.1-1974, ASME, New York, 1974.
91. C J Robert, M M Kurt, " Fundamentals of Machine Components Design", Second Edition, Hamilton 1991 New York, USA
92. L L Msibi, " Development of the Smart Aircraft Bolt", MSc Thesis, Mech. Eng. University of Natal 2002, Durban
93. D Jonson "Finite Element Modelling of Smart TRIP Steel Sensors and Systems", University of Natal, Ph.D. Thesis, January 2003
94. D Francis, M.Sc. Thesis, "An Investigation of the Strength of an Aircraft Wing Bolt with a Centre-Drilled Hole, University of Natal, 2000, Durban

95. H M Otte, Acta Metallurgica, Vol.5, pp 137-141, 1957
96. Smart Aircraft Bolt Technology Project 1999/2000, School of Mechanical Engineering, University of Natal. Prepared for ARMSCOR.
97. D P Rowlands, "The Secrets of Stainless Steels", SA Stainless Steel Development Association (SASSDA), Stainless Steel Information Series No.18

APPENDIX A

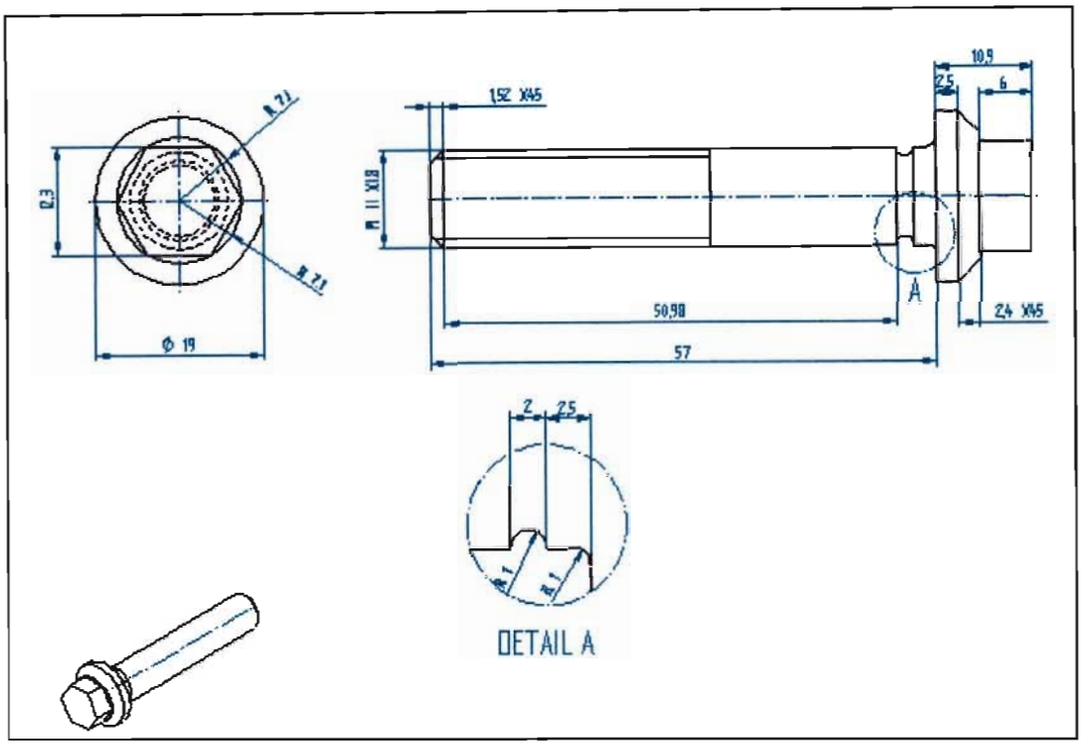

Figure 1 Drawing for prototype aircraft bolt with under head 1mm groove

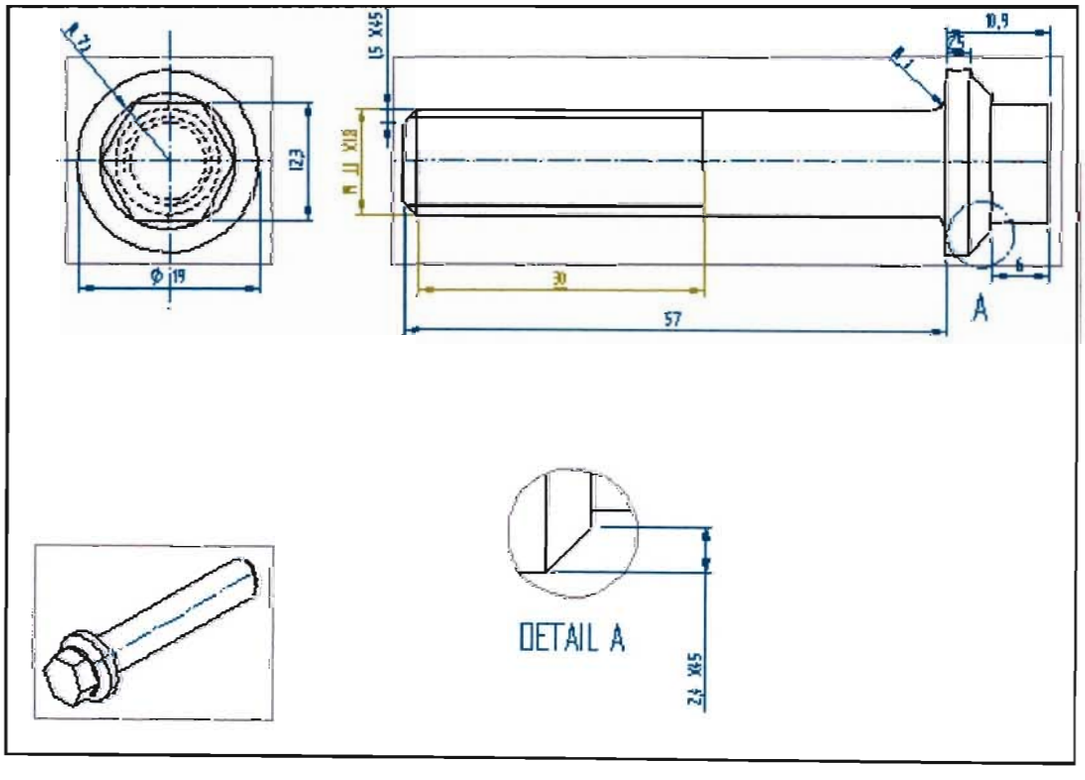

Figure 2 Drawing for aircraft bolt prototype without any groove

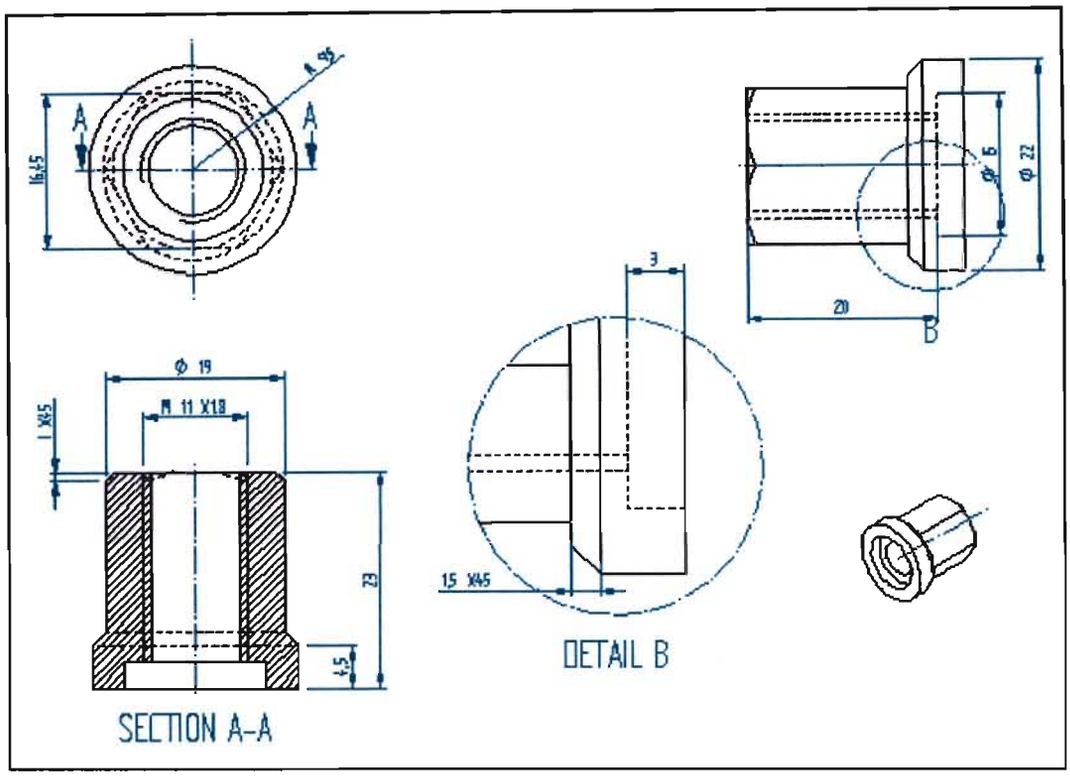

Figure 3 Drawing for a smart nut for aircraft bolt prototype showing a groove to house the magnetic inductance coil

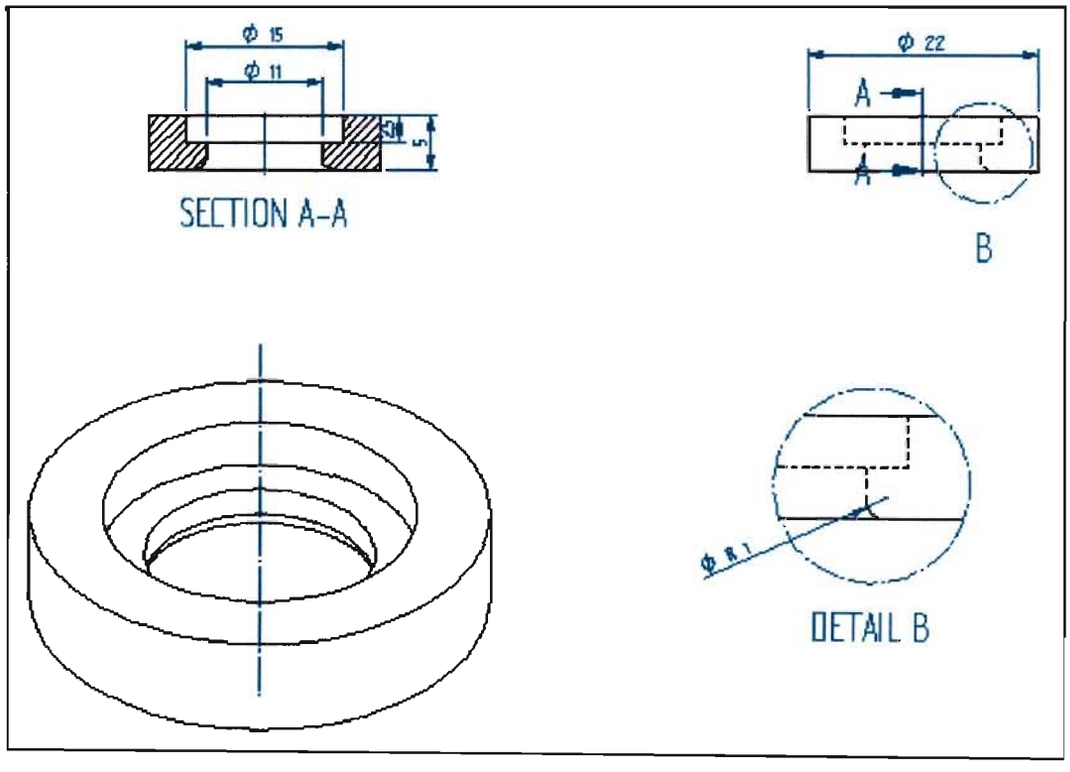

Figure 4 Drawing for a smart washer for aircraft bolt prototype showing a groove to house the magnetic inductance coil

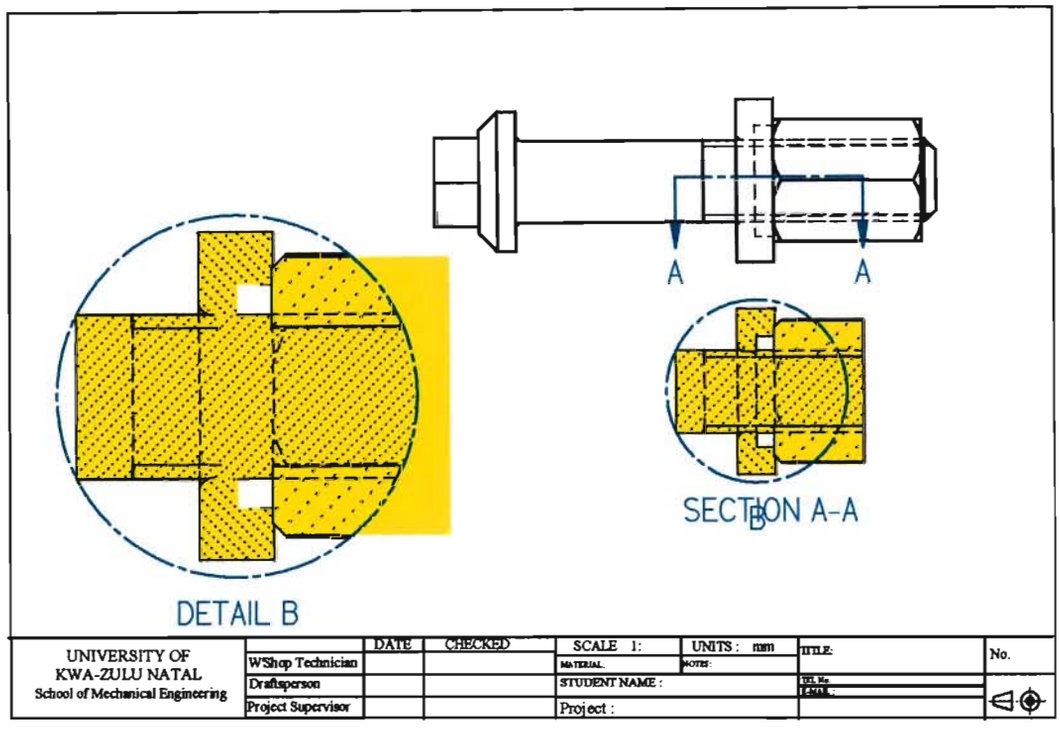

Figure 5 Smart bolt prototype assembly drawing showing an open space where a coil is placed

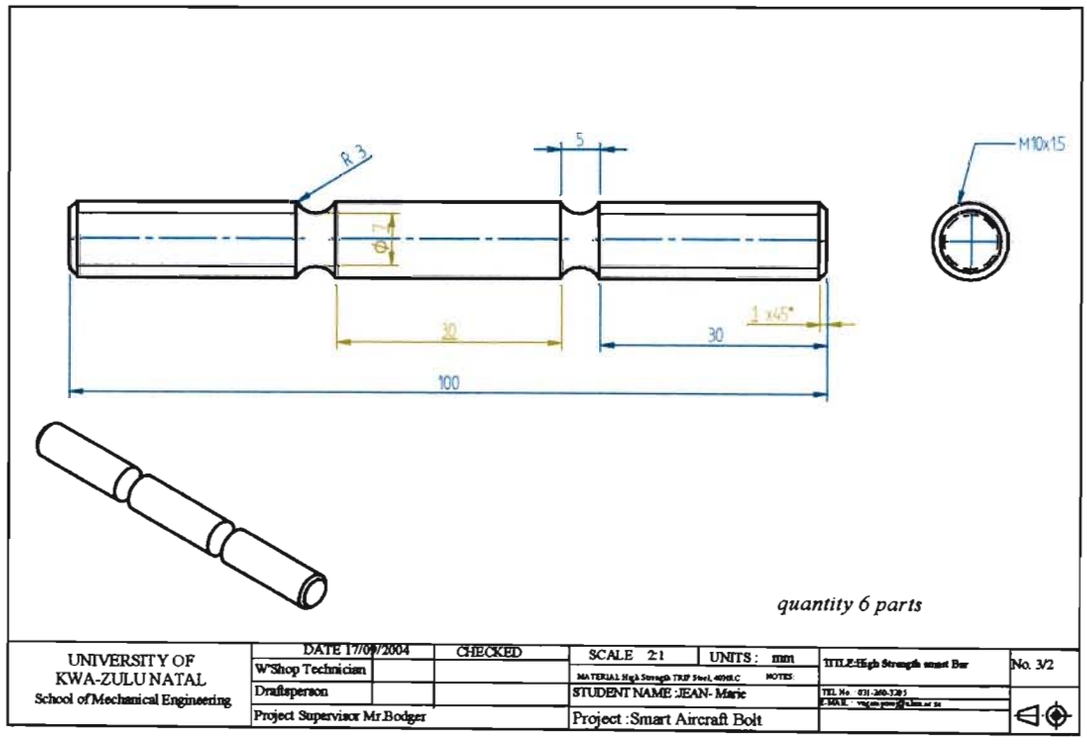

Figure 6 Smart bar (Φ=10mm made in High Strength TRIP steel) drawing designed to simulate smart bolt

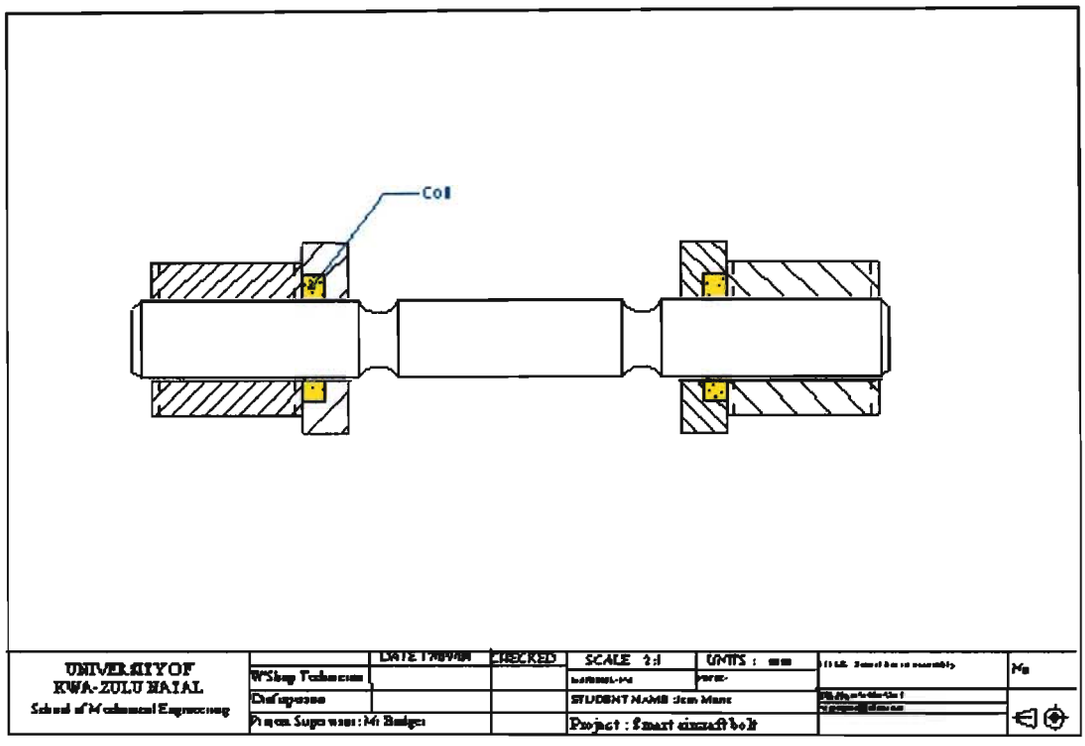

Figure 7 Smart bar drawing in assembly showing a location of the Inductance coil

APPENDIX B

METLAB

Certificate of Test No. 04-3135 B

University of Kwazulu - Natal School of Mec
Engineering Faculty of Eng
Durban
4041
ATT: J.M.V Vugampore

Date received 2004-07-15
Date tested 2004-07-19
Order No.

Identification		Marked 4		
Charpy V Notch				
Impact Size	mm	10 x 10		
Test Temperature	°C	20	-50	
Impact Resistance	J	90	106	
		98	144	
		70	118	
Lateral Expansion	mm	0.24	0.22	
		0.21	0.12	
		0.16	0.28	
Shear	%	100	100	
		100	100	
		100	100	
Material		High strength steel (40 - 42HRC)		
	Note	Specimens machined by the client		
		Test temperatures supplied by the client		

In accordance with specification provided		Not in accordance with specification provided		No requirement provided	X

N/A
Witnessed by

Metallurgist/Designee

Figure 8 Impact test results alloy 4 showing high impact resistances at 20°C and –50°C